TECHNISCHE UNIVERSITÄT DARMSTADT

Impact of ionizing radiation on cardiac differentiation capability of human embryonic stem cells

Fachbereich Biologie der

Technischen Universität Darmstadt

zur Erlangung des Grades

Doktor rerum naturalium

(Dr. rer. nat.)

Dissertation

von Scarlett Nitsch

Erstgutachterin: Prof. Dr. Gisela Taucher-Scholz

Zweitgutachter: Prof. Dr. Gerhard Thiel

Darmstadt 2018

Nitsch, Scarlett: Impact of ionizing radiation on cardiac differentiation capability of human embryonic stem cells
Darmstadt, Technische Universität Darmstadt
Jahr der Veröffentlichung der Dissertation auf TUprints: 2019
URN: urn:nbn:de:tuda-tuprints-80779
Tag der mündlichen Prüfung: 14.12.2018

Ehrenwörtliche Erklärung

Ich erkläre hiermit ehrenwörtlich, dass ich die vorliegende Arbeit entsprechend den Regeln guter wissenschaftlicher Praxis selbstständig und ohne unzulässige Hilfe Dritter angefertigt habe.

Sämtliche aus fremden Quellen direkt oder indirekt übernommenen Gedanken sowie sämtliche von Anderen direkt oder indirekt übernommenen Daten, Techniken und Materialien sind als solche kenntlich gemacht. Die Arbeit wurde bisher bei keiner anderen Hochschule zu Prüfungszwecken eingereicht.

Darmstadt, den 2. Oktober 2018

.....

Scarlett Nitsch

Danksagung

Mein herzlichster Dank gilt Prof. Dr. Gisela Taucher-Scholz für die Vermittlung der Doktorandenstelle und die freundliche Übernahme des Erstgutachtens. Gleichermaßen bedanke ich mich bei Prof. Dr. Gerhard Thiel, der sich unmittelbar als externer Betreuer und zweiter Referent zur Verfügung stellte. Beiden danke ich für das Interesse, die Unterstützung und die hilfreichen Ratschläge während meiner gesamten Zeit als Doktorandin auch außerhalb meiner halbjährigen PhD-Meetings.

Bei Dr. Sylvia Ritter möchte ich mich ganz herzlich für die Aufnahme in ihre Arbeitsgruppe bedanken. Vielen Dank für die fortwährende Unterstützung, die vielen Korrekturen meiner Berichte und die Möglichkeit, jederzeit meine Arbeit zu besprechen.

Dr. Insa Schröder danke ich für die freundliche Betreuung und Vermittlung ihrer Fachkompetenz. Danke für die vielen wertvollen Ratschläge, Korrekturen und Diskussionen meiner Ergebnisse.

Des Weiteren möchte ich der gesamten Arbeitsgruppe *Stem Cell Differentiation and Cytogenetics* danken. Besonders bedanke ich mich bei Dr. Onetsine Arrizabalaga de Mingo, die mir immer wieder wertvolle Tipps gab und mich bei der Durchführung der Durchflusszytometrie unterstützte. Dr. Elena Nasonova danke ich herzlich für die Unterstützung und Durchführung der Chromosomenanalysen. Ein besonders herzliches Dankeschön gilt auch Julia Kunz, die mich durch ihre Hilfe im Labor und bei der Videoauswertung sehr entlastete.

Bei Florian Braun und Dr. Michael Scholz bedanke ich mich für die Entwicklung der Software *cBRA*, durch die die Auswertung der unzähligen Videos im Rahmen meiner Doktorarbeit erst möglich wurde.

Paolo Zuccolini danke ich für seine Zeit und Geduld bei der Durchführung der elektrophysiologischen Messungen der kardialen Cluster.

Außerdem möchte ich mich bei der gesamten Abteilung Biophysik für die herzliche Aufnahme und Unterstützung bedanken.

Lara Muñoz-Rizzo, Céline Schielke, Svenja Lehnung und Kim Röder danke ich für die abwechslungsreichen und lustigen Mittagspausen sowie ihre Unterstützung und Freundschaft.

Mein größter Dank gilt meinen Eltern, die mir mein Studium ermöglicht, mich immer unterstützt und ermutigt haben, meine Ziele zu verfolgen. Meinem Freund David Linde danke ich besonders für sein Verständnis, seine Liebe, Geduld und ständige Ermutigung vor allem auch in stressigen Zeiten.

Bei HGS-HiRE bedanke ich mich für die finanzielle Unterstützung. Die vorliegende Arbeit wurde des Weiteren durch das Bundesministerium für Bildung und Forschung unterstützt (Förderkennzeichen 02NUK025A).

Zusammenfassung

In der medizinischen Diagnostik sind Röntgenstrahlen die am häufigsten verwendete Strahlenart und sie werden zunehmend auch bei schwangeren Frauen angewendet. Eine genaue Einschätzung des Gesundheitsrisikos für den sich entwickelnden Embryo ist daher notwendig. Da es ethisch nicht vertretbar ist, Strahleneffekte und deren Mechanismen im menschlichen Embryo zu untersuchen, wird ein geeignetes Modellsystem benötigt. Pluripotente, humane embryonale Stammzellen (hESCs) können fast unbegrenzt vermehrt und in alle Zellen des menschlichen Körpers differenziert werden und stellen somit ein vielseitiges *in-vitro*-Modell dar. Effekte verschiedener Noxen, wie beispielsweise ionisierende Strahlung (IR) oder Medikamente, auf die frühe menschliche Entwicklung sowie deren molekulare Mechanismen können mithilfe von hESCs untersucht werden. Das Herz ist das erste funktionelle Organ, deshalb ist seine korrekte Bildung die Voraussetzung für alle sich nachfolgend entwickelnden Organe, die mit Sauerstoff und Nährstoffen versorgt werden müssen. Der Einfluss einer pränatalen Strahlenexposition auf die kardiale Entwicklung wurde bisher nur in wenigen Studien untersucht. Diese zeigten, dass die kardiale Entwicklung muriner ESCs beeinträchtigt ist.

In der vorliegenden Dissertation wurde der Einfluss einer Röntgenstrahlenexposition auf die kardiale Differenzierungsfähigkeit von hESCs untersucht. Die Differenzierung wurde eine Woche nach Bestrahlung initiiert. Sowohl Gen- und Proteinexpression verschiedener Marker als auch die Funktionalität der schlagenden kardialen Cluster wurden über 15 Tage hinweg untersucht. Dabei wurde eine dosisabhängige Abnahme der kardialen Genexpression beobachtet: Während 0,1 Gy einen geringen Effekt auf die Expression von *NKX2.5*, *TNNT2*, *MYH6/7* und *MLC2a/v* hatte, war nach Bestrahlung mit 1 Gy eine deutliche Reduktion zu sehen. Diese war durch eine 2 Gy-Bestrahlung noch deutlicher und bereits bei einem Marker des kardialen Mesoderms (*MESP1*) sichtbar. Außerdem wurde in den Kardiomyozyten, die aus den 2 Gy-bestrahlten hESCs hervorgingen, kein MLC2v-Protein detektiert, welches ein früher Marker der ventrikulären Spezifizierung und wichtig für die kardiale Kontraktion ist. Im Vergleich zu den Kontrollen zeigten diese Zellen des Weiteren geänderte Schlagraten und eine niedrigere Antwort auf Isoproterenol, ein Agonist der β-Adrenorezeptoren. Untersuchungen der molekularen Signalwege weisen darauf hin, dass diese Effekte durch ein beeinträchtigtes *non-canonical-WNT-signaling* und gp130-vermitteltes *signaling* bedingt werden.

Da pluripotente Zellen nur vorübergehend während der frühen Schwangerschaft existieren, ist es statistisch wahrscheinlicher, dass eine Strahlenexposition zu einem späteren Zeitpunkt stattfindet. Um den Einfluss von IR auf differenzierende kardiale Kulturen zu untersuchen, wurden diese an bestimmten Zeitpunkten mit 1 Gy bestrahlt. Erste Experimente zeigten keine Änderungen auf molekularer und funktioneller Ebene.

Diese Studie zeigte, dass hohe Dosen (2 Gy) einen deutlich negativen Effekt auf die kardiale Differenzierung von hESCs haben und auch die niedrigste getestete Dosis (0,1 Gy) zu dysregulierter kardialer Genexpression führt. Dies weist darauf hin, dass sich auch eine Dosis von 0,1 Gy, die

Schwellendosis für Missbildungen und geistige Retardierung, schädlich auf den frühen Embryo auswirken könnte, da Entwicklungsprozesse nach einem strikten zeitlichen Muster ablaufen und selbst kleinste Änderungen in den Signalwegen die normale Entwicklung *in vivo* stören. Allerdings muss beachtet werden, dass die gemessene Dosis am Uterus bei den meisten einmaligen diagnostischen Untersuchungen deutlich geringer ist als 0,1 Gy.

Abstract

X-rays are the most commonly used radiation type in medical diagnostics and their application is increasing also in pregnant women. Therefore, a detailed health risk assessment for the developing embryo is needed. Since it is ethically not feasible to investigate radiation effects and their mechanisms directly in human embryos, a suitable model is needed. Pluripotent human embryonic stem cells (hESC) can be propagated almost infinitely and differentiated into all cells of the body, representing a versatile *in vitro* model system. Effects of various noxae, like ionizing radiation (IR) or newly designed drugs, on early human development and the underlying molecular mechanisms can be investigated using hESCs. Since the heart is the first functional organ, its normal formation is a prerequisite for the subsequently developing organs that need to be supplied with oxygen and nutrients. However, studies addressing the cardiac development upon prenatal IR exposure are scarce and based on murine ESCs suggesting that cardiac differentiation is impaired.

The present study investigated the impact of X-ray exposure of hESCs on their cardiac differentiation capability. Differentiation was initiated seven days after exposure. Marker gene and protein expression as well as functionality of the beating cardiac clusters were investigated up to 15 days. A dose-dependent decrease of cardiac gene expression was detected: whereas 0.1 Gy had a mild effect on several cardiac marker genes (e.g. *NKX2.5*, *TNNT2*, *MYH6/7*, *MLC2a/v*), their expression was markedly reduced following the 1 Gy exposure. Upon 2 Gy, this decrease was even more pronounced and already visible at the stage of cardiac mesoderm formation (*MESP1*). In addition, in cardiac clusters derived from 2 Gy-irradiated hESCs, MLC2v protein, an early ventricular marker, which is important for cardiac contraction, was not detected. Furthermore, their beat rates differed from those of controls and a lower response to isoproterenol, an agonist of β-adrenergic receptors, was observed. Molecular signaling pathway analyses suggest that these effects are linked to impaired non-canonical WNT signaling as well as gp130-mediated signaling.

Since pluripotency occurs only transiently in the first days of the blastocyst stage, it is statistically more likely that a prenatal exposure occurs at a later developmental stage. To investigate the impact of IR on the developing cardiac cultures, they were irradiated with 1 Gy at specific stages of differentiation. First experiments did not reveal molecular or functional alterations.

In conclusion, this study showed that a high X-ray dose (2 Gy) has a marked negative impact on cardiac differentiation of hESCs, but also the lowest dose tested (0.1 Gy) led to dysregulated cardiac gene expression. Thus, based on these results, even 0.1 Gy, which is the general threshold dose for malformations and mental retardation, might be harmful to the early embryo since developmental processes have a strict temporal pattern and even small alterations in the signaling pathways may hamper normal development *in vivo*. However, it has to be taken into account that the measured uterus dose of most single diagnostic procedures is much lower than 0.1 Gy.

Contents

Abbreviations

AP	Action potential
APA	Action potential amplitude
App.	Appendix
bpm	Beats per minute
BSA	Bovine serum albumin
CM	Cardiomyocytes
CT	Cycle threshold
cTNT-H9	Cells of the cell line H9-hTnnTZ-pGZ-D2
d	Day
DDR	DNA damage response
DNA	Desoxyribonucleic acid
EB	Embryoid body
ESCs	Embryonic stem cells
FA	Formaldehyde
FCS	Fetal calf serum
GFP	Green fluorescent protein
Gy	Gray
h	Hours
hESCs	Human embryonic stem cells
IR	Ionizing radiation
MDP	Maximum diastolic potential
MEF	Mouse embryonic fibroblasts
mESCs	Murine embryonic stem cells
mFISH	Multicolor fluorescence in situ hybridization
mRNA	Messenger ribonucleic acid
miRNA	Micro ribonucleic acid
mV	Millivolt
qRT-PCR	Quantitative Real-Time polymerase chain reaction
RT	Room temperature
s	Second
SCS	Stem cell signaling
SD	Standard deviation
SR	Sarcoplasmic reticulum
StZG	*Stammzellgesetz*
Sv	Sievert

1 Introduction

In the past years, the application of X-rays for medical diagnoses is increasing also in pregnant patients: From 1997 to 2006, there was a 121 % increase of imaging tests using ionizing radiation (IR) in pregnant women and, for the use of computer tomography (CT) scans, a 25 % increase per year was observed (Chen et al., 2008). The risk of the developing embryo is estimated based on epidemiological studies of atomic bomb survivors (Lee et al., 1999; Schull and Otake, 1999; Tatsukawa et al., 2008) or upon nuclear catastrophes (Hatch et al., 2017; Lie et al., 2017) and on animal model studies (Kimler and Norton, 1988; Pampfer and Streffer, 1988; Saito et al., 2015). However, there are difficulties with the extrapolation of these data. In addition, it is ethically infeasible to investigate the molecular mechanisms of IR-induced effects in human embryos. For this reason, human embryonic stem cells (hESCs) that can be differentiated *in vitro* into all cells of the three germ layers were selected in the present study as a suitable model system to investigate the impact of IR on early development. The development of the heart begins around week 2 - 3 post conception, around week 4 the heart starts to beat and around week 7 it is fully septated and connected to the aorta (Brade et al., 2013). Since it is the first functional organ, all subsequently arising tissues and organs depend on its correct formation. Hence, the presented study investigates the effects of IR on the cardiac differentiation capability of hESCs.

1.1 Physics of ionizing radiation and its effect during prenatal exposure

Organisms on earth are constantly exposed to IR via natural or man-made sources. IR comprises all radiation types that have enough energy to eject single electrons of atoms and thereby, ionize them, which means that a positively charged ion and at least one secondary electron are generated (Hall and Giaccia, 2006). The dose (D), which is received by a target is defined as the energy (E) in Joule (J) absorbed per mass unit (m) in kg and is measured in Gray (Gy):

$$\text{Dose} = \frac{E}{m}\ ;\ [\text{D}] = \frac{J}{kg} = \text{Gy}$$

Today, there is a growing number of radiological examinations in pregnant patients. X-rays are the most commonly used radiation type in medicine. They are photons that are indirectly ionizing, which means that the generated secondary electrons ionize other molecules in the irradiated target, leading to the production of free radicals (Hall and Giaccia, 2006). In biological systems, water molecules are the most likely target, generating hydroxyl radicals, which can lead to DNA damage being the most severe radiation-induced cellular damage type.

An *in utero* exposure to IR can have severe consequences, comprising non-cancer health effects as well as mutagenic and carcinogenic effects. The risks of an *in utero* exposure depend on the stage of development and the dose (De Santis et al., 2007). The pregnancy can be divided into three periods:

the preimplantation period (day 0 - 10 post conception), organogenesis (day 10 - week 8) and the fetal period (3^{rd} - 9^{th} month). As summarized by Williams and Fletcher (2010), an exposure above 0.1 Gy within the first ten days of pregnancy is associated with an increased risk of implantation failure. However, embryos that survive in this stage are unlikely to have non-cancer health effects. Upon an exposure during organogenesis or early fetal development (until week 15), mental retardation and growth restriction are the most common malformations. Whereas non-cancer health effects are not associated with an exposure to doses below 0.05 Gy at any stage of development, there is an increased risk of childhood malignancies like leukemia at any prenatal stage of development and dose (Williams and Fletcher, 2010).

The pregnancy might not always be known at the time when radiological examinations or a radiation therapy are necessary and some examinations cannot be avoided even if the pregnancy is known. The risk of the developing embryo is evaluated by physicians according to the recommendations of the *Deutsche Gesellschaft für medizinische Physik*: 100 mSv, which corresponds to 100 mGy in the case of X-rays, is reported to be the threshold dose for malformations and mental retardation. In 90 % of all cases of X-ray diagnostics, the uterus dose is lower than 20 mSv and there is no increased risk for the embryo. If the exposure occurred within the first ten days of the pregnancy (i.e. pre-implantation phase), no further dose calculation is needed since the embryo will either survive without damage or it will fail to implant with a threshold uterus dose of 100 mSv. However, if the exposure occurs after this phase, the dose should be calculated by the physician. If it is below 100 mSv, the patient will be informed, but an abortion is not recommended. Above 100 mSv, the increased risk of malformations or mental retardation should be considered by the patient. Nonetheless, the physician will only recommend an abortion if the uterus dose is higher than 200 mSv (*DGMP- und DRG-Bericht*, 2002).

Still, there is a need for further investigations of the exact risks and the underlying molecular mechanisms leading to radiation-induced health effects. Since it is ethically unjustifiable and infeasible, this cannot be studied directly in human embryos. The only available human *in vivo* data derive from epidemiological studies of atomic bomb survivors. However, since many other factors like nutrition, mental stress of the mother or uptake of medicine, drugs or chemicals by the mother (Barker, 1999; Mone et al., 2004) influence embryonic development, these data are difficult to extrapolate. Furthermore, mechanistic studies are not possible *in vivo*. Therefore, a suitable *in vitro* model is needed. With the generation of embryonic stem cell (ESCs) lines, such a model was established allowing the investigation of the impact of various noxae, like IR or drugs, on embryogenesis.

1.2 Stem cells

ESCs are pluripotent, which means that they have the potential to proliferate almost indefinitely (self-renewal) and give rise to all cells of the three germ layers (endo-, meso- and ectoderm). In 1981, the first successful establishment of murine ESCs (mESC) line was achieved by two labs (Evans and Kaufman, 1981; Martin, 1981). Human ESCs (hESC) lines, including the H9 line used in the present

study, were first established by Thomson et al. (1998). ESCs are obtained from blastocysts. These are embryos that consist of the outer cell layer, called trophoblast, giving rise to the extraembryonic tissues, and of the inner cell mass, which will give rise to the organism and is the source of ESCs. However, besides species-dependent differences, murine and human ESCs represent slightly different developmental stages of the blastocyst. hESCs are termed "primed", whereas mESCs are termed "naïve" (Morgani et al., 2017; Nichols and Smith, 2009).

Since hESCs derive from human embryos, ethical concerns arise and their use in research is strictly limited. In Germany, the legal basis for their scientific use is provided by the *Embryonenschutzgesetz* and the *Stammzellgesetz*. Research on hESCs must be of high basic or medical interest and it must be justified that it cannot be performed with another model system.

hESCs are a versatile tool for research and medicine. For example, they can be used to study the earliest steps of embryo- and cardiogenesis. Furthermore, hESC-derived cardiomyocytes (CM) are a promising tool for the preclinical screening of newly developed drugs for cardiotoxic and pro-arrythmic effects as well as for regenerative medicine and to treat cardiovascular diseases like myocardial infarction or heart failure. For example, it was recently reported by Liu et al. (2018) that hESC-derived CM were able to implant successfully into infarcted hearts of macaques, thereby restoring cardiac function without the onset of arrhythmias, which were observed in a previous study (Chong et al., 2014). The first human trial using hESC-derived cardiac progenitor cells for treating severe heart failure was initiated in 2013 (ESCORT, Menasché et al., 2015) and first results of this study are promising (Menasché et al., 2017).

1.2.1 Maintenance and markers of pluripotency in hESCs

Pluripotency is maintained by a complex signaling network, comprising TGF-β, FGF, NOTCH and WNT signaling. The strict regulation and interplay of all these pathways leads to the inhibition of differentiation on the one hand and on the other hand to the expression of the core transcriptional regulatory circuit, which is made up of OCT4, SOX2 and NANOG that ensure maintenance of pluripotency and self-renewal (Yeo and Ng, 2013). These three transcription factors are used as a quality-control of hESCs. OCT4, encoded by the *POU5F1* gene, is a homeodomain protein and plays a critical role in the establishment and maintenance of pluripotency. Precise regulation of OCT4 is crucial since even small alterations in its amount lead to differentiation (Niwa et al., 2000; Wang et al., 2012). Its synergistic action with NANOG, another homeodomain protein, and SOX2 ((Sex determining region Y)-box 2), is well described (see Yeo and Ng, 2013 for further references). These three transcription factors co-occupy more than 300 target genes (Boyer et al., 2005). Among others they target their own genes in autoregulatory loops, but they also repress differentiation genes.

1.2.2 Unique features of human ESCs

Apart from pluripotency and infinite self-renewal, ESCs possess additional unique characteristics that distinguish them from differentiated cells and enable them to protect themselves more efficiently against DNA damage to maintain genomic integrity of the stem cell-pool and give rise to normal progeny cells (reviewed by Nagaria et al., 2013). hESCs have a lower mutation frequency compared to differentiated cells (Cervantes et al., 2002) and are able to undergo cell death in a facilitated manner as a means to avoid mutations. For this reason, they express, for example, constitutively active BAX, which is rapidly and p53-dependently translocated to the mitochondria upon apoptotic stimuli to induce cytochrome c release and caspase activation leading to apoptosis (Dumitru et al., 2012). In contrast, BAX is present in an inactive conformation in somatic cells and must be activated prior to its translocation. Therefore, the induction of apoptosis is faster in hESCs.

hESCs originate from the blastocyst that developed under low oxygen tensions in the oviduct and uterus (Fischer and Bavister, 1993) and they proliferate well under hypoxic conditions (Ezashi et al., 2005) using anaerobic glycolysis (Varum et al., 2011). Consistent with this, hESCs have a low number of mitochondria with a rather immature phenotype. Thus, a lower amount of reactive oxygen species (ROS) can be found and, in addition, more antioxidant enzymes are produced (Saretzki et al., 2004). However, during differentiation both, mitochondria number and maturity level, increase (Cho et al., 2006; John et al., 2005).

The cell cycle of hESCs is much shorter than the one of proliferating somatic cells. This is attributable to a short G1 phase (Becker et al., 2006), during which hESCs are the most sensitive to differentiation signals (Pauklin and Vallier, 2013; Sela et al., 2012).

1.2.3 Response of ESCs to IR – state of the art

The response of murine and human ESCs to IR was intensively investigated in the past years using X- or γ-rays. Upon exposure, the first visible reaction of the ESCs is the formation of holes within and a decreased number and size of the colonies. This is attributable to apoptosis and cell death (Momcilovic et al., 2009; Rebuzzini et al., 2012; Wilson et al., 2010). In line with this, a dose- and radiation quality-dependent reduction in the clonogenic survival was described (Luft et al., 2014; Rebuzzini et al., 2012).

The most severe IR-induced cellular damages are those of the DNA and efficient mechanisms exist to allow their repair. A common DNA damage sensor in somatic cells, namely ATM, was found to be activated also in ESCs. It phosphorylates and thereby stabilizes the transducer proteins p53 and CHK2 (Momcilovic et al., 2009). Subsequently, cell cycle arrest occurs to ensure the repair of the IR-induced damage. ESCs are capable of inducing a transient dose-dependent cell cycle arrest at G2/M phase, but not at G1-phase (Filion et al., 2009; Luft et al., 2014; Rebuzzini et al., 2012). The higher the dose, the longer is the duration of the G2/M arrest. For mESCs, Rebuzzini and colleagues found it to last 48 h upon a 5 Gy γ-ray exposure, yet in another study, the arrest was no longer visible at 6 h after 2 Gy X-

rays (Luft et al., 2014). Momcilovic et al. (2009) reported that hESCs returned to cell cycle 16 h after exposure to 2 Gy γ-rays and that the G2/M arrest requires ATM, but is independent of p21. Even though p21 mRNA is increased upon DNA damage induction (Becker et al., 2007; Filion et al., 2009; Sokolov et al., 2015; Wilson et al., 2010), ESCs fail to accumulate p21 protein (Filion et al., 2009; Dolezalova et al., 2012). This is due to hESC-specific microRNAs that prevent its protein expression (Dolezalova et al., 2012), which might explain the lack of a G1-cell cycle-arrest in hESCs.

DNA double strand breaks (DSBs) are the most critical damage to cells and are repaired via two major pathways: The main repair pathway of DSBs in mammalian somatic cells is the Non-Homologous End-Joining (NHEJ) that operates in all cell cycle phases and is considered to be error-prone (Pannunzio et al., 2018). Homologous Recombination (HR) relies on the presence of sister chromatids as repair template and therefore, only takes place during late S and G2 phase and is error-free (San Filippo et al., 2008). mESCs predominantly repair DSBs via HR (Tichy et al., 2010). In contrast, hESCs utilize both, HR as well as a high-fidelity NHEJ and levels of proteins involved in both pathways are elevated enabling a more efficient repair compared to differentiated cells (Adams et al., 2010a, 2010b; Fan et al., 2011).

Whole-genome expression analyses by Sokolov et al. (2015) revealed that exposure to low dose IR leads to a time- and hESC line-dependent genomic response. At an early time point after exposure (2 h upon 0.05 Gy), only expression of *CDKN1A* (encoding p21) was increased in all tested cell lines, whereas all other differentially expressed genes were cell line-dependent. In contrast, a high dose (1 Gy) led to enhanced expression of multiple genes involved in p53 signaling, apoptosis and cell cycle arrest. At a late time point (16 h) after 1 Gy exposure, 16 genes were consistently upregulated, which are involved anti-apoptotic signaling and DNA damage/stress response, whereas upon low dose, no transcriptomic effects were detected.

Furthermore, it is well described that ESCs that survive an IR exposure maintain pluripotency even upon a relatively high 4 Gy-dose as evidenced by the expression of pluripotency markers (Luft et al., 2014; Momcilovic et al., 2009; Rebuzzini et al., 2012) and by teratoma formation in immuno-compromised mice (Wilson et al., 2010). In addition, differentiation markers were not found to be increased upon IR exposure (Sokolov et al., 2010,Wilson et al., 2010).

1.3 The mammalian heart – development, electrophysiology and radioresponse

The heart is the first functional organ during human development and its correct formation is crucial for the supply of the embryo with oxygen and nutrients. *In vitro* studies addressing the influence of noxae, like IR, on heart development contribute to the risk assessment for an *in utero* exposure.

1.3.1 Development of the mammalian heart

With the appearance of the primitive streak in the epiblast of the blastula, gastrulation starts and results in the formation of endo-, ecto- and mesoderm. The mesoderm, from which the mammalian

heart is formed, is further subdivided into the paraxial, intermediate and lateral plate mesoderm. Cells of the latter give rise to the first and second heart fields (SHF). The cells of the first heart fields (FHF) are lateral on both sides of the primitive streak and migrate to fuse at the midline forming the so called cardiac crescent (Fig. 1 A). This structure will give rise to the linear heart tube that starts to beat subsequently (week 4 of human development). The heart tube expands by cell proliferation and recruitment of additional cells originating from the SHF. It consists of multipotent cardiac progenitor cells with increased proliferation and delayed differentiation compared to the FHF cells. Subsequent looping and extensive growth give rise to the fetal heart, which displays well-defined chambers at day 32 of human development (Brade et al., 2013). Whereas the SHF cells give rise to the outflow tract, inflow region/atria and right ventricle, FHF cells contribute partially to the atrial myocardium and exclusively to the left ventricle (reviewed by Brade et al., 2013; Cyganek et al., 2013; Kelly et al., 2014; Fig. 1 B). Around week 7 of human gestation, the heart is fully septated and connected to the vascular system.

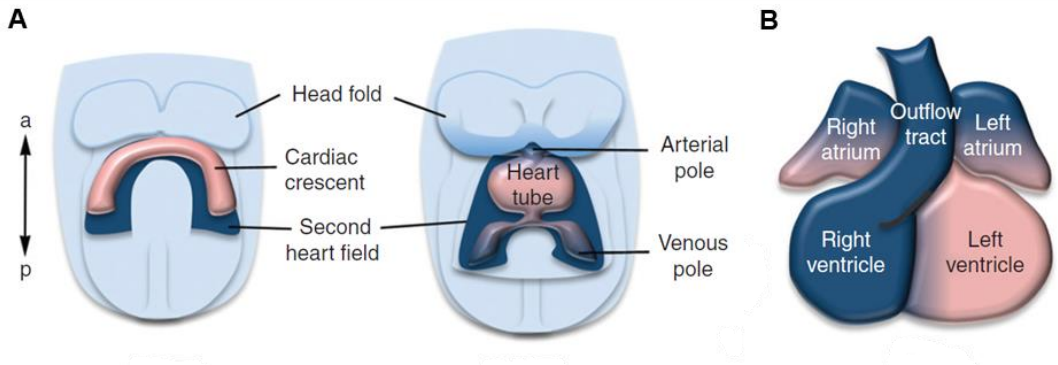

Fig. 1: Contribution of the first and second heart field to the developing mammalian heart. A) The cells of the FHF make up the cardiac crescent (pink). Whereas the cells of the FHF differentiate already at the crescent stage forming the linear heart tube, the cells of the SHF (blue) show delayed differentiation that starts upon their gradual migration into the linear heart tube. B) Contribution of the FHF and SHF cells to the components of the heart. Figure modified and reprinted from Kelly (2012) with permission from Elsevier.

All these developmental steps rely on the complex promoting and inhibiting signaling of multiple pathways. The tissues adjacent to the mesoderm, like endoderm, neurectoderm and the Node, secrete the respective signaling molecules. As described by Burridge et al. (2012) mesoderm induction starts with NODAL signaling in the epiblast, thereby maintaining BMP4 in the adjacent extraembryonic ectoderm. Secretion of BMP4 leads to the induction of canonical WNT signaling in the proximal epiblast via WNT3 (Burridge et al., 2012). Thereby, Brachyury and Eomesodermin are expressed (early primitive streak) and lead to the expression of the transcription factor MESP1, which is a key regulator of the differentiation of mesodermal cells into cardiac progenitor cells (Bondue et al., 2008). For this differentiation step, BMP, FGF, NODAL and Sonic Hedgehog (SHH) signaling are crucial (Wagner and Siddiqui, 2007). MESP1 directly or indirectly promotes expression of key cardiovascular

transcription factors like HAND2, NKX2.5 and GATA4 finally leading to the expression of cardiac structural proteins like MYH6, MYH7, TNNT2 and MLC2v (reviewed by Bondue and Blanpain, 2010).

Canonical WNT signaling plays a biphasic role during cardiac development: whereas it is crucial for mesoderm formation, it is inhibitory for cardiac specification after the formation of cardiac mesoderm (Naito et al., 2006). Therefore, canonical WNT signaling is rapidly downregulated by antagonists like Dickkopf-1 (DKK1) secreted by the surrounding tissues, but also MESP1 was shown to upregulate DKK1 expression (David et al., 2008). In addition, WNT11 was shown to inhibit canonical WNT signaling by caspase-mediated destabilization of β-catenin (Abdul-Ghani et al., 2011). In contrast to canonical WNT signaling, the non-canonical signaling mediated by WNT11 plays a supportive role in the cardiac specification phase (Mazzotta et al., 2016; Pandur et al., 2002a). Furthermore, BMP signaling is required for CM differentiation and the Serum Response Factor (SRF) regulates expression of microRNAs (miR-1 and miR-133) that lead to the withdrawal of the differentiating cells from the cell cycle (Evans et al., 2010).

During the heart tube stage, fundamental patterning events occur that determine chamber and non-chamber myocardium. The chamber specification results from the expression of transcriptional regulators, like IRX4, HAND1 and ANF (encoded by *NPPA*), and connexin proteins. In addition, T-box transcription factors play crucial roles at this step: Whereas TBX5 and TBX20 promote chamber specification, TBX2 and TBX3 inhibit them to maintain non-chamber properties (reviewed by Dunwoodie, 2007). A gradient expression of TBX5 is realized by retinoic acid signaling leading to its expression in atria and the left ventricle. It acts synergistically with NKX2.5 and GATA4 to activate expression of *NPPA* and *GJA5* (encoding connexin 40 expressed in fast-conducting tissue and together with connexin 43 in the working myocardium of the atria and ventricles). TBX3 suppresses chamber specification and leads to the expression of the pacemaker channel HCN4 in the cells that will give rise to the sinoatrial node (SAN).

Another crucial signaling pathway throughout the development of the heart is the NOTCH signaling. It is activated upon cell-cell contact via the interaction of a receptor (NOTCH1-4) with a transmembrane ligand (Jagged and Delta proteins; reviewed by Kopan, 2012) and contributes to cardiogenesis from as early as the cardiac crescent stage to cardiac valve development (reviewed by De la Pompa and Epstein, 2012). It was shown to interact with the non-canonical WNT signaling (Koyanagi et al., 2007). Conflicting data exist suggesting either a promoting or an inhibiting effect of NOTCH signaling on cardiogenesis (e.g. Jang et al., 2008; Koyanagi et al., 2007; Rones et al., 2000). However, there is evidence that active NOTCH signaling promotes proliferation of cardiac precursors by blocking differentiation (Cyganek et al., 2013; Schroeder et al., 2006).

1.3.2 Cardiac electrophysiology and excitation-contraction coupling

All tissues of the human body need to be supplied with oxygen and nutrients. This is realized by the contraction of the heart, which pumps the blood through the vessels and relies on electrical signals, i.e. ion currents. Cardiac action potentials (AP) arise from changes in the transmembrane electrical potential in CMs. The morphology of a typical cardiac AP is depicted in Fig. 2, however, depending on the localization within the heart, the morphology of the APs varies due to distinct ion channels and currents (electrical heterogeneity; Liu et al., 2016). For example, only the atria possess the ultra-rapid outward K^+ current generated by $K_v1.5$ (encoded by *KCNA5*), acetylcholine-activated K^+ current, T-type Ca^{2+} current and Ca^{2+}-activated K^+ current.

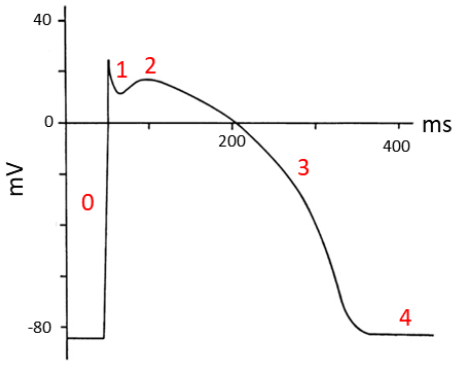

Fig. 2: Morphology of a typical ventricular action potential. The cardiac AP can be divided into five phases: 0 = upstroke, 1 = early repolarization, 2 = plateau, 3 = late repolarization, 4 = diastolic phase. Figure modified from Beeler and Reuter (1977).

As reviewed by Liu et al. (2016) the AP consists of five phases (Fig. 2). Phase 4 is the diastolic phase representing the resting membrane potential. During this phase, K^+ channel activity dominates via the inward rectifier current (I_{K1}). Phase 0 is initiated by depolarization arising from electric coupling between adjacent CMs via gap junctions and is characterized by rapid influx of Na^+ ions via voltage-gated Na^+ channels (Na_v). The membrane potential moves toward the equilibrium potential of Na^+ (around + 50 mV). However, the maximal voltage reached in ventricular and atrial CM is between + 20 and 40 mV. Upon closing of the Na_v-channels, depolarizing Ca^{2+} currents (especially L-type Ca^{2+} currents) as well as repolarizing currents via K_v channels, Ca^{2+}-activated Cl^- channels and the Na^+/Ca^{2+} exchanger (NCX) emerge in phase 1. The NCX operates in the reverse mode during this phase moving three Na^+ ions outward for one Ca^{2+} ion inward. The elevated intracellular level of Ca^{2+} leads to the opening of the RyR2 channels of the sarcoplasmic reticulum (SR), thereby inducing Ca^{2+} release from the SR (Fig. 3 A) leading to the contraction of the CM via excitation-contraction coupling (Fig. 3 B). CM are made up of sarcomeres consisting of thin (actin) and thick (myosin) filaments. Actin filaments are surrounded by tropomyosin, which is associated with troponin T, C and I. Myosin molecules consist of a head, neck and tail domain. Upon the drastically increased intracellular Ca^{2+} concentration, Ca^{2+} ions bind to troponin C leading to a conformational change of the tropomyosin.

Thereby actin is exposed and the myosin head can bind. Via ATP hydrolysis, the myosin head moves and the actin slides across the myosin filament, thereby shortening the muscle (power stroke; contraction). Subsequently, the myosin detaches from the actin. The contraction lasts until the end of phase 2 (plateau). For cardiac relaxation, the intracellular Ca^{2+} concentration is decreased via the SR Ca^{2+}-ATPase (SERCA), which pumps the Ca^{2+} back into the SR, and the NCX as well as Ca^{2+}-ATPases located in the CM membrane to move the Ca^{2+} out of the cell (Fig. 3 B).

Phase 3 is initiated when the net outward K^+ current exceeds the depolarizing currents $I_{Ca,L}$ and I_{NCX}. In this phase, I_{Kr} is the most important current.

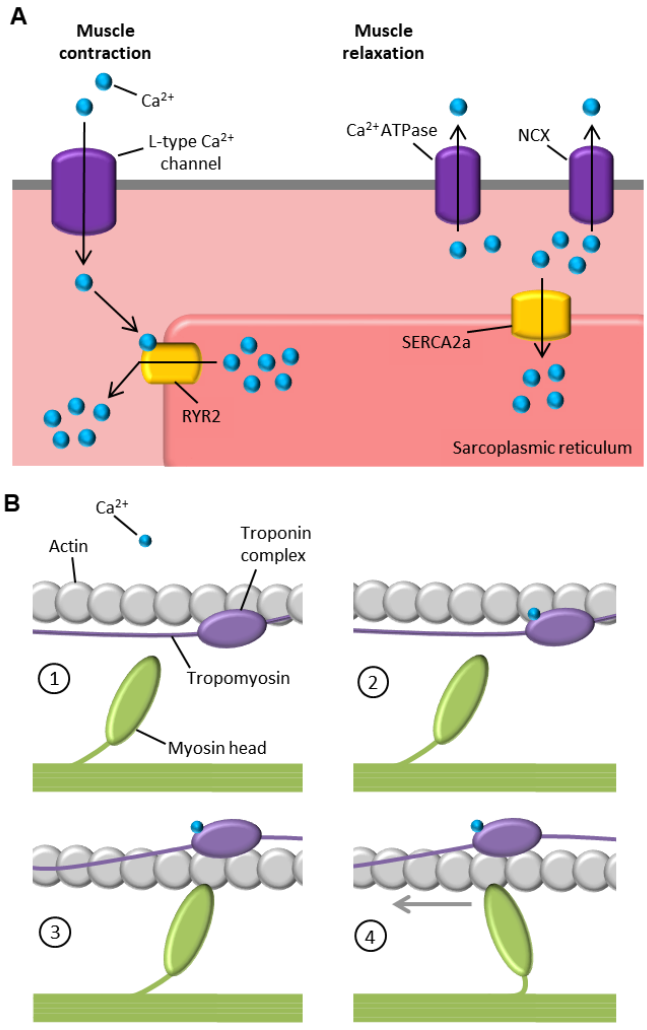

Fig. 3: Mechanism of muscle contraction and relaxation. A) Ca^{2+} ions enter the cell and mediate the Ca^{2+}-induced Ca^{2+}-release from the SR leading to muscle contraction. During muscle relaxation, intracellular Ca^{2+} levels are actively decreased via SERCA2a, NCX and Ca^{2+} ATPases. Figure modified from Shenoy and Rockman (2011). B) The cardiac muscle consists of actin and myosin filaments. Actin is surrounded by tropomyosin, which is associated to the troponin complex consisting of troponin T, C and I (1). When Ca^{2+} ions bind to troponin C (2), the tropomyosin exposes actin, to which the myosin heads can bind (3). Using ATP, the myosin head pulls at the actin, which slides across the myosin filament leading to muscle shortening (4, power stroke; contraction). Figure modified according to Alberts et al. (2009) and Seidman and Seidman (2001).

The cardiac AP is initially generated in the SAN CM driving the depolarization of the adjacent CM via gap junctions consisting of connexin proteins. The AP of the SAN is different to those of the atria and ventricles. There is no stable resting potential in phase 4, instead the SAN AP is characterized by a slow diastolic depolarization phase (Baruscotti et al., 2005). When the maximum diastolic potential (MDP) is reached (between -70 and -55 mV), slow spontaneous depolarization occurs. At around -50 mV, the funny current (I_f, also called "pacemaker current") is provided by the Hyperpolarization-activated cyclic nucleotide-gated (HCN) channels. HCN4 is the major isoform in the SAN (Stieber et al., 2003). The opening potential of these channels depends on the intracellular cAMP-level, which is controlled by β-adrenergic receptors. HCN channels conduct Na^+ and K^+ and their main function is the generation of the sinus rhythm via the SAN AP.

1.3.3 The development of the heart can be recapitulated in vitro *using ESCs*

Using specific protocols, hESCs can be differentiated into all cells of the three germ layers. To generate hESC-derived CM, the distinct stages of the heart development are recapitulated *in vitro* by regulating the same signaling pathways as *in vivo* and can be monitored via marker expression on the mRNA and protein level (Boheler et al., 2002; Fig. 4 A). Cardiac differentiation protocols start with the development of mesodermal cells via the enhancement of canonical WNT signaling. Many protocols additionally regulate BMP and Activin A signaling for the initial step. According to Singh et al. (2012), Activin A leads to the expression of NANOG via SMAD2/3 when PI3K/AKT activity is high and canonical WNT signaling is absent. However, when PI3K/AKT signaling is low and canonical WNT signaling is active, Activin A/SMAD2/3 signaling leads to the expression differentiation-associated genes, like the mesendodermal markers Eomesodermin (EOMES) and MIXL1 (Singh et al., 2012).

Mesodermal cells are *Brachyury* (*T*) positive leading to the expression of *MESP1* when cardiac mesoderm is formed. They represent the early primitive streak and gastrulation stage. Subsequently, WNT signaling is downregulated by addition of specific inhibitors. Depending on the inhibitor used, either canonical and non-canonical or only canonical WNT signaling can be blocked (Chen et al., 2009; Huang et al., 2009). Based on detailed WNT signaling studies in hESCs, Mazzotta et al. (2016) proposed a model for the contributions of the multiple WNT pathways at distinct stages of cardiac differentiation (Fig. 4 B).

Canonical WNT signaling is mediated via accumulation of β-catenin (reviewed by MacDonald et al., 2009). In the absence of WNT ligands, β-catenin is phosphorylated by the destruction complex, which includes the protein kinases GSK3 and CK1α. Subsequently, β-catenin is ubiquitylated and thus targeted for degradation. Thereby, target gene expression is repressed (MacDonald et al., 2009). In contrast, when WNT proteins bind to the Frizzled (FZD) family receptors associated with LRP5/6, the subsequent recruitment of GSK3 and CK1α leads to the phosphorylation of LRP5/6. The destruction complex is disrupted, allowing β-catenin to accumulate in the cytoplasm and translocate into the

nucleus where it associates with LEF/TCF. The transcriptional repressors are removed from the target genes and their transcription takes place (MacDonald et al., 2009). This signaling pathway promotes differentiation of hESCs in a concentration-dependent manner (Blauwkamp et al., 2012; Davidson et al., 2012). In contrast, it is not required for pluripotency maintenance (Singh et al., 2012) and it was shown to be repressed by OCT4 (Davidson et al., 2012) and SOX2 (Zhou et al., 2016) in hESCs.

Non-canonical WNT signaling pathways do not involve β-catenin. An overview of their molecular mechanisms is given by Semenov et al. (2007). WNT/JNK signaling operates via the ROR2 receptor and the activation of PI3K and JNK leading to target gene expression. According to Mazzotta et al. (2016) it is required for the formation of MESP1-positive cardiogenic mesoderm. WNT/Ca^{2+} signaling is promoted via the FZD4/6 receptor (Mazzotta et al., 2016) and leads to an increase of intracellular Ca^{2+} levels. Both non-canonical pathways antagonize the canonical WNT/β-catenin signaling and are required for gastrulation (Semenov et al., 2007). In addition, WNT/Ca^{2+} signaling is required for CM development from cardiac progenitors (Mazzotta et al., 2016).

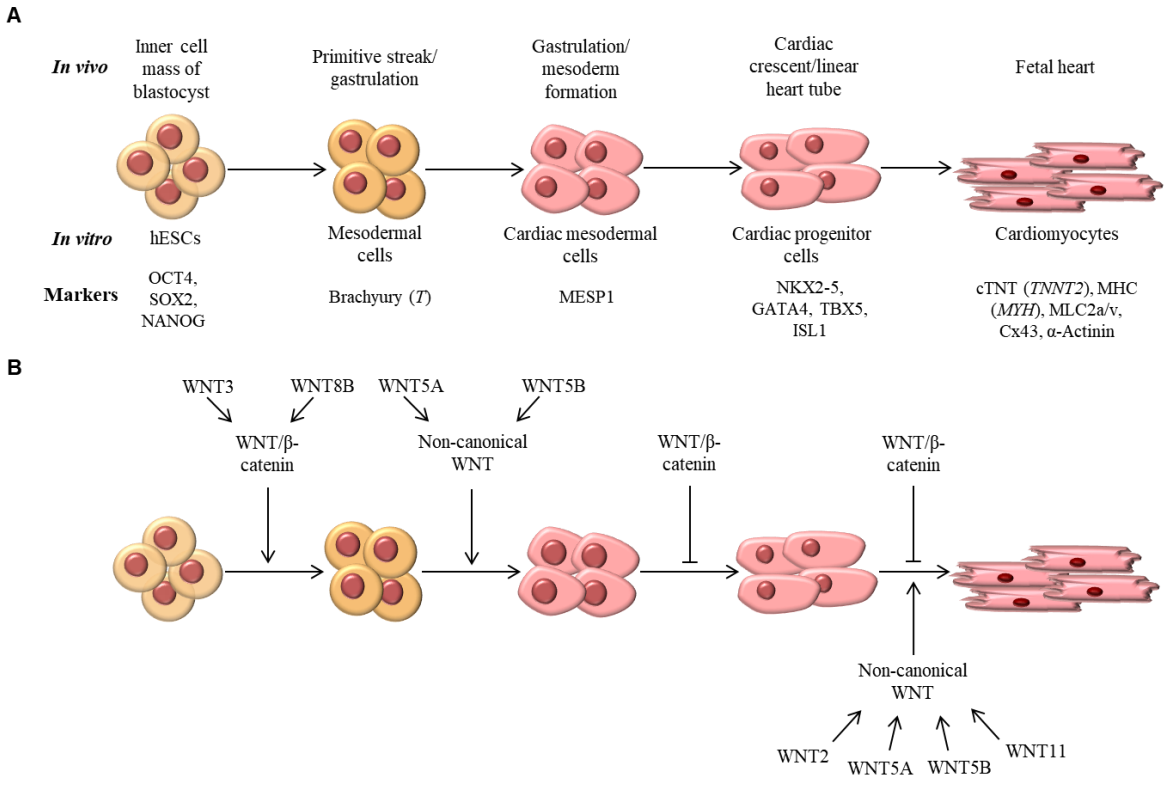

Fig. 4: Cardiac differentiation. A) Each stage of the *in vivo* heart development can be recapitulated *in vitro* with the directed cardiac differentiation of hESCs. B) Canonical and non-canonical WNT signaling during cardiac differentiation. Figure modified according to Mazzotta et al. (2016).

Following *MESP1* expression, cardiac precursor genes, like *NKX2.5*, *GATA4* and *TBX5* are expressed. The developing CM assemble in cardiac clusters, which start to beat spontaneously around day 8 of differentiation. This is accompanied by the expression of cardiac markers like cardiac troponin T (cTNT, encoded by *TNNT2*) and cardiac specific myosins (e.g. *MYH6/7*, *MLC2a*). Depending on the

protocol, atrial (*NPPA*) or ventricular (*IRX4*, *MLC2v*) markers may emerge with ongoing differentiation. There is an increasing number of protocols that allow the generation of the specific cardiac cell types, e.g. atrial differentiation is promoted by retinoic acid and ventricular differentiation is enhanced by blocking retinoic acid signaling (Zhang et al., 2011). However, in the present study, heterogeneous cardiac cultures containing all cardiac cell types as well as non-cardiac cells are desired to mimic the heart as an organ consisting of various cell types as close as possible.

A major problem of hESC-derived CM is, however, their immature morphological and functional properties (Yang et al., 2014). In recent years, several approaches that aim at the maturation of the *in vitro*-generated CM were developed. Kolanowski et al. (2017) provided a comprehensive overview of the current knowledge on CM maturation. Without specific maturation protocols, hESC-derived CM are more similar to early fetal than to adult ones.

1.3.4 Effect of ionizing radiation on the heart and cardiac development – state of the art

It is known that radiation exposure of the heart to high doses leads to cardiac injury. Acute or early cardiac effects are rare, since the heart is known to respond late, i.e. years or decades after the exposure (Boerma et al., 2016). For example, upon radiotherapy of breast cancer, there is an increased risk of mortality due to cardiovascular diseases especially if the women were treated for left-sided breast cancer (Bouillon et al., 2011). Recent reviews on radiation-induced cardiovascular disease are provided by Boerma et al. (2016) and Puukila et al. (2017). Typical cardiac effects comprise chronic inflammation, oxidative stress, damage to microvasculature, ischemia, accelerated atherosclerosis and fibrosis, but also injuries to the cardiac valves are described. Epidemiological studies of atomic bomb survivors who were exposed during childhood or adolescence showed an elevated risk for heart diseases like hypertension, stroke and myocardial infarction also at doses below 1 Gy (Shimizu et al., 2010; Yamada et al., 2004). In addition, increased blood levels of inflammatory cytokines were found (Hayashi et al., 2003).

Animal studies addressing cardiac effects of radiotherapy found that cardiac injury rather depends on the dose per fraction than on the total dose. In rat and mouse hearts, common IR-induced effects were damages to the endothelium, fibrosis and hypertension (Baker et al., 2009; Boerma et al., 2004). In addition, elevated levels of connexin 43 (Cx43) mRNA and protein were detected leading to increased intercellular communication probably to enhance transmission of radiation-induced signals (Amino et al., 2006 and references within). Total body irradiation of postnatal and adult mice leads to an altered cardiac transcriptome and proteome and 0.5 Gy γ-rays or more resulted in reduced expression of cytoskeletal proteins (e.g. actin, myosin) indicating degenerating heart structure (Bakshi et al., 2013; Coleman et al., 2015). Cardioprotective mechanisms were elevated before clinical symptoms in cardiac function were observed according to Coleman et al. (2015). Similarly, Seemann et al. (2012) reported that cardiac function of murine hearts irradiated with high X-ray doses remained normal

despite vascular changes suggesting compensatory mechanisms, which, however, failed after prolonged time. In contrast, whole body proton (0.5 Gy) and iron ion (0.15 Gy) irradiation of adult mice led to impaired cardiac function up to 10 months post irradiation with increased cardiac fibrosis, altered cardiac calcium homeostasis and activation of cardiac hypertrophy signaling (Yan et al., 2014). Primary chicken CM irradiated with 0.5 to 7 Gy X-rays showed dose-dependently increased beat rates, however, upon 0.5 and 1 Gy these alterations were minor (Frieß et al., 2015). When such CM were irradiated with heavy ions, a high functional robustness as well as a low apoptotic rate was observed (Heselich et al., 2018). Only high doses (2 and 7 Gy) of titanium ions were shown to impair their beat rates.

Data on the impact of a radiation exposure on the fetal heart are scarce. Atomic bomb survivors that were exposed *in utero* showed a dose-dependent cancer incidence and the most prominent non-cancer effects were microcephaly and mental retardation (Kodama et al., 1996). No significant association between an *in utero* exposure and non-fatal cardiovascular diseases (stroke and myocardial infarction) or hypertension has been reported (Tatsukawa et al., 2008).
Although ESC maintain their pluripotent potential upon IR exposure, whole-genome transcription studies indicated that gene expression of several signaling pathways is altered (Sokolov et al., 2015, 2011; Wilson et al., 2010) and thus, their differentiation capability may be affected. For example, a downregulation of *ACVR1B* and *ACVR2A* expression in hESCs exposed to 1 Gy X-rays was reported (Luft et al., 2017). Since these genes encode activin receptors, not only differentiation into definitive endoderm as reported by the authors, but also cardiac differentiation could be impaired (compare section 1.3.3).
Whether specifically cardiac differentiation is affected by an IR exposure was analyzed in only three studies up to date. Two of them used mESCs and the same differentiation technique demonstrating an impaired cardiac differentiation (Helm et al., 2016; Rebuzzini et al., 2013). Whereas Rebuzzini and coworkers found an increased expression of several cardiac marker genes (*Nkx2.5*, *Gata4*, *Alpk3* and *Tnnc1)* upon an exposure to 5 Gy γ-rays, Helm and colleagues described a rather decreased expression (*Tnnt2*, *Myh7*, *Myl4*, *Hcn4*) with C-ions being more effective than X-rays. Additionally, decreased beat rates and contraction force were described and correlated to a decreased density of Cx43 (Rebuzzini et al., 2013). Both studies show that cardiac differentiation of mESCs is affected by IR exposure, which may markedly impair the complex signaling networks and correct development of the developing fetus. Still, the effect of an IR exposure on human cardiac development was only investigated in one study up to date using human induced pluripotent stem cells (Baljinnyam et al., 2017). However, the culture conditions are artificial and the observed effects are questionable. For example, ROCK inhibitor is used for a prolonged time to enhance cell attachment and, furthermore, low dose α-particles were used leading to a very small fraction of cells that are hit by a particle (i.e. only 3 % of the cell population).

1.4 Objective

The medical use of X-rays for diagnostics in pregnant patients is increasing, therefore, a detailed risk assessment for the developing embryo is needed. Even though many studies showed that ESCs maintain pluripotency upon IR exposure, they also revealed that several signaling pathways are affected as indicated by altered gene expressions (see section 1.2.3). These alterations could lead to an impaired subsequent differentiation and organ formation. During human development, the heart is the first functional organ and it meets the metabolic demands of the developing embryo. For this reason, its correct development is crucial to ensure growth and health of the fetus. Although it is known that there is an association between IR exposure of the heart and an increased risk for cardiovascular diseases, the impact of an *in utero* exposure on the early heart and its further development is not clear yet. Studies directly addressing the impact of an IR exposure on cardiac development are scarce. Two of these reported altered gene expressions in cardiac cultures derived from mESCs and impaired CM functionality (Helm et al., 2016; Rebuzzini et al., 2013). Since these results are difficult to extrapolate to human heart development due to species-dependent differences, the objective of this study is to characterize the influence of an X-ray exposure on cardiac differentiation capability of hESCs. Upon optimization of the cardiac differentiation conditions, the effect of multiple X-ray doses was investigated via marker gene and protein expression as well as functional assessments of the beating CM. For this, videos were recorded and beat rates as well as beat variability were analyzed with a recently developed software called cardiac Beat Rate Analyzer (cBRA; Nitsch et al., 2018). With the same method, the functionality of β-adrenergic receptors and HCN channels was tested using isoproterenol and ivabradine. Furthermore, pathway analyses based on qRT-PCR arrays and literature research were performed to shed light on possible mechanisms underlying IR-induced effects.

2 Material and Methods

In the following section, methods applied in this study are described. Kits, media, supplements and chemicals are listed separately in the appendix (App. Tables 1 - 3) including their manufacturers and ordering numbers. Furthermore, manufacturers of devices and softwares are also listed in the appendix (App. Tables 4 and 5).

2.1 Cell lines and culture conditions

Mouse embryonic fibroblasts (PMEF-NL) were obtained from Millipore, Germany, in passage 3 and used as feeder layer for the hESC line H9. The work with hESCs was approved by the Robert-Koch-Institute (registry number: 1710-79-1-4-69) in concordance with the German stem cell law (§ 11 *StZG)*. Two hESC lines obtained from the WiCell Research Institute, Wisconsin were used: the wildtype cell line WA09 (H9) and the transgenic cell line H9-hTnnTZ-pGZ-D2 (cTNT-H9). The wildtype H9 cells were delivered at passage 26 and co-cultured with mitotically inactivated mouse embryonic fibroblast (MEF) feeder cells in H9-medium (see Table 1) and supplemented with 10 ng/ml FGF2. For experiments, H9 cells from passage 37 to 74 were used.

Table 1: Composition of H9-medium.

Component	**Final concentration**
Knockout DMEM	
+ Knockout Serum Replacer	20 %
+ L-Glutamine	1 mM
+ Non-Essential Amino Acids	1x
+ β-Mercaptoethanol	100 µM
+ Penicillin/Streptomycin	50 U/ml Pen., 50 µg/ml Strep.

The transgenic cTNT-H9 cell line was generated at the University of Wisconsin by Dr. Timothy Kamp's lab (Wrighton et al., 2014). In these cells, GFP is under the control of the cardiac troponin T-promoter making this cell line suitable to monitor cardiac differentiation. They were obtained at passage 37 and cultured feeder-independently on Laminin-521-coated petri dishes in mTeSR1-medium (see Table 2). For experiments, cTNT-H9 cells from passage 57 to 82 were used. All hESCs were cultured at 37 °C with ambient oxygen and 5 % CO_2.

Table 2: Composition of mTeSR1-medium.

Component	**Final concentration**
mTeSR1 Basal Medium	
+ 5x mTeSR1-supplement	1 x
+ Penicillin/Streptomycin	50 U/ml Pen., 50 µg/ml Strep.

2.1.1 Mouse Embryonic Fibroblasts (MEFs) expansion and storage

PMEF-NL were obtained from Millipore in passage 3 and propagated until passage 6, in which they were mitotically inactivated to be used as feeder cells. Thawed MEFs were transferred into MEF-medium (DMEM + 9 % FCS + 1 % Penicillin/Streptomycin) and centrifuged for 5 min at 300 x g. The pellet was solved and 1.5 - 2.5 x 10^6 cells were seeded per T75 culture flask in a total of 15 ml MEF-medium. Before reaching confluency, MEFs were passaged as follows: medium was aspirated, cells were washed with $PBS^{+/+}$ and incubated with trypsin for 5 min at 37 °C. After detachment, they were resuspended in MEF-medium, transferred into a 50 ml reaction tube and centrifuged at 200 x g for 5 min. The pellet was resuspended and 2.5 x 10^6 cells were seeded per T75 culture flask in a total volume of 15 ml MEF-medium.

At passage 6, MEFs were mitotically inactivated. For this purpose, they were harvested as described before, collected in a T25 culture flask on ice and exposed to 60 Gy X-rays. Afterwards, the cells were transferred into a 50 ml reaction tube and centrifuged. The pellet was solved in freezing medium (90 % FCS + 10 % DMSO). Aliquots of either 3 or 6 x 10^6 cells in 1.8 ml were frozen over night at -80 °C and then transferred to liquid nitrogen.

2.1.2 Preparation of MEF conditioned medium

MEF conditioned medium was used for the immediate culture of H9 cells upon thawing. For its preparation, 4.5 x 10^6 MEFs were seeded per T75 flask and cultured in H9-medium including 10 ng/ml FGF2. The medium was changed after 24 h and subsequently, the conditioned medium was collected for four days, filtered through a 20 µm pore filter and stored at -20 °C.

2.1.3 H9 cells – thawing

H9 cells were cultured upon delivery and frozen at passage 32 in freezing medium and liquid nitrogen. Since H9 cells were grown on mitotically inactivated MEFs, petri dishes needed to be prepared one day before the H9 cells were thawed. For this purpose, Ø 6 cm petri dishes (21 cm^2) were coated with 0.1 % gelatin in PBS by incubating for at least 1 h at 37 °C. The gelatin solution was aspirated, 2 ml MEF-medium were added and the dishes were returned to the incubator. Mitotically inactivated MEFs (see section 2.1.1) were thawed in the water bath until only a small piece of frozen cells remained. The cells were transferred to 10 ml cold MEF-medium and centrifuged for 5 min at 200 x g. The pellet was resuspended in prewarmed (37 °C) MEF-medium, cells were counted with an automatic cell counter and seeded at a density of 0.24 x 10^5 cells/cm^2. On the next day, the medium was aspirated, cells were washed with $PBS^{+/+}$ and incubated for at least 1 h in conditioned medium, which was supplied with 10 ng/ml FGF2. Then the feeder layer was ready for use.

H9 cells were thawed in a water bath until only a small frozen piece remained, transferred into cold H9-medium and centrifuged for 8 min at 300 x g. The pellet was carefully resuspended in conditioned medium without disrupting small cell clumps and seeded onto the MEF feeder cells. After 24 h,

medium was switched to H9-medium including 10 ng/ml FGF2. Subsequently, medium change was performed every day.

2.1.4 Manual passage of the H9 cells

For routine culture, H9 cells were passaged manually once a week. For this, petri dishes containing mitotically inactivated MEF were prepared as described before. One hour before passage of the H9 cells, the MEF containing petri dishes were washed with $PBS^{+/+}$ and H9-medium was added. To avoid daily medium change, 8 µl/ml (= 10 ng/ml) StemBeads® FGF2 were added to the H9-medium supplying the cells with a steady release of FGF2 for four days.

Colonies with undifferentiated morphology were chosen for propagation (Fig. 5 A, red arrow), while differentiated ones (Fig. 5 B, blue arrows) were excluded. The selected colonies were dissected with a scalpel (Fig. 5 C) at a microscope with 100 x magnification under an open laminar flow cabinet (ENVAIReco) and transferred to the prepared petri dishes. After four days, daily medium change with H9-medium including 10 ng/ml non-beads-coupled FGF2 was performed.

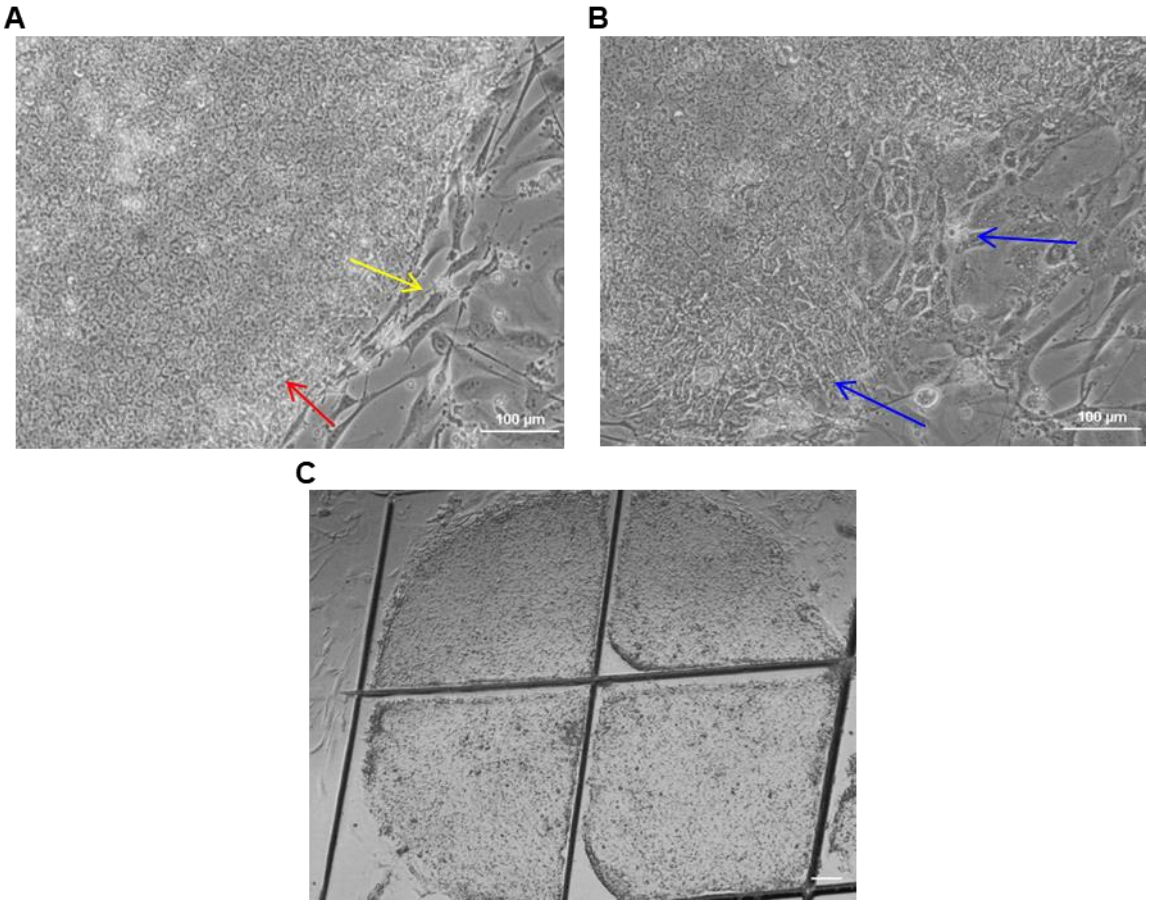

Fig. 5: Manual passage of H9 cells. A) Undifferentiated H9 colonies (red arrow) grown on MEF feeder cells (yellow arrow) were chosen for passage based on their morphology, whereas B) colonies containing differentiated cells (blue arrows) were excluded. C) Dissection of selected colonies into squares with a scalpel, followed by their transfer into a new petri dish, which was preseeded with MEF feeders. After 7 days in culture, manual passage was repeated. Scale bars: 100 µm.

2.1.5 Passage of H9 cells with the non-enzymatic passaging reagent ReleSR™

For radiation experiments, H9 cells were passaged with ReleSR™, a non-enzymatic passaging reagent from STEMCELL Technologies that preferentially detaches pluripotent stem cells from the culture dish. Thereby, the yield of H9 cells was enhanced and the effort of manual passaging was reduced. Briefly, the medium was aspirated and cells were rinsed with 200 µl ReleSR™. It was aspirated completely and the cells were incubated for 2 - 4 min at 37 °C. After 2 min, detachment of the pluripotent cells was controlled at the microscope. To stop the reaction, the cells were rinsed with H9-medium and subsequently split 1:3. Cells were exposed four days after passaging (section 2.4).

2.1.6 H9-hTnnTZ-pGZ-D2 human embryonic stem cells (cTNT-H9)

cTNT-H9 cells were thawed in a 37 °C water bath until only a small piece of frozen cells remained, transferred into H9-medium and centrifuged for 5 min at 200 x g. The pellet was resuspended carefully in mTeSR1-medium (see Table 2) and distributed to four Laminin-coated wells (10 µg/ml Laminin-521) of a Nunc™ 6-well-plate (Thermo Fisher Scientific). Medium change was performed every day. Upon propagation, cTNT-H9 cells were frozen at passage 54 in freezing medium over night at -80 °C and then transferred to liquid nitrogen.

cTNT-H9 cells were subcultured using the ReleSR™-method (compare section 2.1.5) to ensure that only undifferentiated cells were passaged (Fig. 6 A, red arrow). After aspiration of the reagent, cells were incubated for 2 min at 37 °C. When the pluripotent cells detached (Fig. 6 B, red arrows), the reaction was stopped by addition of prewarmed mTeSR1-medium. Split ratios between 1:3 and 1:15 were used depending on how many cells detached. Medium was changed every day. Upon recovery from thawing, the cells were cultured routinely on 5 µg/ml Laminin-521.

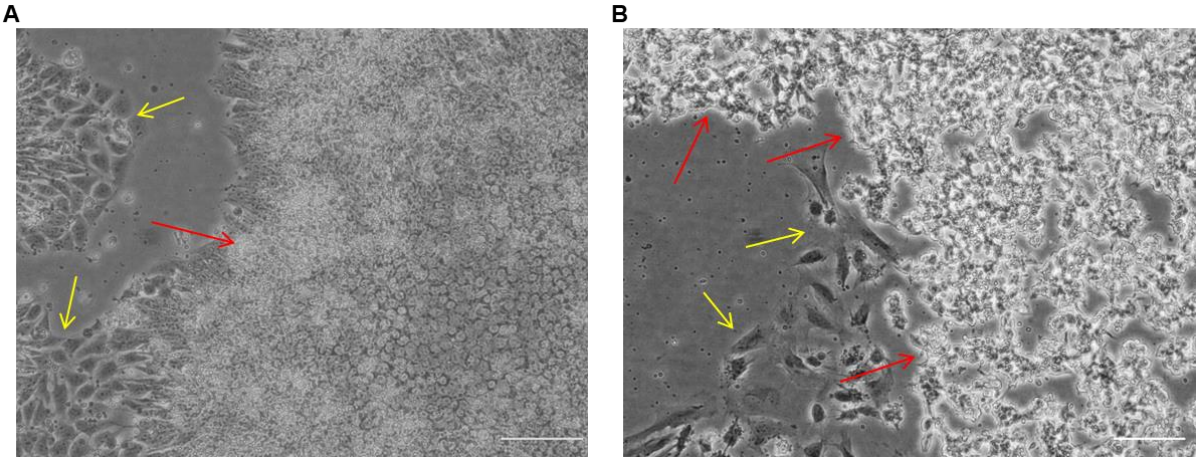

Fig. 6: Passage of cTNT-H9 cells using the ReleSR™-method. A) During culture in mTeSR1-medium on Laminin-521-coated petri dishes, some cTNT-H9 cells started to differentiate spontaneously (yellow arrows). To ensure that only undifferentiated, pluripotent cells (red arrow) were passaged, the ReleSR™-method was applied. B) ReleSR™ only detaches pluripotent stem cells (bright cells, red arrows), whereas differentiated cells (yellow arrows) stay attached to the surface of the culture dish. Scale bars: 100 µm.

2.2 Cytogenetic analyses of cTNT-H9 cells

Since genomic stability of hESCs is influenced by the method of passaging, ReleSR™-passaged cTNT-H9 cells were analyzed via multicolor Fluorescence *in situ* hybridization (mFISH) for chromosomal aberrations at various passages. To accumulate the cells in metaphase, 0.1 µg/ml colcemide (stock concentration: 10 µg/ml) was added 2 h before harvest. Subsequently, the medium was collected in a 15 ml reaction tube and cells were incubated with ReleSR™ for 2 min at 37 °C. Detaching cells were collected and transferred to the reaction tube. The cell suspension was repeatedly pipetted up and down to obtain single cells and subsequently, centrifuged for 5 min at 200 x g. The supernatant was discarded and the pellet was solved in prewarmed 0.075 M KCl (ad 10 ml) and incubated for 8 min at 37 °C followed by 8 min centrifugation at 200 x g. Fixative solution (methanol:acetic acid 3:1) was added to the pellet dropwise (ad 10 ml). The suspension was centrifuged for 10 min at 300 x g. Afterwards, the pellet was resuspended in 10 ml fixative, incubated for 30 min at room temperature (RT) and again centrifuged (10 min, 300 x g). The supernatant was removed, the pellet was resuspended in fixative (200 - 400 µl) and subsequently, the cell suspension was dropped onto wet microscope slides. The spreads were air dried and finally hybridized with the 24xCyte Human Multicolor FISH Probe Kit according to the manufacturer's protocol. Images of the metaphase spreads were taken with an Axio Imager Z2 microscope and Metafer 4 software. Their analysis was performed with the ISIS Software.

2.3 Cardiac differentiation of hESCs

Two protocols for directed cardiac differentiation were compared: the GiWi (GSK3-inhibitor, WNT-inhibitor)-protocol published by Lian et al. (2013a; Lian protocol) and an enhanced protocol published by Kadari et al. (2015; Kadari protocol). For both, the hESCs were seeded on Matrigel® at high density and the same basal medium is used. However, according to Kadari et al., ascorbic acid is additionally added and thus, present during the entire differentiation process (see Table 3). The factors used and the exact time table of the two protocols is depicted in Fig. 7. For their comparison, H9 cells were seeded four days before initiation of differentiation (d-4) on Matrigel®-coated (42 µg/cm²) 6-well-plates (Sarstedt), Ø 6cm or Ø 3.5 cm (8.8 cm²) Nunc™-petri dishes at a density of 0.3×10^6 cells/cm². For the first 24 h, 5 µM Y-27632 ROCK inhibitor was added to prevent apoptosis and help single cells to attach. Until initiation of differentiation (d0), the cells were cultured in mTeSR1-medium, which was changed every day.

Table 3: Composition of the basal medium for cardiac differentiation depending on the protocol.

Lian protocol		Kadari protocol	
Component	Final concentration	Component	Final concentration
RPMI-1640 (w. stable glutamine)		RPMI-1640 (w. stable glutamine)	
+ B-27 minus insulin	1 x	+ B-27 minus insulin	1 x
+ Penicillin/Streptomycin	0.5 %	+ Ascorbic acid	50 µg/ml
		+ Penicillin/Streptomycin	0.5 %

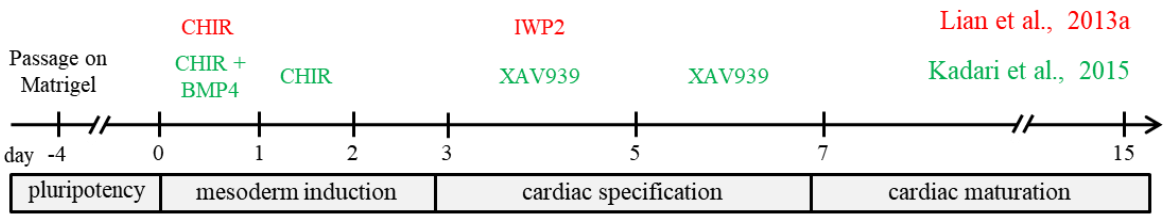

Fig. 7: Directed cardiac differentiation protocols. CHIR99021 is used by Lian et al. (2013a) to initiate cardiac differentiation and IWP2 from day 3 to day 5 to promote cardiac specification. In contrast, Kadari et al. (2015) additionally used BMP4 in the first 24 h and addition of CHIR99021 was prolonged. Instead of IWP2, XAV939 was used from day 3 to day 7. Starting from day 7, medium was changed every two to three days.

2.4 X-ray irradiation

X-ray exposure was carried out at an Isovolt DS1 X-ray tube with 250 kV and 16 mA at RT. The dose was measured with a SN4-dosimeter, the dose rate was approximately 1 Gy/min. cTNT-H9 cells were irradiated with either 0.1, 1 or 2 Gy and three days later, they were seeded on Geltrex® (0.12 - 0.18 mg/ml protein)-coated culture plates. Controls were sham-irradiated. Seven days after irradiation, cardiac differentiation was initiated (Fig. 8 a).

In another setup, differentiating CM derived from cTNT-H9 cells were irradiated at day 5 or 8 of differentiation with 1 Gy (Fig. 8 b).

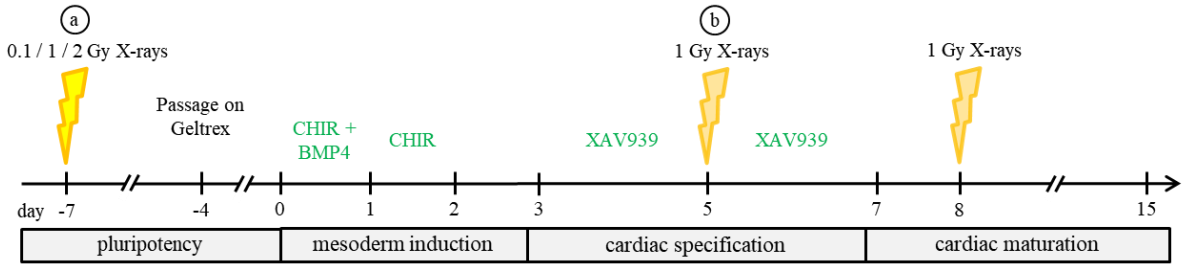

Fig. 8: Setup of X-ray irradiation experiments. (a) Pluripotent cTNT-H9 cells were irradiated with 0.1, 1 or 2 Gy X-rays. Three days later, they were seeded on Geltrex®-coated culture plates and seven days after irradiation (day 0), cardiac differentiation according to Kadari et al. (2015) was initiated. (b) In another setup, differentiating cTNT-H9 cells were irradiated at day 5 or at day 8 with 1 Gy X-rays.

2.5 Quantification of cell death upon X-ray irradiation

To compare the apoptotic rate of wildtype H9 and cTNT-H9 cells, both cell lines were passaged with the ReleSR™-method and cultured feeder-free on Laminin-coated Ø 3.5 cm Nunc™-petri dishes in mTeSR1-medium. Using the CellEvent™ Caspase-3/7 Green Flow Cytometry Assay Kit, living (instead of fixed) cells are required. For this reason, cells were irradiated with 1 Gy after 4, 5 and 6 days of culture on Laminin-coated dishes to quantify the apoptotic and necrotic fraction at all time points (72, 48 and 24 h after irradiation, respectively) at the same day (see Fig. 9). Medium was changed directly after exposure and then every 24 h.

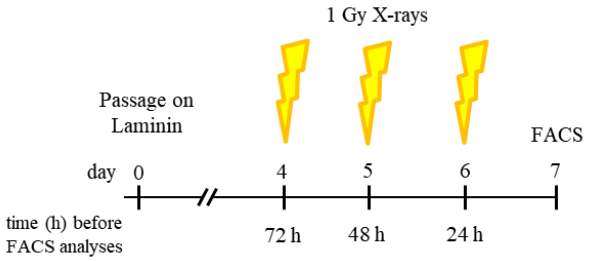

Fig. 9: Quantification of the apoptotic and necrotic fraction at several time points after X-ray exposure of hESCs. Cells were seeded on Laminin and after 4, 5 or 6 days, they were irradiated with 1 Gy X-rays. At day 7 after passage, they were harvested for FACS analysis to determine the apoptotic and necrotic fraction at the indicated time points.

For cell harvest, the medium was passed through a 40 µm cell-strainer (Corning) and collected in a 15 ml reaction tube for each sample. The cells were detached and singularized by incubation with Accutase® for 5 - 10 min at 37 °C. They were collected with cell scrapers and passed through the strainers into the 15 ml reaction tubes. Subsequently, the strainers were rinsed with cold $PBS^{+/+}$, the cell suspensions were carefully mixed and cells were counted. The suspensions were centrifuged for 5 min at 300 x g (RT). Pellets were resuspended and diluted in 2 % BSA in $PBS^{+/+}$ to obtain cell suspensions with 1 x 10^6 cells/ml. 1 ml of the samples was incubated with 1 µl CellEvent™ Caspase-3/7 Green Detection Reagent at 37 °C for 25 min to mark apoptotic cells. Subsequently, 1 µl of 1 mM SYTOX AADvanced was added for another 5 min to stain necrotic cells. For each cell line, an unstained control and controls for each dye were prepared. Fluorescence intensity was measured using a BD FACSCanto™II flow cytometer with the BD FACSDiva™ v7.0 software and the 530/30 and 670/LP filters for Caspase-3/7 Green Detection Reagent and SYTOX AADvanced dyes, respectively.

2.6 qRT-PCR-based marker gene expression analyses

RNA samples were taken at specific days of cardiac differentiation by lysing the cells with 700 µl QIAzol Lysis Reagent. They were stored at -80 °C until further processing. RNA was isolated from the cell lysates based on phenol-chloroform extraction and affinity chromatography with the RNeasy MiniKit according to the miRNeasy Mini Handbook from QIAGEN. For collecting the RNA from the

columns, they were centrifuged for 2 min at 8000 x g with 30 µl RNase-free water. Eluated samples were put on ice immediately and RNA concentrations were measured at a nanophotometer (Colibri, Titertek Berthold). Until further processing, RNA samples were stored at -80 °C.

2.6.1 Markers of pluripotency and differentiation

4 µg RNA were transcribed into cDNA using the RevertAid RT Kit according to the manufacturer's protocol in a 40 µl approach. The reaction was performed in the PCR Thermal Cycler Peqstar. Upon cDNA synthesis, samples were diluted in an equal volume of nuclease-free water. For each target gene, triplicates of each sample were pipetted into a 96-well-plate (Sarstedt). For the housekeeping gene (18sRNA, as used by Luft et al., 2017), samples were diluted 1:100 in nuclease-free water. The plates were sealed, briefly centrifuged and placed into the StepOnePlus RT PCR System or QuantStudio3. The cycling program was: 15 min at 95 °C, followed by 45 cycles of 15 s at 95 °C, 20 s at 60 °C and 20 s at 72 °C. A melt curve cycle of 15 s at 95 °C, 60 s at 60 °C and 15 s at 95 °C completed each PCR run. The results were analyzed with the ABI StepOne Software v2.3 or with QuantStudio™ Design & Analysis Software v1.4. For each target, the threshold was adjusted manually to match between experiments to be compared. Since the primer pairs used in these analyses are not equally efficient, the standard curve method was applied. RNA samples used for the generation of standard curves are listed in App. Table 6. mRNA levels were normalized to 18sRNA. To compare the mRNA expression of marker genes between the Lian and Kadari protocol, or between controls and irradiated samples, a second normalization was performed: All values were normalized to the highest expression level of each target achieved with the Lian protocol, or with control samples in case of irradiation experiments. Primers were produced by the company *biomers.net* (sequences are listed in App. Table 7) and solved in 1 x TE buffer upon arrival. They were used at a concentration of 1 µM.

2.6.2 microRNA-1

1 µg RNA was transcribed into cDNA using the miScript II RT Kit according to the manufacturer's instructions. Afterwards, cDNA concentration was measured at the nanophotometer and the cDNA was diluted to 250 ng/µl in 100 µl with nuclease free water. miR-1-content of the samples was investigated in triplicates of the prepared cDNA. As a housekeeping gene, SNORD25-11 was used (see Luft et al., 2017). qRT-PCR was performed using the miScript SYBR Green PCR Kit and primers were obtained from QIAGEN (Hs_miR-1_2 and Hs_SNORD25_11 miScript Primer Assays). The following cycling program was used: 15 min at 95 °C, followed by 45 cycles of 15 s at 94 °C, 30 s at 55 °C and 30 s at 70 °C. PCR analysis was completed with a melt curve cycle of 15 s at 95 °C, 60 s at 60 °C and 15 s at 95 °C. Subsequently, the standard curve method was applied to determine the relative amount of miR-1. Values were normalized to SNORD25-11 and to the miR-1 level of controls at day 15 of differentiation.

2.7 qRT-PCR-array based analyses of DNA Damage Response and Stem Cell Signaling

cTNT-H9 cells were irradiated with 1 Gy X-rays and RNA samples were taken 1 h, 6 h, 24 h, and 7 d after exposure by lysing the cells with QIAzol Lysis Reagent. RNA isolation was performed as described in section 2.6. RNA was eluated with 25 µl RNase-free water. After RNA isolation, n = 6 samples were pooled for each time point (2 µg of each sample). For subsequent cDNA-synthesis with the RT² First Strand Kit, 1 µg RNA was used. The cDNA synthesis was performed according to the manufacturer's protocol in the Peqstar PCR Thermal Cycler. Afterwards, cDNA was diluted in equal volume of RNase-free water and stored at -20 °C until further analyses. According to the manufacturer's protocol, cDNA and the RT² SYBR Green ROX qPCR Mastermix were mixed and diluted in nuclease-free water. Using a multichannel pipette (VWR), 25 µl of the mixes were pipetted into the wells of the Human Stem Cell Signaling PCR Array (PAHS-047ZA, QIAGEN) and the Human DNA Damage Signaling Pathway PCR Array (PAHS-029ZC, QIAGEN) plates. They were sealed, centrifuged and placed into the StepOnePlus RT PCR System. The following cycling program was used: 10 min at 95 °C, followed by 40 cycles of 15 s at 95 °C and 60 s at 60 °C. The PCR run was completed by a melt curve cycle with 15 s at 95 °C, 60 s at 60 °C and 15 s at 95 °C. Subsequent analyses were performed with the ABI StepOne Software v2.3 and the Data Analysis Center of www.qiagen.com using the ΔΔCT method. Both PCR arrays contained five housekeeping genes for normalization. However, not all of them were suited for normalization since their expression differed markedly between the samples. For the Stem Cell Signaling Array, *GAPDH, HPRT1* and *RPLP0* were selected for normalization due to very similar CT-values among all samples. For the DNA Damage Response Signaling Pathway Array, two normalization methods were chosen and compared with each other: in a first approach, *B2M* and *HPRT1* were used for normalization. In a second approach, the genes *NBN, FEN1, PPP1R15A, FANCA, H2AFX* were chosen since their expression was comparable between all samples.

2.8 Immunocytochemical analyses of pluripotency and differentiation markers

For immunocytochemical analyses of proteins, cells were grown in petri dishes on Ø 12 mm round coverslips, which were either preseeded with MEF feeder cells (H9 cells, see section 2.1.3) or Laminin-coated (cTNT-H9 cells). Cells were fixed at several days to analyze for pluripotency markers (day 0), endothelial markers (day 5 and 8) and cardiac markers (day 8 and 15). Briefly, the medium was aspirated, cells were washed with PBS and fixed with 3.7 % formaldehyde (FA) for 15 min on ice. Subsequently, they were washed three times and stored at 4 °C in PBS until immunocytochemical staining.

To permeabilize the cells, they were treated 30 min at RT with 0.5 % Triton X-100 diluted in 1 % BSA. Subsequently, unspecific binding sites were blocked by incubating with 1 % BSA for 30 min (RT). Then, the cells were incubated with the primary antibody diluted in 1 % BSA (antibodies and dilutions are listed in Table 4) over night at 4 °C in a humidifying chamber. Cells were washed and

subsequently incubated with the secondary antibody (diluted 1:400 in 1 % BSA, see Table 5) for 30 - 45 min at 37 °C in the dark. After another washing step, DNA was stained with Hoechst-33342 (diluted 1:1000 in ultrapure water) for 4 min (dark, RT). Cells were washed once with PBS and two times with ultrapure water. Coverslips were mounted on slides (Carl Roth) with Fluorescent Mounting Medium, sealed with nail polish and stored at 4 °C until microscopy. A Leica DMI 4000B microscope was used to take Z-stack images and focus stackings of these were generated in ImageJ/Fiji. For intensity measurements, average intensity projections were used.

Table 4: Primary antibodies for immunocytochemical analyses.

Antigen	**Manufacturer ID**	**Antibody raised in**	**Dilution**
Alpha Actinin (sarcomeric)	Sigma-Aldrich/Merck A7732	mouse	1:1500
ATM	Millipore/Merck 04-200	rabbit	1:100
Cardiac Troponin T	Santa Cruz sc-20025	mouse	1:400
CD31	Abcam ab28364	rabbit	1:25
Connexin 43 (GJA1)	Abcam ab11370	rabbit	1:1000
HCN4	Abcam ab66501	rabbit	1:2000
MLC2	Abcam ab79935	rabbit	1:1500
MYL7	Santa Cruz sc-365255	mouse	1:400
Nanog (Alexa Fluor® 488 anti-human Nanog)	BD Pharmingen 560791	mouse	1:10
OCT-3/4	Santa Cruz sc-5279	mouse	1:400
p21	Calbiochem OP64	mouse	1:100
SOX2	Santa Cruz sc-17319	goat	1:300
vWF	Sigma-Aldrich/Merck 3520	rabbit	1:500

Table 5: Secondary antibodies.

Antibody	**Manufacturer ID**	**Reactivity**	**Dilution**
Alexa Fluor® 488	Life technologies A11070	goat-anti-rabbit	1:400
Alexa Fluor® 488	Life technologies A11001	goat-anti-mouse	1:400
Alexa Fluor® 568	Life technologies A11036	goat-anti-rabbit	1:400
Alexa Fluor® 568	Life technologies A11004	goat-anti-mouse	1:400
Alexa Fluor® 594	Life technologies A11058	donkey-anti-goat	1:400

The noise signal was generally high in all samples. However, using 4 % goat serum for blocking instead of 1 % BSA as well as fixing the cells for a shorter time (15 min) on ice instead of a prolonged time at RT did not reduce the unspecific signal. Nonetheless, specific signals could clearly be distinguished from noise.

2.9 Video analyses of the beating hESC-derived cardiac clusters

Spontaneous beating of the hESC-derived cardiac clusters was first observed between day 6 and 8 of differentiation. To evaluate the beating characteristics (beat rate and beat variability), the software cBRA (cardiac Beat Rate Analyzer) was developed (Nitsch et al., 2018). Videos were recorded at day 8, 10 (or 11) and 15 of differentiation (for details see Nitsch et al., 2018).

To analyze the presence and functionality of β-adrenoreceptors, two clusters for each condition were recorded before and after addition of 1 µM isoproterenol.

Furthermore, presence and functionality of HCN4 channels were investigated with ivabradine. Therefore, the same clusters were recorded before and after addition of ivabradine. Increasing concentrations between 2 - 100 µM were added to the cultures derived from sham and 1 Gy-irradiated cTNT-H9 cells.

2.10 Electrophysiological measurements of cTNT-H9-derived cardiomyocytes

cTNT-H9-derived cardiac cultures at day 15 of differentiation were exemplarily measured in the whole-cell configuration of the current clamp technique in collaboration with the group of Prof. Dr. Gerhard Thiel at Technical University Darmstadt. The clusters were not dissociated into single cells since dissociation with trypsin or Accutase® was not successful. Therefore, current clamping was more difficult and only three CM, which were located at the edges of beating clusters, could be measured. Intra- and extracellular solutions were prepared according to Spencer et al. (2014). 4 GΩ capillaries were pulled and heated up for 15 min. Before measurement, 2 mM ATP was added to the intracellular solution, which was subsequently warmed in a 37 °C water bath. Culture medium was removed and replaced by the extracellular solution. Using an EPC-9 (Vers. C) Patch Clamp Amplifier (HEKA Elektronik), spontaneous AP were recorded with the I0-current at RT with the software PatchMaster v2x90 (HEKA Elektronik). The maximum diastolic potential and AP amplitudes were calculated and compared to literature values.

2.11 Statistical analyses

PCR data are presented in column scatter plots with the median line or as dose effect-curves showing the median of all experiments with the standard error of the median. Beat rates determined via video analyses in cBRA are presented in box plots with the median and the 25 % and 75 % quartiles for each experiment. All results are based on $n \geq 3$ independent experiments if not denoted differently. Statistical significance was determined by Student's t-test (* $p < 0.5$, ** $p < 0.01$, *** $p < 0.001$).

3 Results

3.1 Characterization of the H9-derived cardiac cultures using two different protocols

Two recent protocols for directed cardiac differentiation (Kadari et al., 2015; Lian et al., 2013a) were compared using the H9 cells in n = 6 independent experiments. Cells were seeded on Matrigel®-coated plates (see section 2.3) and four days later (d0) their pluripotency was confirmed by immunocytochemical detection of OCT4, SOX2 and NANOG (Fig. 10). However, some cells were negative for these markers and had a different morphology hinting at spontaneous differentiation (not shown). Directed cardiac differentiation was performed as shown in Fig. 7. From day 1 to 3 massive cell death was observed microscopically independent of the culture protocol (not shown).

Cardiac development was confirmed by the onset of spontaneous contraction of the clusters between day 6 and 8 of differentiation. However, the cluster morphology differed depending on the protocol: Whereas the clusters resulting from the Kadari protocol were round and compact, those derived from the Lian protocol were strand-like and developed a higher degree of interconnectedness until day 15 (Nitsch et al., 2018).

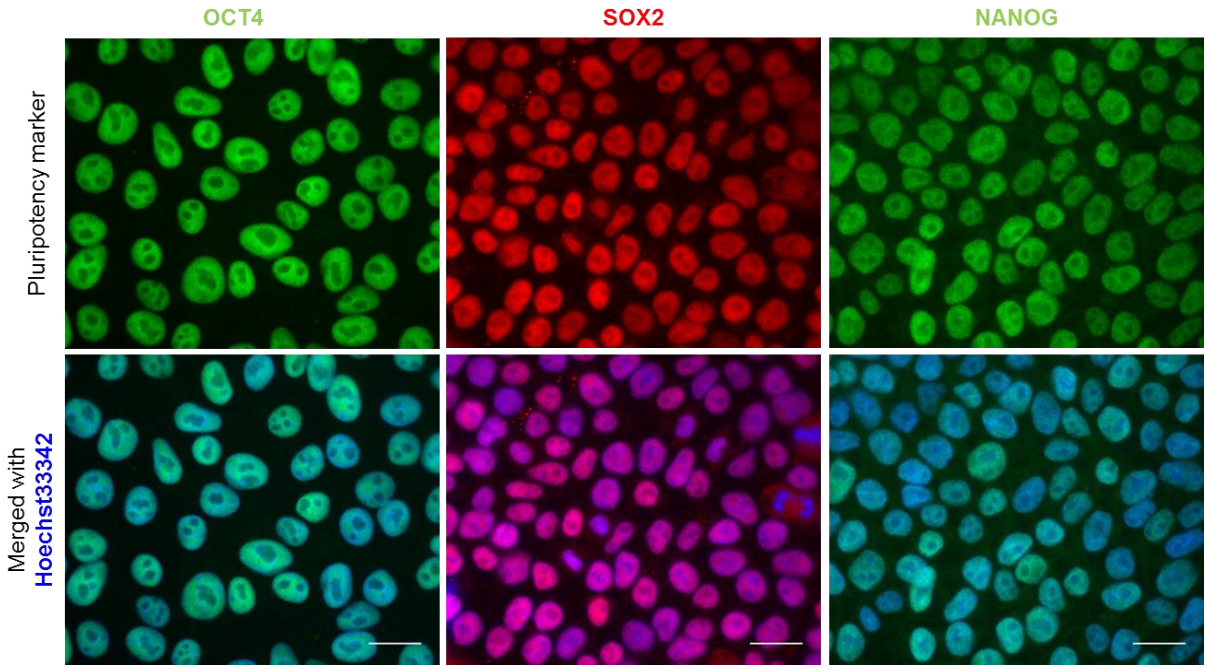

Fig. 10: Immunocytochemical staining of the core pluripotency transcription factors in H9 cells before initiation of cardiac differentiation. After four days of feeder-free culture on Matrigel®-coated coverslips, H9 cells were fixed and stained for OCT4, SOX2 and NANOG. DNA was stained with Hoechst-33342. Scale bars: 20 µm.

3.1.1 qRT-PCR based analyses of stage-specific cardiac marker gene expression

The cardiac cultures generated with the two protocols were compared based on qRT-PCR analyses of known marker genes of cardiac differentiation. Absolute gene expressions varied among experiments,

as shown in Fig. 11 - 13. However, the general trend was similar. After initiation of differentiation, expression of the pluripotency marker genes *POU5F1* (encoding OCT4) and *NANOG* decreased with both protocols (Appendix (App.) Fig. 1 A, B).

At day 1 and 2 of differentiation, expression of *T* (encoding Brachyury) and *MESP1*, which are markers for mesodermal and cardiac mesodermal cells (Saga et al., 2000; Showell et al., 2004), is upregulated, respectively, with both protocols (Fig. 11 A, B). Interestingly, *MESP1* expression was induced simultaneously with *T* at day 1 using the Kadari protocol, whereas with the Lian protocol *MESP1* was only upregulated at day 2.

Following the downregulation of *T* and *MESP1*, cardiac progenitor markers like *GATA4* and *NKX2.5* (Fig. 11 C, D) were upregulated at day 5. Since their expression varied markedly among the experiments, no clear difference between the two protocols could be observed. However, by trend, especially the expression of *NKX2.5* was higher using the Kadari protocol. Expression of *ISL1*, another marker for cardiac progenitors, was by trend higher with the Kadari protocol until day 8 where it peaked for this protocol. In contrast, using the Lian protocol, its expression peaked at day 15 (App. Fig. 1 C).

WNT11, a marker for non-canonical WNT signaling, was first detected at day 2. With the Lian protocol, its mRNA level peaked at day 15, however, with the Kadari protocol, it peaked already at day 8 and its expression remained high until day 15 (App. Fig. 1 D).

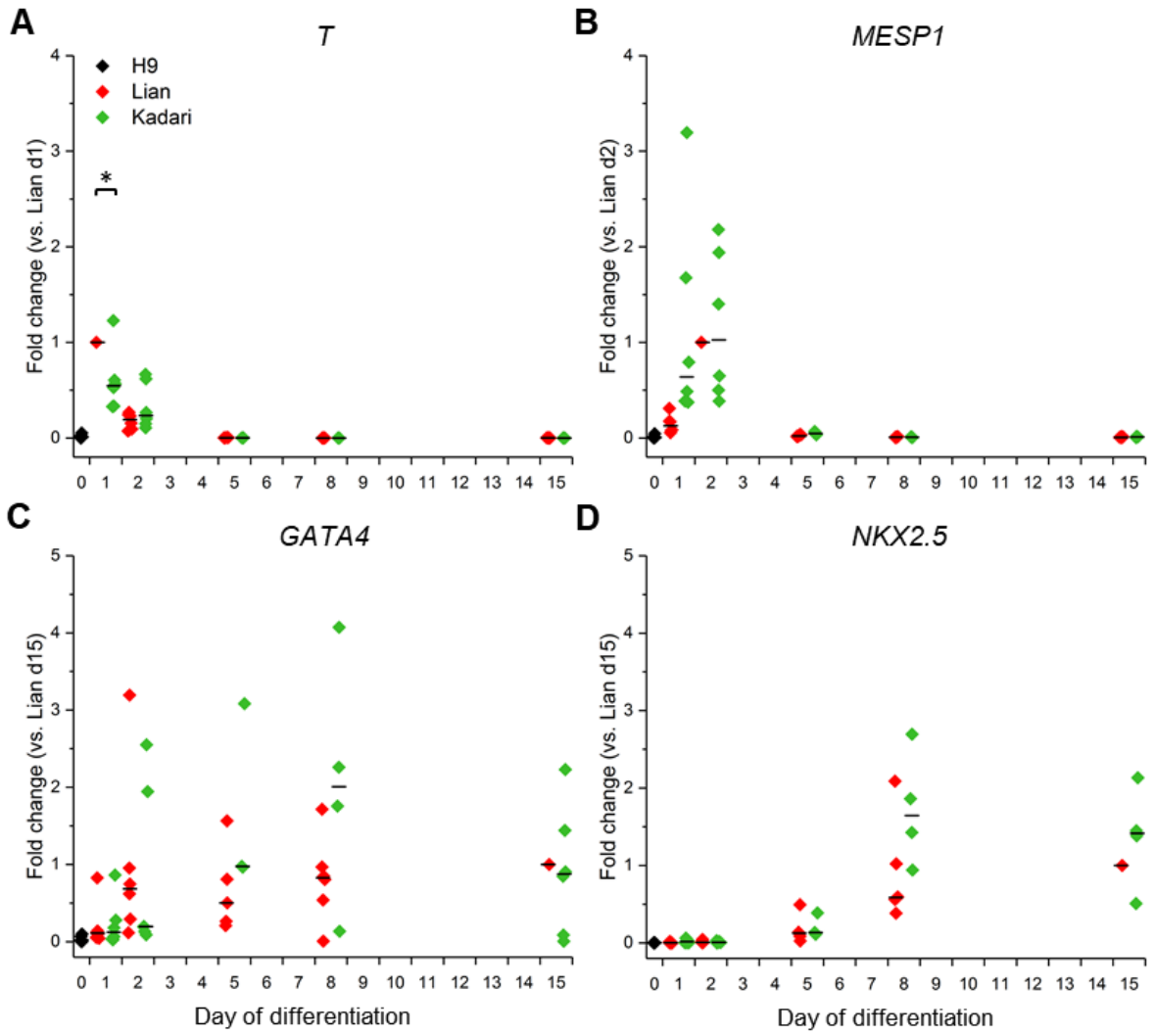

Fig. 11: qRT-PCR based analyses of early cardiac differentiation marker genes comparing two protocols. Pluripotent H9 cells (black) were differentiated according to the Lian (red, n = 6) and Kadari protocol (green, n = 6 until day 5, n = 4 at day 8 and 15). At multiple days during differentiation, expression of *T* (A), *MESP1* (B), *GATA4* (C) and *NKX2.5* (D) were investigated via qRT-PCR. Values were normalized to 18sRNA and the highest mRNA level of each target achieved with the Lian protocol. Student's t-test was performed among experiments. * $p < 0.05$; black lines: median; d, day.

Cardiac troponin T (cTNT) is essential for CM contraction (Sehnert et al., 2002, see section 1.3.2). It is encoded by the gene *TNNT2* whose expression appeared at day 5 and increased until day 15 (Fig. 12 A) independent of the protocol. However, its expression was higher in the cardiac cultures derived from the Kadari protocol.

The pacemaker marker *HCN4* was already expressed in undifferentiated cells (Fig. 12 B). Starting from day 8, its expression was elevated and peaked at day 15. With the Kadari protocol, HCN4 expression was higher.

Myosins are essential for CM contraction and consist of heavy and light chains (England and Loughna, 2013). Together with the onset of spontaneous contraction, expression of *MYH6* and *MLC2a*

was observed at day 8 and maintained until day 15 (Fig. 13 C, D). Both are markers for fetal/immature as well as for atrial CM (England and Loughna, 2013; Hailstones et al., 1992; Reiser et al., 2001) and were stronger expressed with the Kadari protocol.

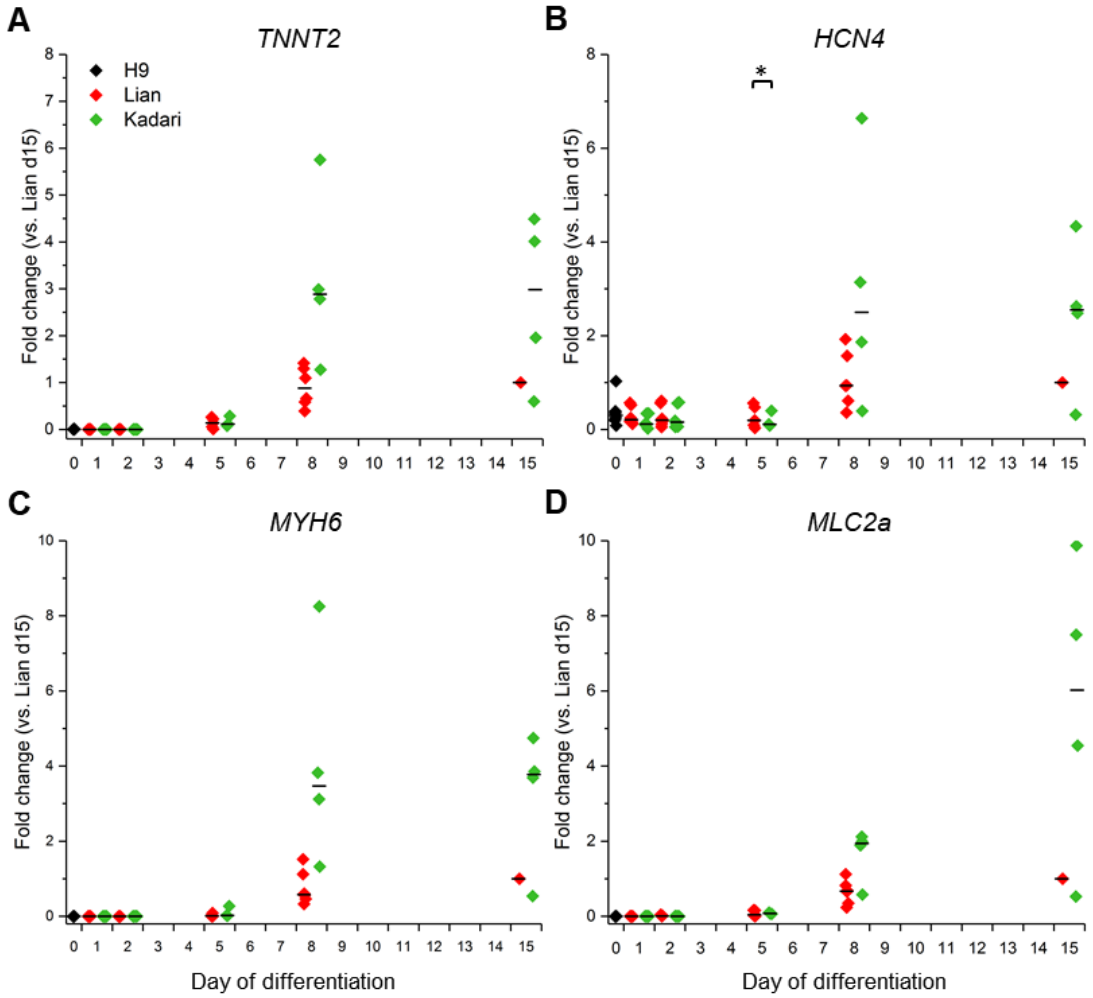

Fig. 12: Comparison of the expression of immature cardiac marker genes between two protocols. Expression of *TNNT2* (A), *HCN4* (B), *MYH6* (C) and *MLC2a* (D) was investigated via qRT-PCR at various days during differentiation according to Lian et al. (2013a; red, n = 6) and Kadari et al. (2015; green, n = 6 until day 5, n = 4 at day 8 and 15). Values were normalized to 18sRNA and for each target to the day 15-mRNA level achieved with the Lian protocol. Student's t-test was performed among experiments. * $p < 0.05$; black symbols: target gene expression before differentiation; black lines: median; d, day.

Marked differences between the two protocols were observed in the expression of chamber specific markers. Expression of *MYH7* as well as *MLC2v*, marking more mature and ventricular CM (England and Loughna, 2013), was much higher in the cultures resulting from the Kadari protocol compared to those of the Lian protocol (Fig. 13 A, B). Likewise, expression of *IRX4*, another ventricular marker (Bao et al., 1999; Nelson et al., 2016), was higher with the Kadari protocol. In contrast, with the Lian protocol, its levels were generally low with CT-values near baseline level and it was only expressed at day 15 (Fig. 13 C).

Atrial natriuretic factor (ANF) is a marker for initiation of working myocardium and is used as a marker for atrial development (Houweling et al., 2005). The expression of its gene, *NPPA*, was observed starting from day 8 with both protocols (Fig. 14 D), but with higher levels resulting from the Kadari protocol. Two other genes generally used as atrial markers, namely *NR2F2* (Devalla et al., 2015; Wu et al., 2013) and *KCNA5* (Devalla et al, 2015) were investigated. For *NR2F2*, no protocol-dependent differences were observed (App. Fig. 1 E). *KCNA5* mRNA level was above baseline level starting from day 1 and peaked at day 2 with the Lian protocol. With the Kadari protocol, its expression was initiated at day 2, peaked at day 5 and was reduced afterwards (App. Fig. 1 D). By trend, its level was higher with the Kadari protocol from day 5 to 15.

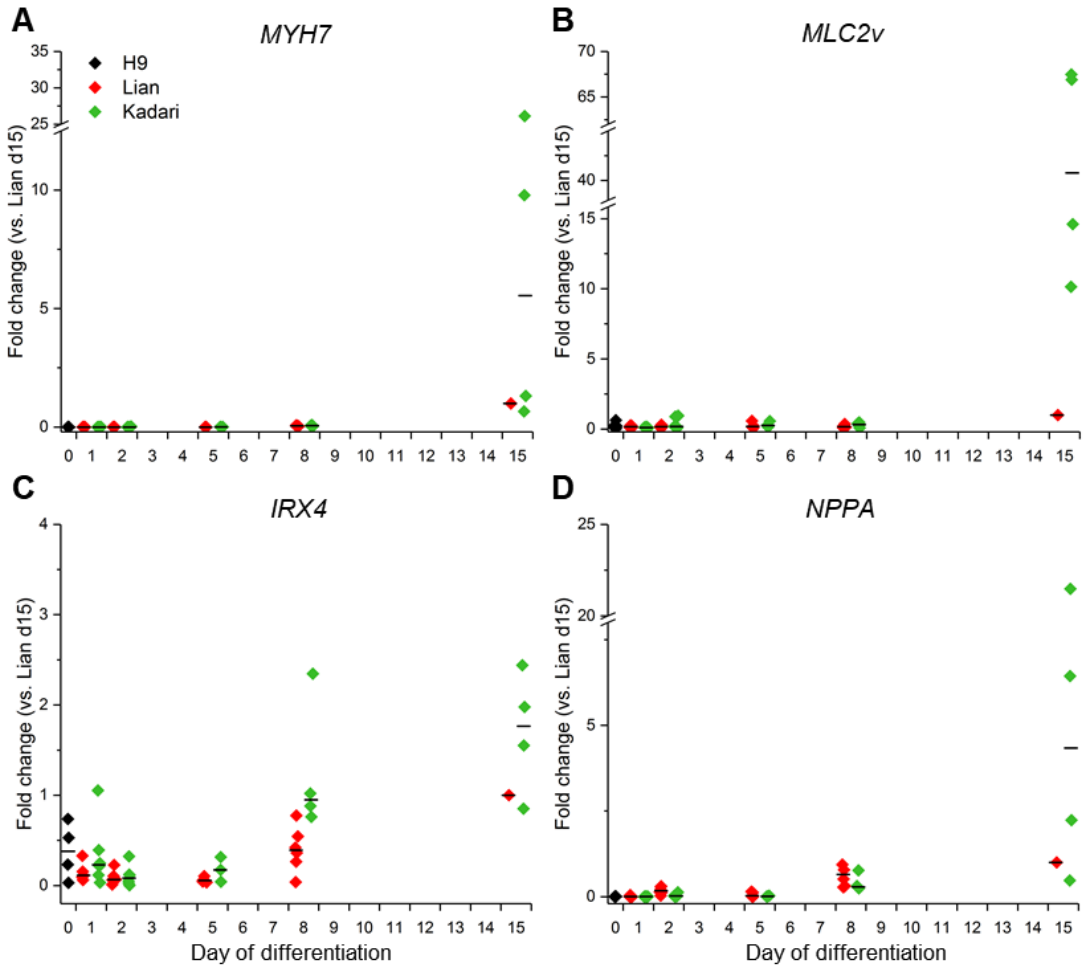

Fig. 13: Expression of chamber specific cardiac marker genes analyzed via qRT-PCR comparing two differentiation protocols. RNA samples were taken at multiple days during differentiation according to Lian et al. (2013a; red symbols; n = 6) and Kadari et al. (2015; green symbols; n = 6 until day 5, n = 4 at day 8 and 15) and analyzed for expression of *MYH7* (A), *MLC2v* (B), *IRX4* (C) and *NPPA* (D). Values were normalized to 18sRNA and for each target to its highest expression level achieved with the Lian protocol. Black symbols: target gene level before differentiation; black lines: median; d, day.

In summary, cardiac marker gene expression was higher in the cultures derived from the Kadari protocol. This was especially obvious for the chamber specific markers *MYH7*, *MLC2v* and *NPPA*.

3.1.2 Immunocytochemical analyses of the structural organization of cardiac proteins

The CM derived from both protocols were additionally analyzed for the cardiac proteins α-Actinin, cTNT, MLC2a and MLC2v at day 15 of differentiation via immunocytochemistry. Both protocols led to their expression, except for MLC2v (Fig. 14). This protein was not expressed in the CM derived from the Lian protocol, while it was observed in some, but not all clusters resulting from the Kadari protocol. CM derived from the Kadari protocol had a higher level of protein organization, i.e. their sarcomeric structure was more pronounced.

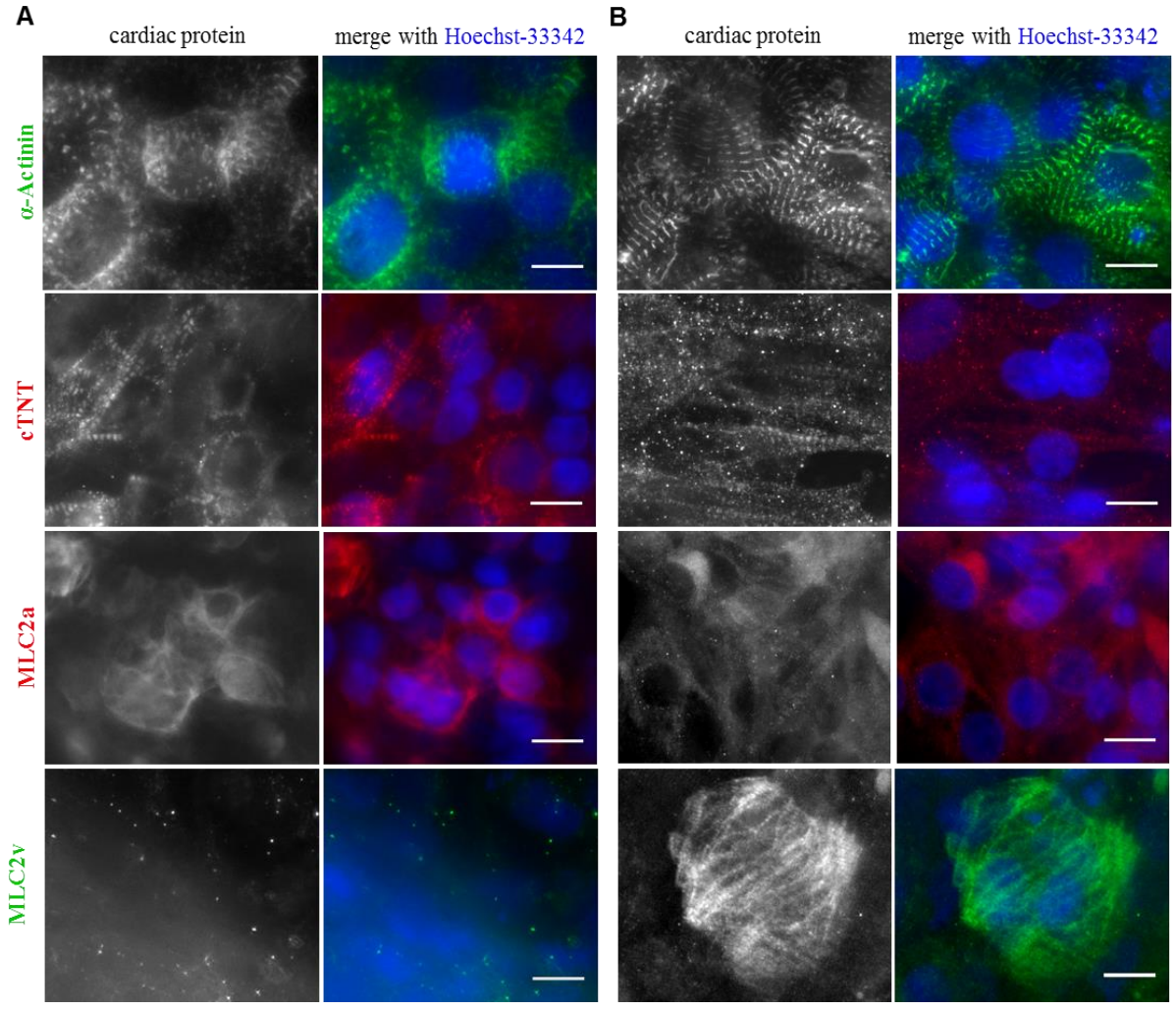

Fig. 14: Immunocytochemical detection of typical markers in H9-derived CM. H9 cells were differentiated according to the Lian (A) or Kadari (B) protocol. At day 15, cells were fixed and stained with antibodies against α-Actinin, cTNT, MLC2a and MLC2v. DNA was stained with Hoechst-33342. Scale bars: 10 µm.

3.1.3 Functional analyses of the beating cardiac clusters

Functionality of the CM generated with both protocols was evidenced by the onset of spontaneous contractions between day 6 and 8 of differentiation. To assess their beating features, videos were recorded and analyzed with the software cBRA (Nitsch et al., 2018) for their beat rates and beat variability. In four out of n = 6 independent experiments, maximum five beating clusters were recorded. However, since the beat rates varied markedly within one experiment and among the clusters derived from one protocol, at least 20 videos per protocol were recorded in all subsequent experiments. The two experiments comparing the Lian and Kadari protocols with 20 videos per protocol showed opposing trends in terms of the beat rates (Fig. 15).

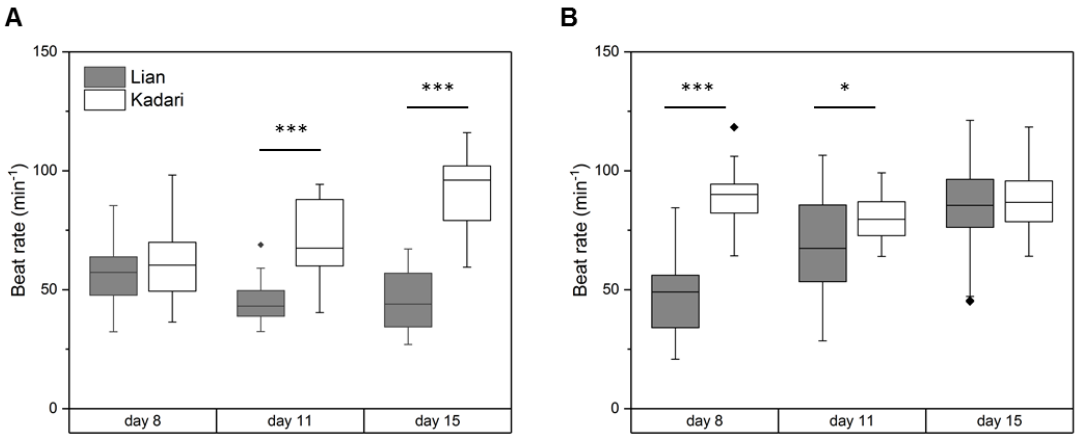

Fig. 15: Beat rates of the H9-derived cardiac clusters. 20 videos were recorded per protocol (gray boxes: Lian protocol, white boxes: Kadari protocol) at day 8, 11 and 15 of differentiation and beat rates of the cardiac clusters were determined with the software cBRA. The results of two independent experiments are shown. Boxes, 25 % quartile – median – 75 % quartile. Whiskers, 1.5 coefficient.

The videos were additionally analyzed for the beat variability of the cardiac clusters. Therefore, beat intervals and their standard deviations (SD1 and SD2) were determined and depicted in Poincaré plots as shown representatively in Fig. 16 A and B for the Lian and Kadari protocol, respectively. SD1 is the standard deviation of the long term variability and SD2 of the short term variability. A high SD1 means that the beating became faster or slower during the video, whereas a high SD2 means that the beat intervals were very irregular. The beat variability of the clusters generated with the Lian protocol was high at each day of video recording (Fig. 16 C, E). The clusters resulting from the Kadari protocol showed a high beat variability at day 8, however, at day 15 it was very low (Fig. 16 D, F).

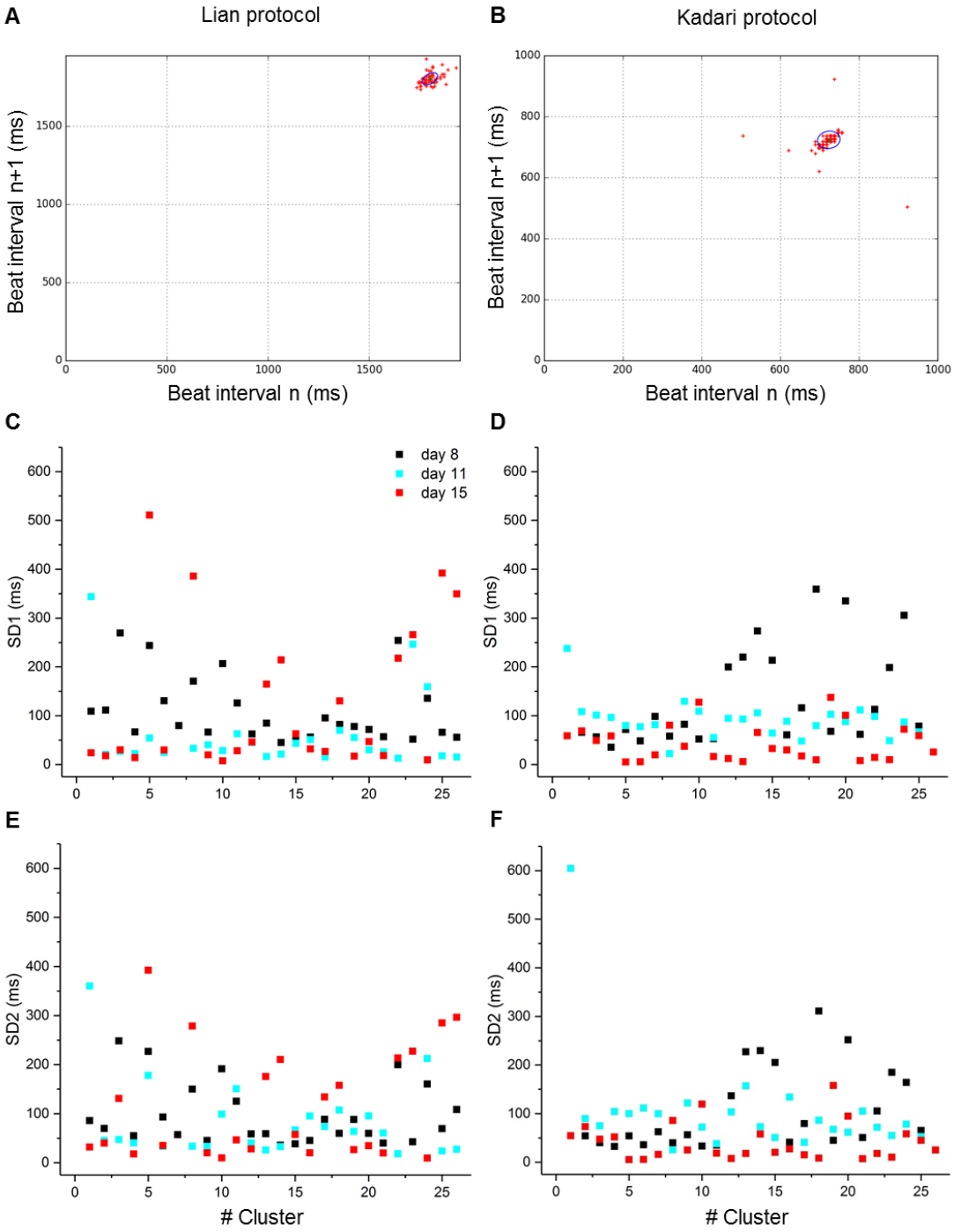

Fig. 16: Beat variability assessed with the software cBRA. A, B) Representative Poincaré plots of the clusters resulting from the Lian (A) and Kadari (B) protocol at day 15 of cardiac differentiation. C-F) At day 8 (black), 11 (blue) and 15 (red) the same clusters were video-recorded to monitor their development over time. The medians of the standard deviations of the long term (C, D) and short term (E, F) variability were calculated and plotted for each cluster at each day for the Lian (C, E) and Kadari (D, F) protocol. Plots of one out of two independent experiments are shown.

Presence and functionality of β-adrenoreceptors of the day 15-CM was investigated via addition of 1 µM isoproterenol, a non-selective agonist of these receptors. Two clusters were recorded per protocol before and after its addition. In general, all clusters reacted with an increased beat rate

(App. Fig. 2). However, one of the two clusters derived from the Kadari protocol showed a delayed response: During the first two minutes upon addition of isoproterenol, its beat rate remained the same as before. Starting from ~ 3 min until the end of the video, it increased by around 24 %. At day 22 and 29 of differentiation, the same cluster showed a normal response to isoproterenol (i.e. 1.4- and 1.8-fold increased beat rate, respectively).

Since differentiation according to Kadari et al. (2015) led to a higher cardiac marker gene expression, a higher level of protein organization and a more regular beating, this protocol was used in all following experiments.

3.2 Characterization of the cell line H9-hTnnTZ-pGZ-D2 and comparison to the wildtype H9 cell line

The transgenic cell line H9-hTnnTZ-pGZ-D2 (cTNT-H9) has several advantages compared to the wildtype H9 cell line: it is adapted to feeder-free conditions and cardiac differentiation can easily be observed since GFP is under the control of the cTNT-promoter (Fig. 17). Before this cell line was routinely used, the cells were characterized with respect to their cardiac differentiation capability, their karyotype and response to X-ray irradiation compared to the wildtype H9 cell line.

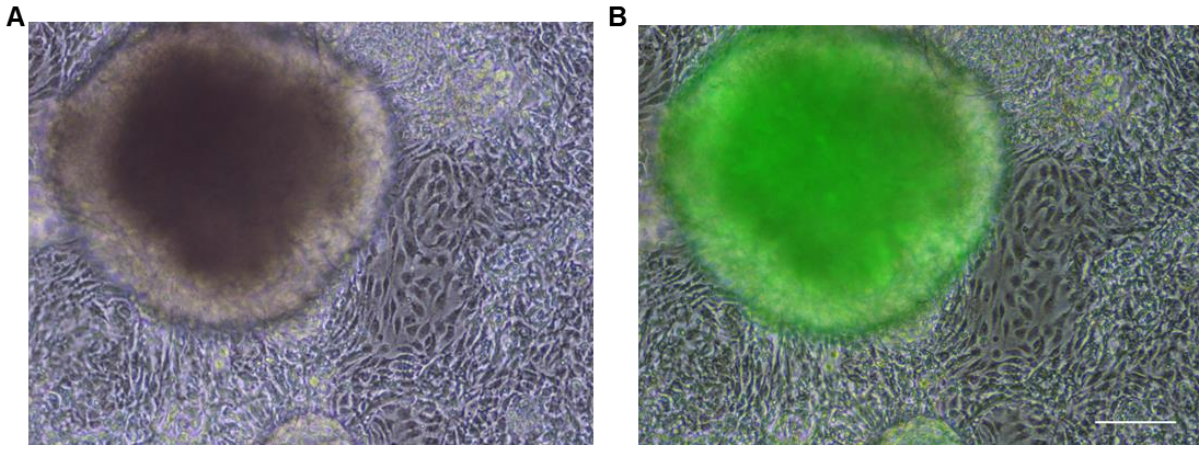

Fig. 17: cTNT-H9-derived cardiac cultures. A) Cardiac clusters were surrounded by non-cardiac cells that were morphologically distinguishable from non-cardiac cells. B) The CM express GFP, which is under the control of the cTNT-promoter, while non-cardiac cells do not fluoresce. Scale bar: 100 µm.

3.2.1 Cytogenetic analyses of cTNT-H9 cells during ReleSR™-passage and after X-ray exposure

During prolonged culture of hESCs, chromosomal aberrations may accumulate, which is in part depending on the method of culture and passaging (Luft et al., 2017; Nguyen et al., 2013). In this study, several passaging methods were tested for the cTNT-H9 cell line, however, only passage with ReleSR™ led to a high amount of pluripotent cells (data not shown). Since no cytogenetic analyses of the cTNT-H9 cells passaged with ReleSR™ exist, their karyotype was analyzed at multiple passages

using mFISH. As depicted in Fig. 18 A, even cTNT-H9 cells of a high passage (i.e. p75) displayed a normal female karyotype consisting of 46 chromosomes. In 111 analyzed cells, no aberrant ones were detected.

24 h after exposure to 1 Gy X-rays, 15.8 % of the cTNT-H9 cells showed chromosomal aberrations (15 aberrant out of 95 analyzed cells, Fig. 18 B). The most frequent aberrations were breaks (9.5 breaks per 100 cells) and translocations (5.3 %). Seven days after irradiation, only 3.3 % cells were aberrant. Additionally, cells irradiated with 2 Gy were analyzed seven days after exposure. However, due to a low number of mitotic cells, only 57 cells were analyzed. Four of them were aberrant including one complex aberration. The results of the cytogenetic analyses after X-ray exposure are summarized in App. Table 8.

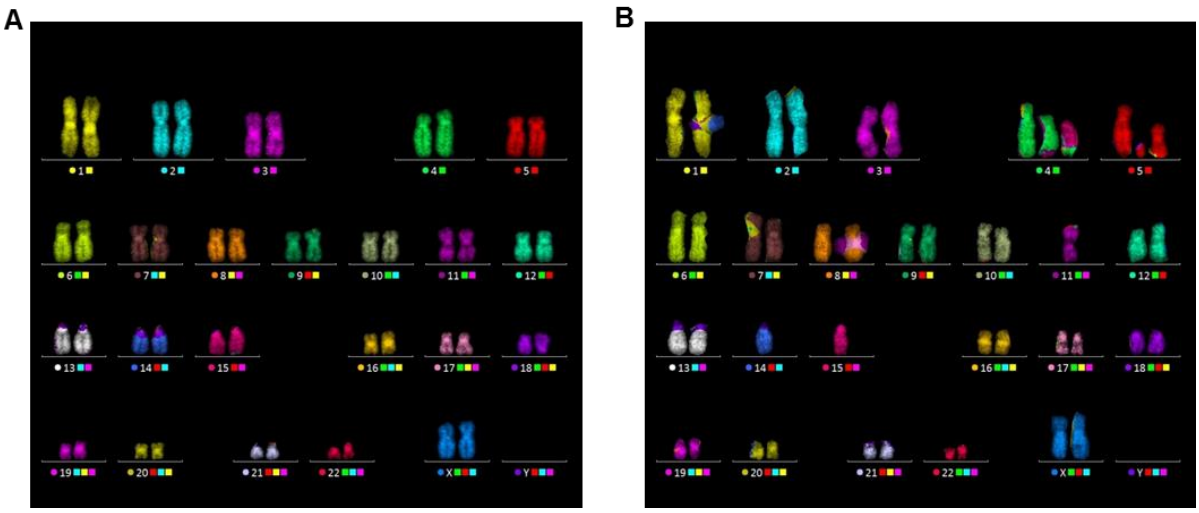

Fig. 18: Cytogenetic analyses of cTNT-H9 cells based on mFISH. A) cTNT-H9 cells at passage 75 had a normal female karyotype with 46 chromosomes. B) 24 h after exposure to 1 Gy, there are several aberrations, like translocations (t 4‘-15 + t 15‘-4) or acentric and truncated chromosomes (ace5 + T5’).

3.2.2 Cell death upon X-ray exposure of cTNT-H9 cells

24 – 72 h after exposure to 1 Gy, massive cell death was observed by many free-floating cells in the culture medium. To quantify necrotic and apoptotic cells, three independent experiments were performed and analyzed by means of the CellEvent™ Caspase-3/7 Green Flow Cytometry Assay Kit. Fig. 19 shows the results of one representative experiment and the data of all three experiments are summarized in App. Table 9 and 10.

24 and 48 h after exposure, the measured percentage of apoptotic cells was on average twice as high as in sham controls (Q4 in Fig. 19 A, B). The amount of necrotic cells (Q2) varied among experiments, but was by trend comparable between controls and irradiated samples. 72 h after irradiation, there were, in the mean, four times more apoptotic cells than in sham controls and the number of necrotic cells was increased two fold (Fig. 19 C). Compared to controls, there were substantially less living cells (Q3) at 48 and 72 h after irradiation. This is in line with the smaller colony size at these time

points. However, it has to be taken into account that the medium was changed every 24 h. Therefore, the number of dead cells determined 48 and 72 h after irradiation represents only those cells that initiated cell death in the last 24 h before measurement and not the overall amount of dead cells since irradiation.

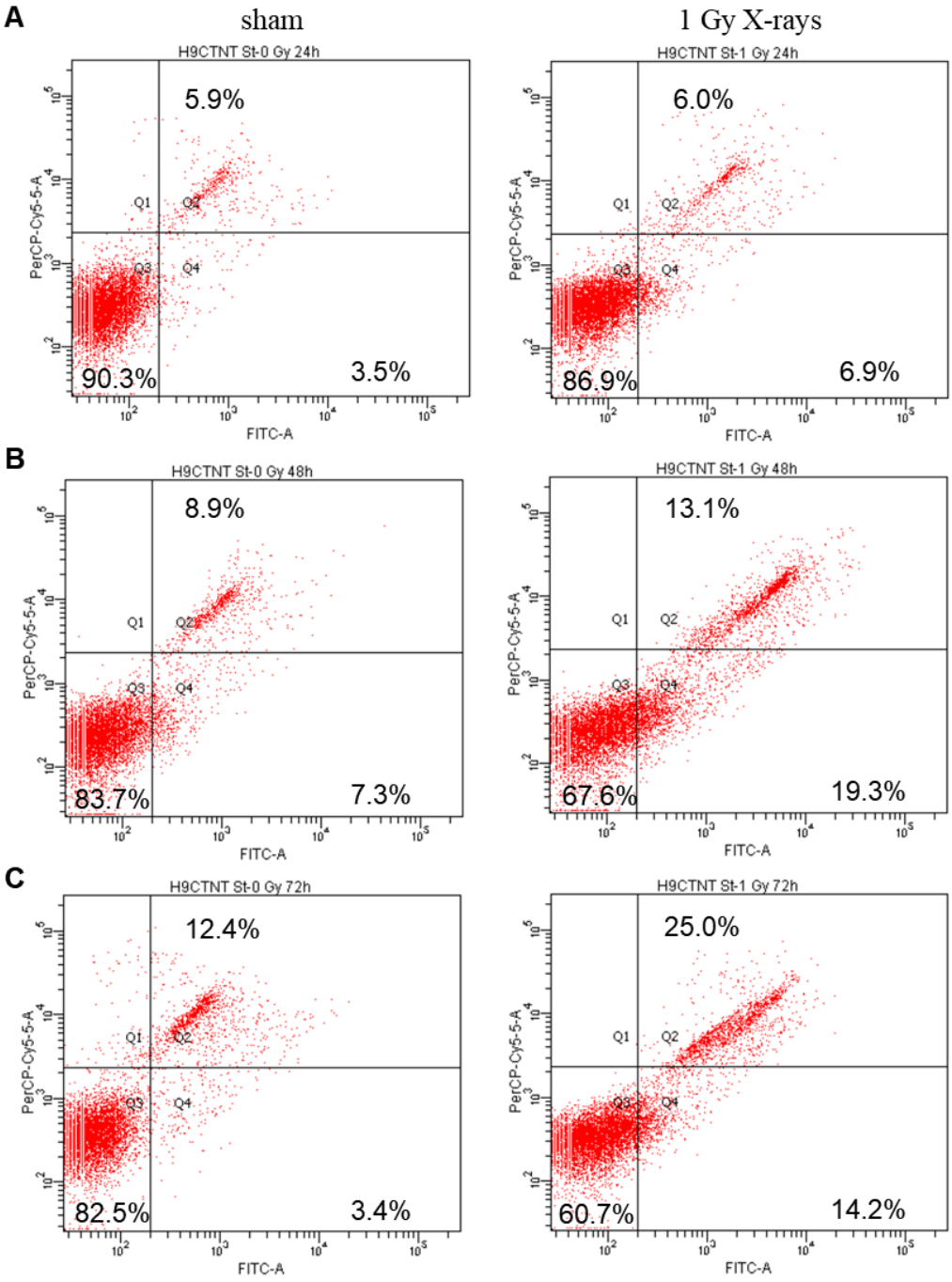

Fig. 19: FACS-based quantification of the necrotic and apoptotic fraction of cTNT-H9 cells upon irradiation. Cells were irradiated (sham or 1 Gy X-rays) and stained with the CellEvent™ Caspase-3/7 Green Flow Cytometry Assay Kit after 24 h (A), 48 h (B) and 72 h (C) for apoptotic (Q4) and necrotic (Q2) cells. Living cells (Q3) were unstained.

3.2.3 Comparison of the cardiac differentiation efficiency using the H9 and cTNT-H9 cell lines

H9 and cTNT-H9 cells were differentiated according to Kadari et al. (2015) in two independent experiments. In the cTNT-H9 cultures, more beating cardiac clusters formed compared to the H9 cultures. This observation was confirmed by marker gene expression analyses (Fig. 20). Whereas at day 2, the early mesodermal marker *T* was expressed at the same level with both cell lines (Fig. 20 A), markedly increased gene expression levels were observed starting from the cardiac progenitor stage (*NKX2.5*, Fig. 20 B) to the immature CM (Fig. 20 C - E) using the cTNT-H9 cells. One exception was the pacemaker marker *HCN4*: its expression was the same at day 8 in both cell lines. However, at day 15 it was slightly (experiment 1, data not shown) or significantly higher (experiment 2, Fig. 20 F) in the cTNT-H9 cultures.

Beat rates of the H9 and cTNT-H9 cultures were the same (App. Fig. 3). The only exception was that in two out of three independent experiments the cTNT-H9-derived clusters were beating significantly faster at day 11 than those derived from the wildtype cell line.

These results suggest that cardiac differentiation is more efficient using the cTNT-H9 cells. Therefore, all subsequent experiments were performed with this cell line.

Cardiac clusters derived from the cTNT-H9 cells detached to a very high extent from the Matrigel®-coated culture plates in all experiments and were thus removed when medium was exchanged. Since this was not the case when the plates were instead coated with Geltrex®, cTNT-H9 cells were differentiated on Geltrex®-coated plates in all subsequent experiments.

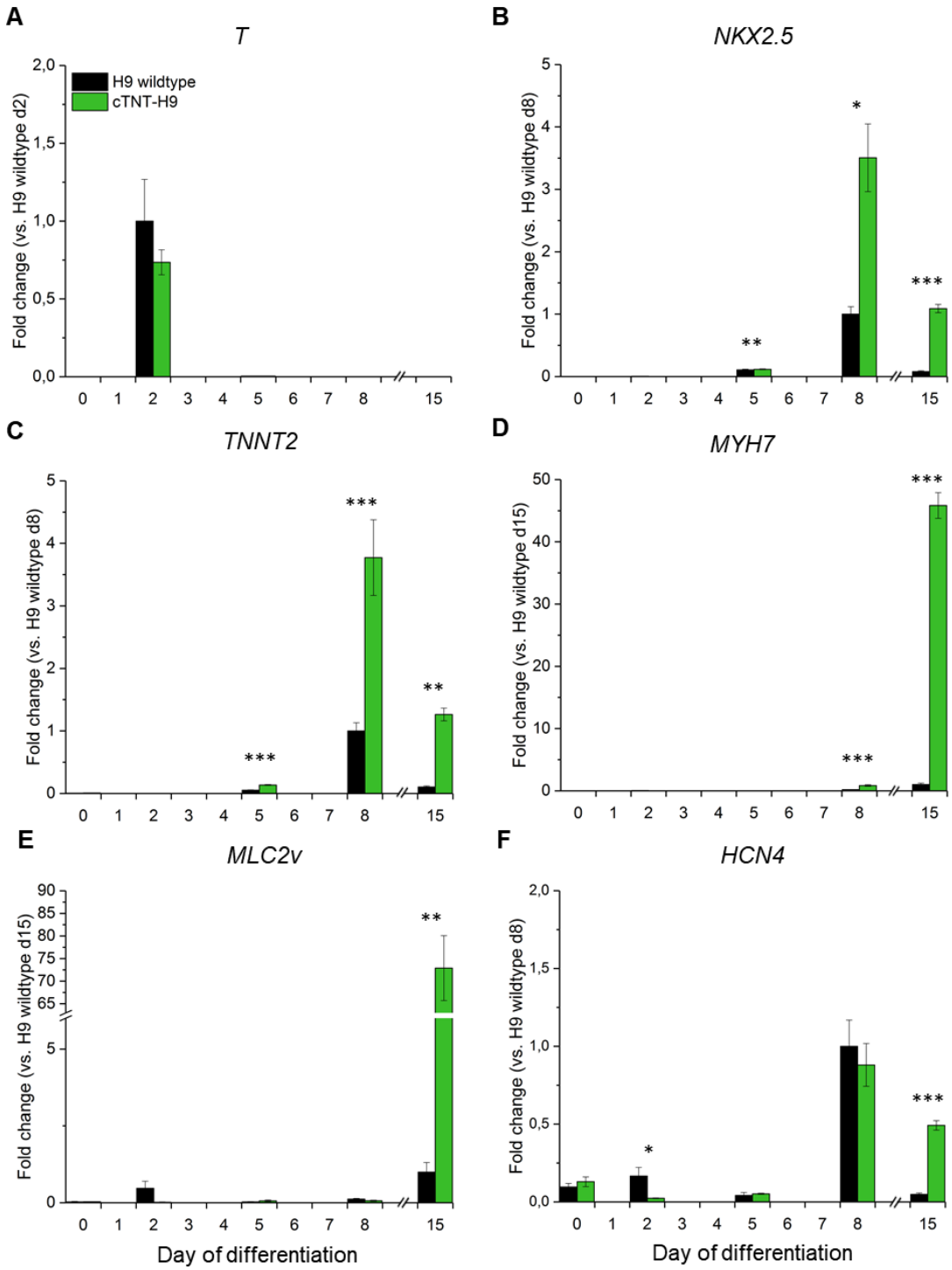

Fig. 20: Marker gene expression of H9- and cTNT-H9-derived cardiac cultures grown on Matrigel®. Expression levels of *T* (A), *NKX2.5* (B), *TNNT2* (C), *MYH7* (D), *MLC2v* (E) and *HCN4* (F) were compared via qRT-PCR analyses at various days of differentiation of H9 (black bars) and cTNT-H9 (green bars) cells. Values were normalized to 18sRNA and to the highest expression level of each target gene achieved with the H9 wildtype cells. Results of one out of two independent experiments are shown. Statistical significance was determined for all values above baseline level by Student's t-test within one experiment. * $p < 0.05$, ** $p < 0.01$, *** $p < 0.001$; d, day.

3.3 Impact of exposure to various X-ray doses on cardiac differentiation of cTNT-H9 cells

Preliminary experiments with the H9 cells indicated that 1 Gy X-rays lead to decreased cardiac gene expression at all differentiation stages starting from *T* to *MLC2v* compared to controls (App. Fig. 4), but no overall effect was detected regarding the beat rates (n = 4) and all clusters were responding to isoproterenol (data not shown).

Pluripotent cTNT-H9 cells were irradiated with 0 (sham), 0.1, 1 or 2 Gy and seven days later, cardiac differentiation was initiated. From n = 8 experiments, there was one outlier experiment with marker gene expressions clearly differing from the other seven experiments and thus, it was not taken into account for the comparison. In another experiment, cardiac differentiation of cTNT-H9 cells exposed to 0.1 Gy failed. Here, starting from *MESP1*, all cardiac markers were significantly decreased. Therefore, only six out of eight experiments were considered to investigate the impact of 0.1 Gy and data of seven experiments were compared for the 1 and 2 Gy doses.

Upon irradiation with 2 Gy, massive cell death occurred already within the first 24 h as indicated by a high number of free-floating cells in the culture medium. The surviving colonies were very small compared to control (App. Fig. 5). To seed the same amount of cells for differentiation initiation, more petri dishes were prepared for the 2 Gy irradiation. Still, in two experiments the cell number was not sufficient and therefore, no RNA sample could be taken for 2 Gy at one (or two) time point(s).

Pluripotency before initiation of differentiation (day 0) was evidenced via immunocytochemical detection of OCT4, SOX2 and NANOG protein (data not shown).

3.3.1 qRT-PCR based analyses of cardiac marker genes upon exposure of pluripotent cTNT-H9 cells

The pluripotency markers *POU5F1* and *NANOG* were expressed in undifferentiated cells. Upon initiation of differentiation, their level was steadily decreased and at day 5, they were no longer expressed (App. Fig. 6 A, B). No general radiation-induced alteration of their expression was observed in the pluripotent cells at day -4, however, at day 0, their expression was by trend reduced upon the 1 and 2 Gy exposure.

For all following markers, dose effect-curves are shown at those day(s) when their expression was above baseline levels. For a detailed time course of their expression for each experiment, column scatter plots are depicted in the appendix (App. Fig. 6 and 7).

At day 2, no alterations were detected for *T* expression upon irradiation with any dose (Fig. 21). *MESP1* expression was not affected by 0.1 Gy, however, upon 1 Gy, it was decreased in five experiments and 2 Gy led to its reduction in all seven experiments (Fig. 21).

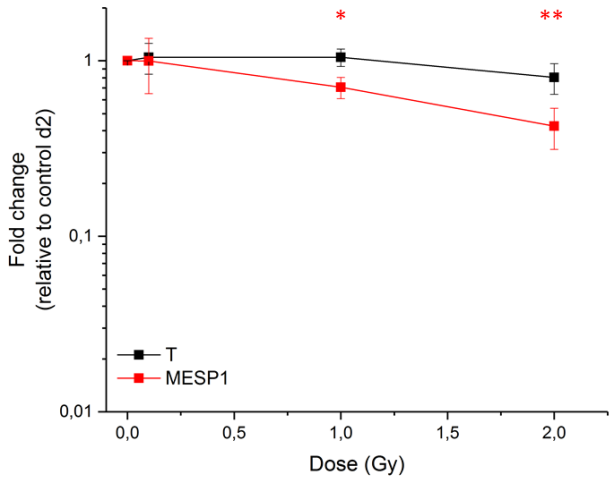

Fig. 21: Dose effect-curves of *T* and *MESP1* expression at day 2 of differentiation. cTNT-H9 cells were irradiated with 0 (sham control), 0.1, 1 or 2 Gy X-rays and seven days later, they were differentiated. Expression of *T* (black) and *MESP1* (red) at day 2 was analyzed via qRT-PCR. Values were normalized to 18sRNA and to the expression level of controls at day 2 of each gene in each experiment. Medians with the standard error of the median are shown. Student's t-test was performed among experiments; * $p < 0.05$; ** $p < 0.01$.

NKX2.5 expression was not affected at day 5 and 8 by 0.1 and 1 Gy exposure (Fig. 22 A). However, at day 15, it was decreased upon both doses and upon 2 Gy, it was decreased at day 8 and 15.
Already before differentiation, *HCN4* mRNA was detected (App. Fig. 6 F). When cardiac differentiation was initiated, its expression first decreased, then increased again after day 5 accompanying the onset of spontaneous beating between day 6 to 8. By trend, *HCN4* amount was decreased at day 15 in cultures derived from irradiated cTNT-H9 cells (Fig. 22 B).

TNNT2 expression appeared at day 5 and peaked at day 15 (Fig. 22 C). Starting from day 6, GFP-fluorescence could be observed in the cardiac clusters at the microscope confirming the expression of cTNT. Upon 0.1 Gy, no significant changes were observed at day 8, however, at day 15, in five out of six experiments *TNNT2* expression was decreased at least 2.0-fold. At day 8 and 15, it was decreased upon 1 Gy in six out of seven experiments, and upon 2 Gy in all seven experiments.

Markers of immature, but also atrial CM, namely *MYH6*, *MLC2a* and *NPPA* appeared at day 8 and peaked at day 15 in control samples (Fig. 22 D - F), whereas more mature and ventricular markers, *MYH7* and *MLC2v*, were detected only at day 15 (Fig. 23).
Exposure to 0.1 Gy did not lead to altered *MYH6*, *MLC2a* and *NPPA* expression at day 8 (Fig. 22 D - F). However, at day 15 expression of all three markers was reduced.

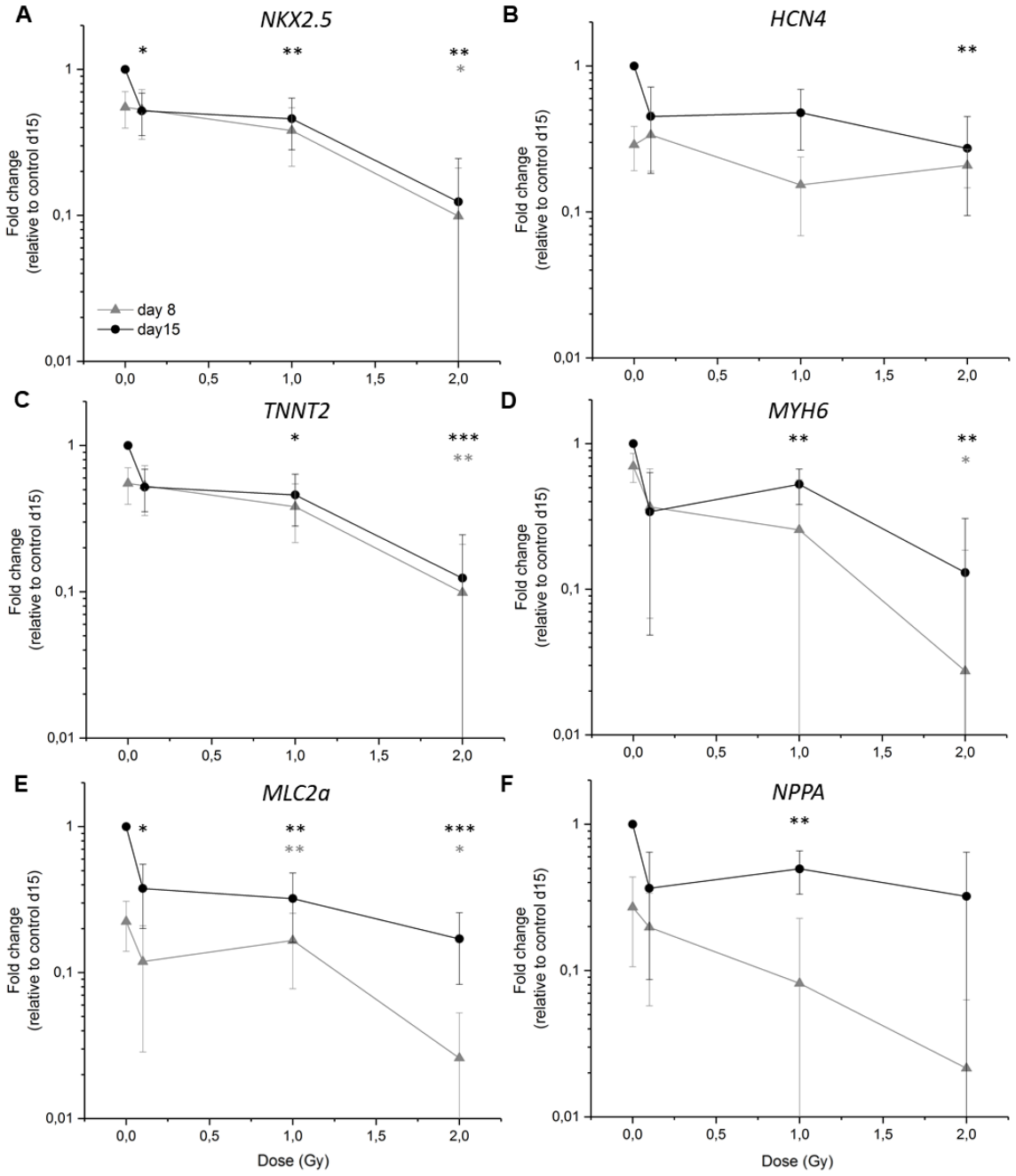

Fig. 22: Expression of cardiac marker genes in differentiating cTNT-H9 cells upon exposure to various X-ray doses. Seven days after irradiation with 0 (sham control), 0.1, 1 or 2 Gy X-rays, cTNT-H9 cells were differentiated. Dose effect-curves are shown for *NKX2.5* (A), *HCN4* (B), *TNNT2* (C), *MYH6* (D), *MLC2a* (E) and *NPPA* (F) expression at day 8 (gray) and 15 (black) of differentiation as analyzed via qRT-PCR. Values were normalized to 18sRNA and to the expression level of controls at day 15 for each gene in each experiment. Medians with the standard error of the median are shown and statistical significance among experiments was determined with Student's t-test; * $p < 0.05$; ** $p < 0.01$; *** $p < 0.001$; d, day.

In cultures derived from 1 Gy-irradiated cTNT-H9 cells, cardiac gene expression varied strongly among experiments (Fig. 22 D - F and Fig. 23). However, by trend all of them were decreased compared to controls. This was even more pronounced upon exposure to 2 Gy where a clear reduction of *MYH6*, *MLC2a*, *NPPA*, *MYH7* and *MLC2v* expression was detected.

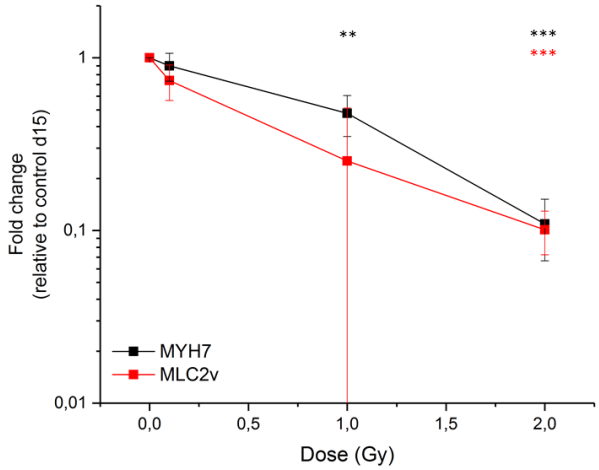

Fig. 23: Expression of ventricular marker genes at day 15 of differentiation of irradiated cTNT-H9 cells. Seven days after irradiation with 0 (sham control), 0.1, 1 or 2 Gy X-rays, cTNT-H9 cells were differentiated. Expression of *MYH7* (black) and *MLC2v* (red) were analyzed via qRT-PCR. Values were normalized to 18sRNA and for each target gene to expression levels of controls at day 15. Student's t-test was performed among experiments; ** $p < 0.01$; *** $p < 0.001$; d, day.

3.3.2 Impact of the exposure on the expression and structural organization of cardiac proteins

To investigate whether X-ray exposure of hESCs has an impact on the structural organization of cardiac proteins, α-Actinin, cTNT and MLC2a were investigated via immunocytochemistry in the day 15-CM. The sarcomeric structures needed for contraction were observed and no difference between controls and irradiated samples was detected (data not shown).

In contrast to controls and CM derived from 0.1 and 1 Gy-irradiated cTNT-H9 cells, those derived from 2 Gy-irradiated cells did not express MLC2v protein (Fig. 24).

HCN4 was stained, too, but the signal was not clearly distinguishable from noise (App. Fig. 8). A positive control of the antibody confirmed its specific binding to HCN4, however (App. Fig. 9).

Gap junctions allow the propagation of electrical activity in the heart and are built up of connexins, with Cx43 being the most abundant one in the mammalian heart (Gros and Jongsma, 1996). Its immunocytochemical detection revealed only few Cx43-foci in the cell membranes of the CM (Fig. 25, right side; representative picture of controls) and no differences between controls and irradiated cells were detected. In non-cardiac cells, the Cx43-signal was stronger not only in the membranes, but also in the whole cytoplasm and more concentrated near the nucleus (Fig. 25, upper left side), however, no foci as in the cardiac cell membranes were detected.

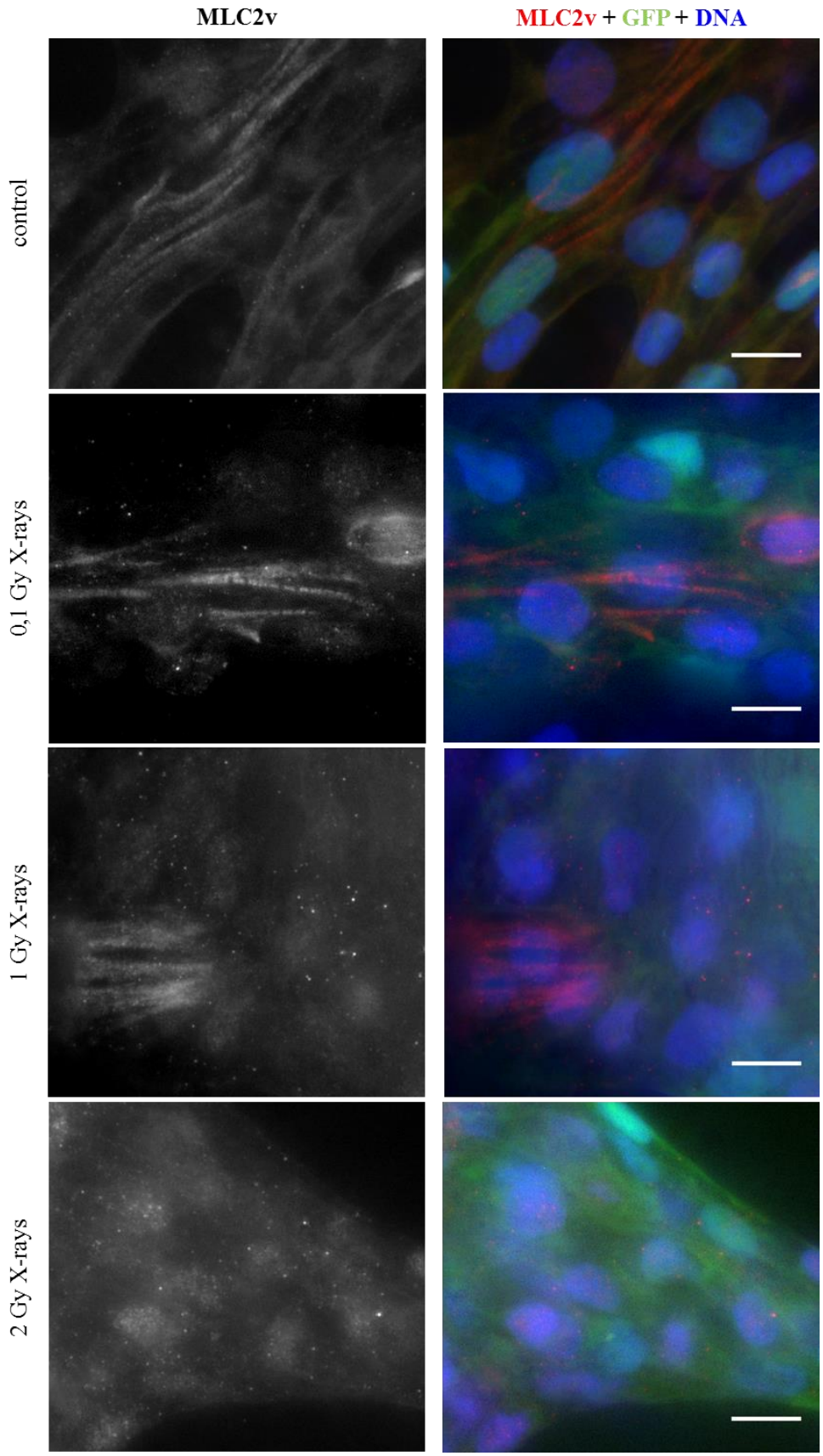

Fig. 24: MLC2v protein expression in sham and irradiated cTNT-H9-derived CM. cTNT-H9 cells were exposed to 0, 0.1, 1 or 2 Gy X-rays and seven days later they were differentiated. At day 15 of differentiation, cells were fixed and stained for MLC2v (red). DNA was counterstained with Hoechst-33342 (blue). Green, GFP-expressing CM. Scale bars: 10 µm.

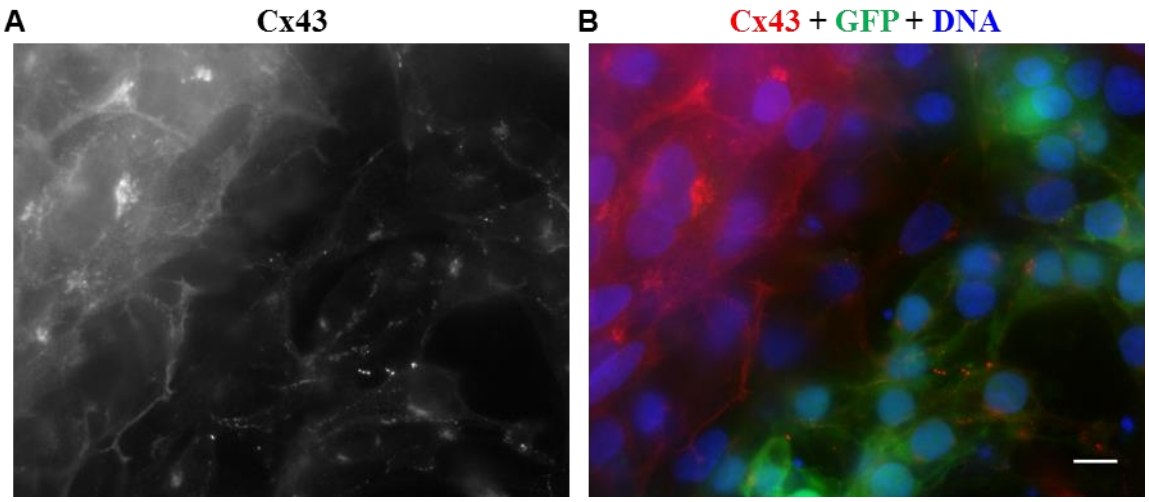

Fig. 25: Connexin 43 in cTNT-H9-derived cardiac cultures. At day 15 of differentiation, cardiac cultures were fixed and stained for Cx43 (A). B) Merged picture with DNA (blue) and GFP-expressing cTNT-H9-derived CM (green). Scale bar: 10 µm.

3.3.3 Functional analyses of beating cardiac clusters derived from exposed cTNT-H9 cells

Beat rates of the cardiac clusters were analyzed at day 8, 10 (or 11) and 15 of differentiation with the software cBRA (Nitsch et al., 2018) and results of each experiment are depicted in Fig. 26 since results varied greatly among experiments. In general, no marked overall differences were observed in the beat rates of control clusters and those derived from 0.1 and 1 Gy-irradiated cTNT-H9 cells. However, in one experiment (Fig. 26 A), a low differentiation efficiency was observed following the 1 Gy exposure: only ten beating clusters developed until day 8 with beat rates comparable to controls and twelve clusters until day 15 with a significantly lower mean beat rate.

Beat rates derived from cells exposed to 2 Gy were distinguishable from controls in most experiments: in one experiment no beating clusters were detected at day 8, one at day 10 and three at day 15 (Fig. 26 A), in two other experiments they were beating faster at day 15 compared to controls (Fig. 26 B, C) and in another one, they were beating faster at day 8 and spanning a smaller range than controls at day 15 (Fig. 26 D).

In two experiments (Fig. 26 D, E) a different cluster morphology was observed: Here, only few compact round clusters formed, but rather thin layers of CM (App. Fig. 10 A - C) that were - in some samples - spanning almost the whole culture dish starting from day 10. Thereby, the majority of the CM was connected with each other and beat rates were beyond physiological rates (between 150 and more than 300 bpm).

As stated previously, in the last experiment (Fig. 26 E), differentiation of the 0.1 Gy irradiated cTNT-H9 was not successful: at day 8 no cardiac clusters were detected, at day 11 there was one and at day 15 there were five beating clusters with a “normal” morphology (i.e. compact beating clusters, App. Fig. 10 D).

Analyses of the beat variability did not show a significant IR-induced effect. Instead, for each experiment a different trend was observed (data not shown).

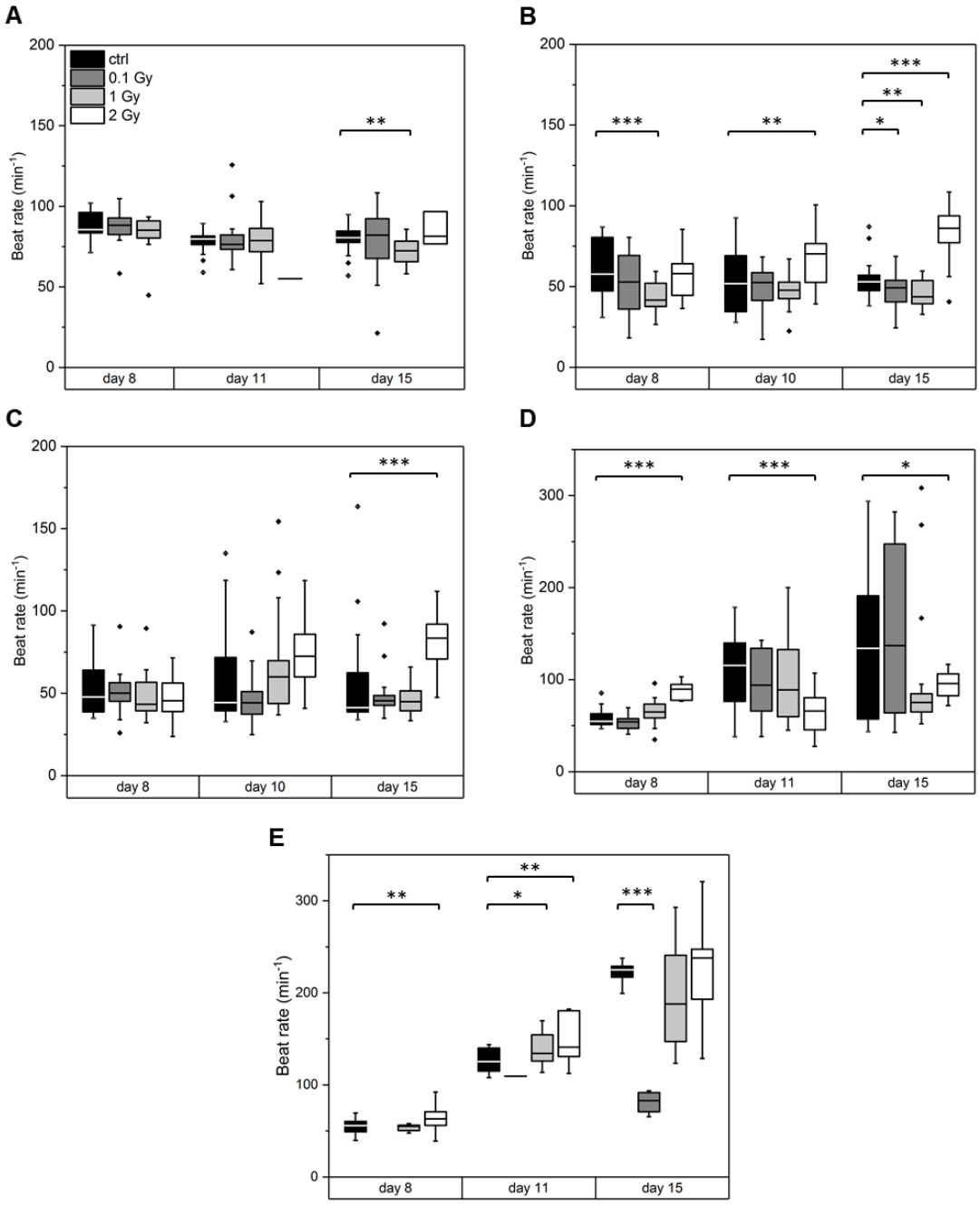

Fig. 26: Beat rates of cardiac clusters derived from cTNT-H9 cells exposed to various X-ray doses. Pluripotent cTNT-H9 cells were irradiated with 0 (control, black boxes) 0.1 (dark gray boxes), 1 (light gray boxes) and 2 Gy (white boxes) and differentiated seven days later. At day 8, 10 or 11 and 15 of differentiation, videos of the beating clusters were recorded and analyzed with the software cBRA. Each plot shows the results of one experiment. Statistical significance was determined with Student's t-test, * $p < 0.05$; ** $p < 0.01$; *** $p < 0.001$. Boxes, 25 % quartile – median – 75 % quartile. Whiskers, 1.5 coefficient.

3.3.4 Impact of isoproterenol on cardiac clusters derived from irradiated cTNT-H9 cells

Addition of 1 µM isoproterenol led to a positive chronotropic response of the cardiac clusters in controls (Fig. 27 A) and irradiated cultures (Fig. 27 B - D). Only one cluster derived from cTNT-H9 cells exposed to 0.1 Gy showed a rather abnormal beat rate before and no enhanced beat rate after addition of isoproterenol (Fig. 27 B, cluster #8). Furthermore, two clusters derived from 1 Gy- (Fig. 27 C, cluster #3, 4) and one cluster derived from 2 Gy-irradiated cells (Fig. 27 D, cluster #4) did not increase their beat rates. However, when the same clusters were analyzed one and two weeks later (at days 22 and 29), their beat rates increased upon addition of isoproterenol (data not shown).

Control clusters were beating around 43 % upon addition of isoproterenol and those derived from 0.1 or 1 Gy-irradiated cTNT-H9 cells were beating about 54 % or 51 % faster, respectively. The lowest increase was observed after the 2 Gy exposure: clusters were beating only about 25 % faster with isoproterenol.

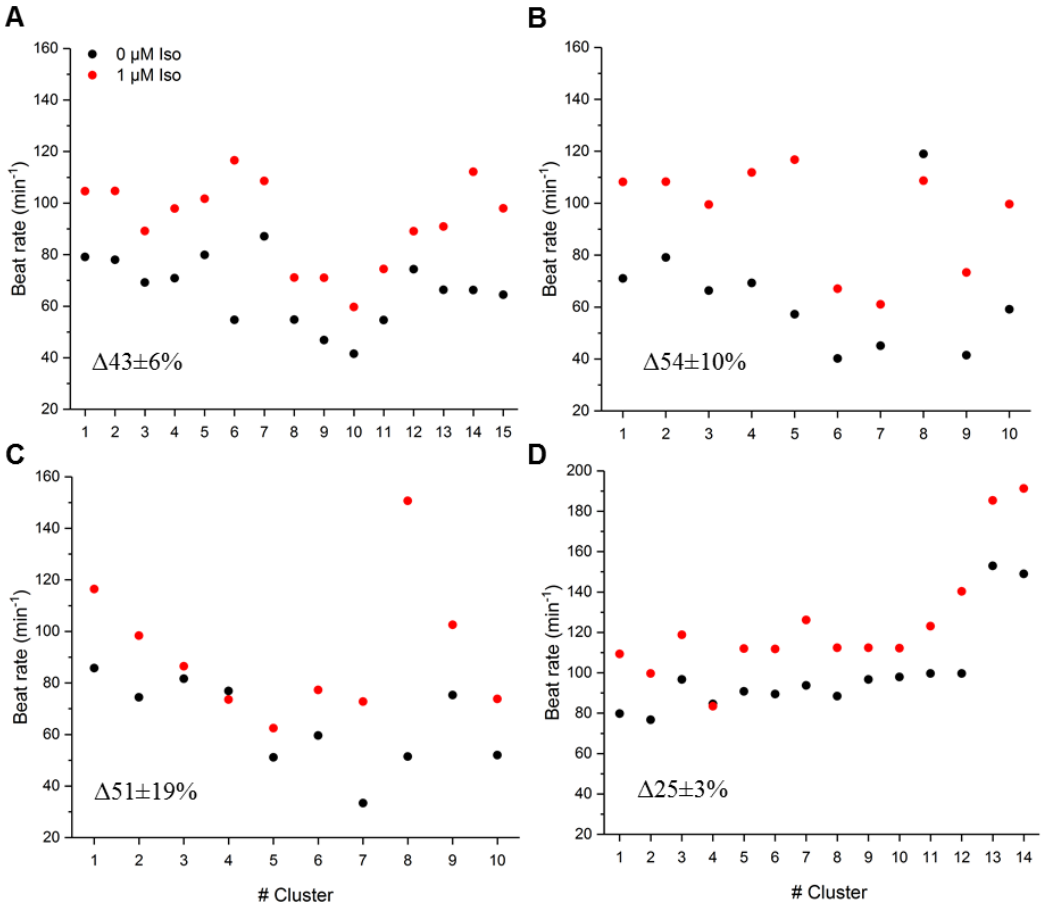

Fig. 27: Increased beat rates upon addition of isoproterenol to cardiac cultures derived from irradiated cTNT-H9 cells. Seven days before initiation of cardiac differentiation**,** cTNT-H9 cells were exposed to 0 (sham control, A), 0.1 (B), 1 (C) and 2 Gy X-rays (D). At day 15 of differentiation, videos of beating cardiac clusters were recorded before (black) and after addition of 1 µM isoproterenol (red). For each dose, the mean difference (Δ) of the beat rates is indicated with the standard error of the mean in percent.

3.4 qRT-PCR array-based pathway analyses of alterations in Stem Cell and DNA Damage Response Signaling upon X-ray exposure of cTNT-H9 cells

To investigate possible mechanisms underlying the described alterations in cardiac markers upon X-ray irradiation (see section 3.3), pluripotent cTNT-H9 cells were irradiated with 1 Gy and RNA samples were collected after 1 h, 6 h, 24 h and 7 days in n = 6 independent experiments. The samples for each time point were pooled and analyzed with a qRT-PCR array containing 84 different primers for targets either of Stem Cell Signaling (SCS) or of DNA Damage Response (DDR) Signaling. For analyses, pooled controls for each time point were set as one control group automatically.

3.4.1 Alterations in Stem Cell Signaling

Three of the proposed housekeeping genes were used for normalization (*GAPDH*, *HPRT1*, *RPLP0*). 1 h after exposure to 1 Gy, drastic gene expression changes occurred with most genes being upregulated compared to controls (Table 6 and App. Fig. 11). *SP1* was markedly affected with a 42-fold downregulation. Most genes with altered expression levels belong to TGF-β signaling and WNT signaling, but also FGF, NOTCH and Sonic Hedgehog signaling were affected. 6 h and 24 h after exposure, the expression of many genes was decreased compared to controls and 7 d after exposure, many genes were again upregulated with the most dramatic changes in gene expression of the activin receptors *ACVR1*, *ACVR1B*/*C* (5.0- to 8.0-fold upregulation) and *ACVR2A/B* (18- and 12-fold upregulation, respectively) and of *FZD3* (13-fold upregulation).

It has to be mentioned that sham controls of each time point were treated as one group by the algorithm in the Data Analysis Center at www.qiagen.com. However, it was not clear how they were summarized. Individual analysis of each sham control revealed that their gene expressions varied markedly. Especially 1 h after sham irradiation, many genes were elevated compared to controls of later time points (data not shown). Since cardiac differentiation was initiated seven days after irradiation in this study, this time point was further investigated. Gene expression changes were again analyzed comparing only the sham control of day 7 with the respective irradiated sample. Most genes that were already identified to be upregulated, were confirmed with this method. Still, six of them were not confirmed (*CREBBP*, *FZD1/8/9*, *IL6ST*, *LTBP3*), but four additional ones were found (*FZD5*, *GLI1*, *NFATC3*, *SMAD1*).

Genes connected to (early) cardiac differentiation that were upregulated seven days after irradiation according to the qRT-PCR array are listed in Table 7 and were further investigated in each of the samples that were pooled for the arrays (subsequently termed “individual array samples”) and in the samples of the experiments described in section 3.3.

Table 6: Stem Cell Signaling-related genes with altered expression levels after exposure to 1 Gy X-rays compared to sham controls at different time points (all sham controls were calculated as one control group). Genes whose expression is altered more than 2-fold are shown (black: upregulated, blue: downregulated)

	1 h	**6 h**	**24 h**	**7 d**
FGF signaling	*FGFR1-4, STAT3*	*FGFR1-3*	*STAT3* *FGFR3/4,*	*FGFR1-3, STAT3*
TGF-β signaling	*ACVR1, ACVR1B/C, ACVR2A/B, ACVRL1, AMHR2, BMPR1A/B, BMPR2, ENG, LTBP3/4, (RGMA), SMAD7/9, TGFBRAP1*	*LTBP1, SMAD1* *ACVR1C, ACVR2A/B, BMPR1A, BMPR2, ENG, SMAD6*	*LTBP1-4, SMAD3/7, TGFBR2/3* *ACVR1, ACVR1B/C, ACVR2A/B, BMPR1A/B, BMPR2,*	*ACVR1, ACVR1B/C, ACVR2A/B, ACVRL1, BMPR1A/B, BMPR2, ENG, LTBP1/3* *SMAD6, TGFBRAP1*
WNT signaling	*BCL9, BCL9L, CTNNB1, FZD1/2/7/8/9, LEF1, LRP5, PYGO2* *FZD3*	*FZD3, LRP5/6* *BCL9, BCL9L, CTNNB1, FZD1/2/7, LEF1*	*FZD3, LRP6, TCF7* *BCL9, BCL9L, CTNNB1, FZD1/2, LEF1*	*BCL9, BCL9L, CTNNB1, FZD1/3/6-9, LEF1, LRP6*
NOTCH signaling	*EP300, NOTCH1/3, PSEN2, PSENEN*	*NOTCH1/2* *EP300*	*NOTCH1/2* *EP300*	*EP300, NOTCH1/2*
Sonic Hedgehog signaling	*GLI1-3, SMO*			*GLI2/3* *SMO*
Other	*CDX2, CREBBP, E2F5, EP300, IL6ST, NFATC1/3, PTCHD2, RBL1, RBPJL, RGMA, STAT3* *SP1*	*CREBBP, LIFR, NFATC4, RBL2, SP1* *EP300*	*LIFR, STAT3, NFATC1/4, RBL2, RBPJL, SP1, STAT3* *CREBBP, E2F5, EP300*	*CREBBP, E2F5, EP300, IL6ST, LIFR, NFAT5, NFATC1/4, RBL2, SP1, STAT3*

Table 7: Stem Cell Signaling-related genes which were more than 2-fold upregulated 7 days after irradiation and connected to cardiac development.

Upregulated gene	**Link to cardiac development**	**Reference/species**
FGFR1	crucial in heart development	Dell'Era et al., 2017 (mouse)
IL6ST	activation of gp130 leads to phosphorylation of STAT3 which directly controls NKX2.5 expression	Snyder et al., 2010 (mouse)
LEF1	OCT4 and TCF/LEF bind to Mesp1 promoter leading to its expression	Li et al., 2013 (mouse)
NOTCH1	inhibits mesoderm formation	Schroeder et al., 2006 (mouse)
SP1	involved in control of Mesp1 expression	Beketaev et al., 2015 (mouse)

3.4.2 Verification of the SCS-array results

FGFR1

The 6.4-fold upregulation of *FGFR1* seven days after irradiation observed with the SCS-array could not be confirmed via individual qRT-PCR (data not shown). Analyzing the experiments of section 3.3 for *FGFR1*, no marked differences between pluripotent and differentiated cells were observed (App. Fig. 12 A) as well as between control, 0.1 and 1 Gy-irradiated samples. An altered amount of *FGFR1* mRNA was, by trend, detected at day 2, 5 and 15 following the 2 Gy exposure, however, the magnitude of the alteration was low.

IL6ST

Activation of glycoprotein 130 (gp130), the receptor protein encoded by *IL6ST*, leads to the activation of STAT3 also in the heart (Fischer and Hilfiker-Kleiner, 2008). According to the results of the SCS-array, *IL6ST* expression was increased 2.1- to 3.5-fold 1 h and 7 d after irradiation with 1 Gy. qRT-PCR analyses of the individual array samples did not confirm these results (data not shown).

In the experiments described in section 3.3 (n = 7) *IL6ST* expression steadily increased until day 15 (Fig. 28). In cultures derived from exposed cTNT-H9 cells, *IL6ST* expression was decreased in all but one experiment at day 8 and 15. Following the 2 Gy exposure, the trend of its reduction was already visible at day 2 (low magnitude) and at day 8 it was reduced with statistical significance according to Student's t-test within three experiments and at day 15 within six experiments.

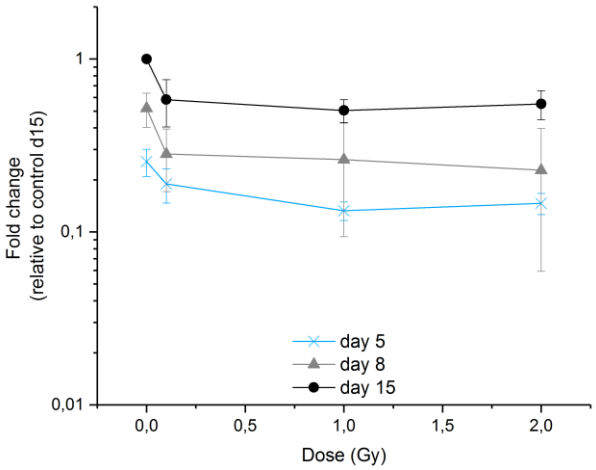

Fig. 28: qRT-PCR-based expression analyses of *IL6ST* during cardiac differentiation of irradiated cTNT-H9 cells. Cells were irradiated with 0 (sham control), 0.1, 1 and 2 Gy X-rays and seven days later, differentiation was initiated (n = 7). Values were normalized to 18sRNA and day 15-control levels in each experiment. Medians with the standard error of the median are shown. Student's t-test was performed among experiments; ** $p < 0.01$, *** $p < 0.001$; d, day.

LEF1

Expression of *LEF1* was very low in the SCS-array (CT-values between 28 and 32). qRT-PCR of the individual array samples showed that *LEF1* was nearly not detectable (data not shown). Also in the experiments of section 3.3, it was not expressed in the pluripotent cells. However, with initiation of differentiation, its expression appeared at day 2 and peaked at day 5 in controls. No differences were observed between controls, 0.1 and 1 Gy-irradiated samples at these time points. However, the 2 Gy-exposed cells showed an increased level at day 2 and 5. At day 15, there was a low magnitude-reduction of *LEF1* mRNA in the 1 and 2 Gy-irradiated cells (App. Fig. 12 B).

NOTCH1

NOTCH1 levels were very low according to the SCS-array. In contrast, it was clearly expressed in the individual array samples, but no IR-induced effect was detected up to 7 days (data not shown). In the experiments of section 3.3, *NOTCH1* mRNA was already present in the pluripotent cells and during differentiation, its level varied with low magnitude. No radiation-induced effects were detectable, except for the day 15 samples resulting from the 2 Gy-irradiated cells showing an increased amount of *NOTCH1* mRNA by trend (App. Fig. 12 C).

SP1

According to the SCS-array, *SP1* expression was downregulated 1 h after irradiation. However, CT-values were low in controls and no expression was detected in the irradiated samples at this time point. Changes in CT-values at 6 h, 24 h and 7 d were of low magnitude and normalization resulted in a 4.9-

fold increase of *SP1* in irradiated samples after 7 d. Individual qRT-PCR analyses did not confirm this, instead, *SP1* expression varied and no overall effect was observed (data not shown).
Investigating *SP1* expression in the experiments described in section 3.3 did not show any alterations, neither between pluripotent and differentiated cells, nor between controls and irradiated samples (App. Fig. 12 D).

ACVR1B and ACVR2B

Using the same SCS-array, Luft et al. (2017) demonstrated the downregulation of activin receptors, like *ACVR1/2B*, 24 h after irradiation of H9 cells. Comparable results were obtained at 24 h post exposure in the study at hand using cTNT-H9 cells. However, analyses of the individual array samples for *ACVR2B* did not confirm this. Likewise, the 11-fold increase at day 7 revealed by the array, was not confirmed (App. Fig. 13 A). Instead, in two experiments, there was a 2.0- and 3.0-fold decrease in *ACVR2B* mRNA.
CT-values for *ACVR1B* were very low in the individual array samples. The 5.0-fold increase seven days after irradiation, which was observed with the array, was not confirmed (App. Fig 13 B).

3.4.3 Alterations in DNA Damage Response Signaling

Depending on the normalization method, the results differed based on the sensitivity of the method. Therefore, two methods were chosen and compared. In one approach, values were normalized to the housekeeping genes *B2M*, *GAPDH* and *HPRT1* (method 1); in the other approach, values were normalized to genes whose expressions did not change among all samples, namely *NBN*, *FEN1*, *PPP1R15A*, *FANCA* and *H2AFX* (method 2). Comparison of the two normalization methods led to an overlapping set of multiple genes whose levels were altered at least 2-fold upon irradiation (Table 8). Generally, method 1 was more sensitive than method 2.

At 1 h after exposure, all 14 genes that were revealed to be upregulated with method 2, were also identified with method 1. However, the latter resulted in additional 21 upregulated genes.
Five of the 14 genes are related to apoptosis, four to cell cycle (*CDKN1A*, which encodes p21, is related to both, apoptosis and cell cycle) and four to various DNA repair pathways. Furthermore, the genes encoding ATM and ATR, which are known DNA damage sensors, as well as *BARD1* and *BRCA1*, whose proteins form a complex to regulate a variety of functions (Gudmundsdottir and Ashworth, 2006), were upregulated. *XPA* and *XPC* were decreased according to both methods. However, CT-values of these two genes were low in controls and irradiated samples, indicating that they were almost not expressed. Therefore, they were not taken into account for further analyses.
Results at 6 h after irradiation varied the most between the two methods. Only 4 genes were found to be upregulated with both methods and their proteins are involved in apoptosis, cell cycle and Nucleotide Excision Repair pathway (NER). Only one gene, namely *MAPK12*, was downregulated.

24 h after exposure, 12 genes were upregulated with both methods, among them *ATM* and *ATR*. Most of the other upregulated genes are related to cell cycle and apoptosis.

Seven days after exposure, there was again a very high number of upregulated genes. 18 genes were upregulated according to both methods, among them *ATM*, *ATR*, *BARD1* and *BRCA1*. Most of the other upregulated genes are related to cell cycle and apoptosis.

Table 8: DNA Damage Response Signaling-related genes with more than two-fold altered expression levels according to both normalization methods after irradiation of cTNT-H9 cells (black: upregulated genes; blue: downregulated genes).

		1 h	6 h	24 h	7 d
Apoptosis		*BAX, BBC3, CDKN1A, DDIT3, GADD45G*	*BBC3, CDKN1A*	*BAX, BBC3, CDKN1A*	*BBC3, CDKN1A, CSNK2A2*
Cell cycle		*BARD1, CDC25C, CDK7, CDKN1A*	*CDKN1A, HUS1*	*CDC25C, CDK7, CDKN1A, GADD45A, HUS1*	*BARD1, CDC25C, CDK7, CDKN1A, CSNK2A2, HUS1, MCPH1, RAD17*
DNA damage sensors		*ATM, ATR* *(XPC)*		*ATM, ATR*	*ATM, ATR*
DNA repair	**BER**	*APEX1*		*APEX1*	*APEX1*
	DSB-repair	*BLM, BRCA1*		*BRCA1*	*BLM, BRCA1*
	MMR				*EXO1, MBD4*
	NER	*DDB2* *(XPA, XPC)*	*DDB2*	*DDB2*	*DDB2*
Genomic stability		*BARD1, BRCA1*		*BRCA1*	*BARD1, BRCA1*
Other			*(MAPK12)*		*ATRX, CSNK2A2*

3.4.4 Verification of the DDR-array results

ATM

ATM expression was increased at 1 h, 24 h and 7 d after irradiation according to the DDR-array. In three out of the six experiments that were pooled for the array, its expression was investigated via individual qRT-PCR. Unlike the results of the array, *ATM* expression remained at the same level as in controls except for one experiment (App. Fig. 14, Experiment 1).

In addition, ATM protein expression was investigated via immunocytochemistry seven days after irradiation in cells that were seeded only for this purpose. No marked difference between controls and irradiated samples were observed at the microscope (App. Fig. 15). To analyze the intensity of the ATM-signal, 20 Z-stacks were taken using the same exposure time in sham and irradiated samples and intensity was measured in average intensity projections with the software Fiji. The measurements revealed a trend towards an increased ATM-signal intensity upon irradiation (App. Table 11), however, this effect was not statistically significant according to Student's t-test.

CDKN1A

qRT-PCR analyses of *CDKN1A* expression in the individual array samples confirmed the results of the DDR-array by trend: At 1, 6 and 24 h after irradiation, *CDKN1A* expression was markedly increased in the irradiated samples compared to controls in most of the six experiments (Fig. 29). However, seven days after irradiation, *CDKN1A* expression was not elevated compared to controls anymore.

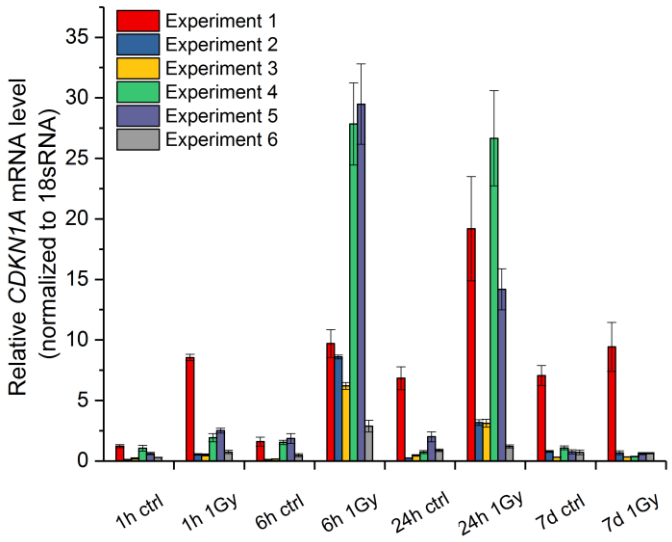

Fig. 29: Individual qRT-PCR analyses of *CDKN1A* expression. cTNT-H9 cells were irradiated with 0 (sham control) or 1 Gy X-rays and RNA samples were taken at 1 h, 6 h, 24 h and 7 d after irradiation (n = 6).

At day 7 after irradiation, immunocytochemical staining of p21 was performed to verify the results of the array (7.0- to 8.8-fold increase seven days post irradiation). Neither in controls nor in 1 Gy-irradiated cells p21 protein was observed (App. Fig. 16).

3.5 Impact of an X-ray exposure on important signaling pathways of cardiac differentiation

Cardiac differentiation is the result of a complex interaction between several signaling pathways. As shown in section 3.3, differentiation is impaired by an X-ray exposure of the hESCs. In addition to the qRT-PCR-arrays of the previous chapter, WNT signaling as well as miR-1 expression were investigated in order to reveal further mechanisms that are impaired by X-ray exposure.

3.5.1 WNT signaling

WNT11-mediated non-canonical WNT signaling plays a crucial role in cardiac differentiation (Mazzotta et al., 2016; Pandur et al., 2002b; Terami et al., 2004). Its expression was investigated via qRT-PCR in the experiments described in section 3.3. *WNT11* was markedly expressed at day 5 and peaked at day 8 (Fig. 30 A). Irradiation of the cTNT-H9 cells with 0.1 Gy led to a rather decreased expression at day 8, and at day 15 this reduction was enhanced. Upon exposure to 1 and 2 Gy, there was a clear and statistically significant reduction of *WNT11* mRNA level from day 5 to 15.

Expression of another WNT-member involved in the non-canonical pathway, namely *WNT5B*, did not reveal an IR-induced effect (Fig. 30 B). Only at day 15, its expression was decreased by trend in cultures derived from 2 Gy-irradiated cells.

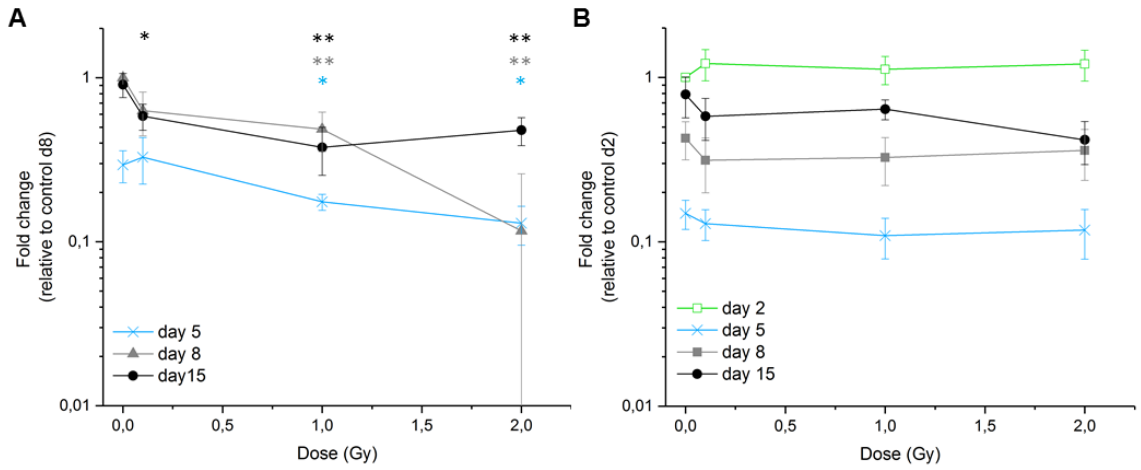

Fig. 30: Expression of *WNT11* and *WNT5B* during cardiac differentiation of cTNT-H9 cells upon irradiation. Seven days before initiation of differentiation, cTNT-H9 cells were exposed to 0 (sham control), 0.1, 1 or 2 Gy X-rays. Dose effect-curves of *WNT11* (A) and *WNT5B* (B) expression at several days of differentiation are shown. Values were normalized to 18sRNA and to control samples with the highest expression level. Medians with the standard error of the median are shown and Student's t-test was performed among experiments; * $p < 0.05$, ** $p < 0.01$; d, day.

On the protein level, no difference in WNT11 expression was observed between controls and irradiated samples at day 15 (see App. Fig. 17 D for exemplary picture of controls). Instead, a time-dependent difference was observed between day 5, 8 and 15 samples. In cells with low GFP-levels (indicating the onset of cTNT expression) at day 5 and 8, WNT11 was detected all over the cells and it accumulated in several foci per cell (App. Fig. 17 A, B). The surrounding non-GFP cells showed a similar pattern, but the nuclear WNT11 signal was lower compared to GFP cells. In contrast, cells with a high GFP-level at day 8 and 15, which were already beating, showed a different pattern: whereas there was a uniform higher signal in the nucleus of most of these cells, no foci were detected anymore. However, the surrounding non-GFP cells had a low overall WNT11 signal, but showed a few (or at least one) big foci mostly near the nucleus (App. Fig. 17 C, D).

3.5.2 microRNA-1

miR-1 plays a central role in cardiac development (Fu et al., 2011; Zhao et al., 2007, 2005). Its expression was investigated via qRT-PCR analyses of the experiments described in section 3.3. Before initiation of differentiation, *miR-1* was not detected in controls and irradiated samples (data not shown). It first appeared at day 8 and increased until day 15. (Fig. 28 A). For the 1 Gy samples, there was a consistent trend towards a decreased *miR-1* expression. In contrast, the data were inconclusive

for the 0.1 and 2 Gy samples: in three out of six experiments, the amount of *miR-1* was reduced, in the other three, it was several fold increased compared to controls leading to high standard errors.

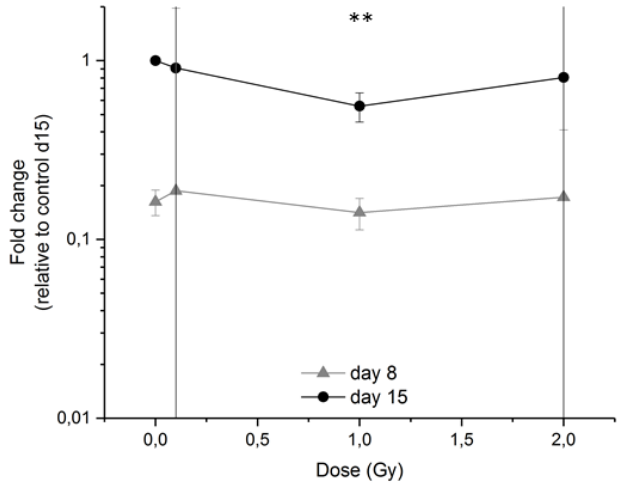

Fig. 31: *miR-1* expression at day 8 and 15 of cardiac differentiation of irradiatied cTNT-H9 cells. Cells were irradiated with 0 (sham control), 0.1, 1 or 2 Gy X-rays and one week later, cardiac differentiation was initiated. At day 8 and 15, RNA samples were investigated via qRT-PCR for *miR-1* expression. Values were normalized to SNORD25-11 and to day 15-control levels. Medians with the standard error of the median are shown and statistical significance was determined via Student's t-test among experiments, ** $p < 0.01$; d, day.

3.6 Contribution of the pacemaker channel HCN4 to the spontaneous beating of the cardiac clusters

HCN4 is the major isoform of the HCN-family in the human sinoatrial node and, thus, it is used as a marker for pacemaker cells. To investigate the presence of pacemaker cells in the cardiac cultures resulting from the Kadari et al. protocol, HCN4 expression was analyzed on the mRNA (Fig. 12 B and Fig. 22 B) and protein level (App. Fig. 8). Irradiated cells showed a lower mRNA level of *HCN4* than controls (Fig. 22 B). However, HCN4 protein signal was hardly distinguishable from noise in the cardiac cultures. Cells with a distinct signal were rare and only present in or near a few clusters. Some of these cells also had a morphology that was different from the cardiac cells and no GFP-cTNT was expressed (App. Fig. 8). Therefore, it was not clear whether these cells were cardiac pacemaker cells or neuronal cells, which also express HCN4 (He et al., 2014). To investigate its contribution to the spontaneous beating of the cardiac clusters at day 15, their electrophysiological properties as well as the effect of ivabradine, a specific blocker of the I_f-current mediated by HCN channels, were investigated.

3.6.1 Electrophysiological properties of cTNT-H9-derived cardiomyocytes

On the basis of their electrophysiological properties, CM can be characterized as atrial-, ventricular- or pacemaker-like (He et al., 2003; Mummery et al., 2003). In order to characterize the contracting CM, they were measured in the whole-cell configuration of the current clamp technique. Since it was not possible to dissociate the cardiac clusters into single cells with trypsin or Accutase®, measurements

were performed in normal cTNT-H9 derived-cultures with cells that were at the margin of beating clusters. Still, only three cells of control samples could be measured and therefore, no statistically significant results were obtained. The characteristics of the measured cells are summarized in Table 9 and recorded traces of their spontaneous AP are shown in Fig. 32. Maximum diastolic potentials (MDP) were around -35 and -23 mV and their AP peaked between 40 and 60 mV.

In the 4 s-traces (Fig. 32 A), a sharp upstroke is dominant for cell 1 and 2. In the 1 s-traces (Fig. 32 B), it becomes apparent that their repolarization first started slowly, then more rapidly. The AP of cell 3 shows a steady slow depolarization and the upstroke is not as sharp as in cells 1 and 2.

Table 9: Electrophysiological characteristics of three cTNT-H9-derived CM.

# Cell	n (AP)	Beat rate (bpm)	APA (mV)	MDP (mV)
1	16	96	73.3	-35.2
2	12	72	84.6	-22.8
3	15	90	68.8	-22.7

n (AP), number of AP; MDP, maximum diastolic potential; APA, AP amplitude

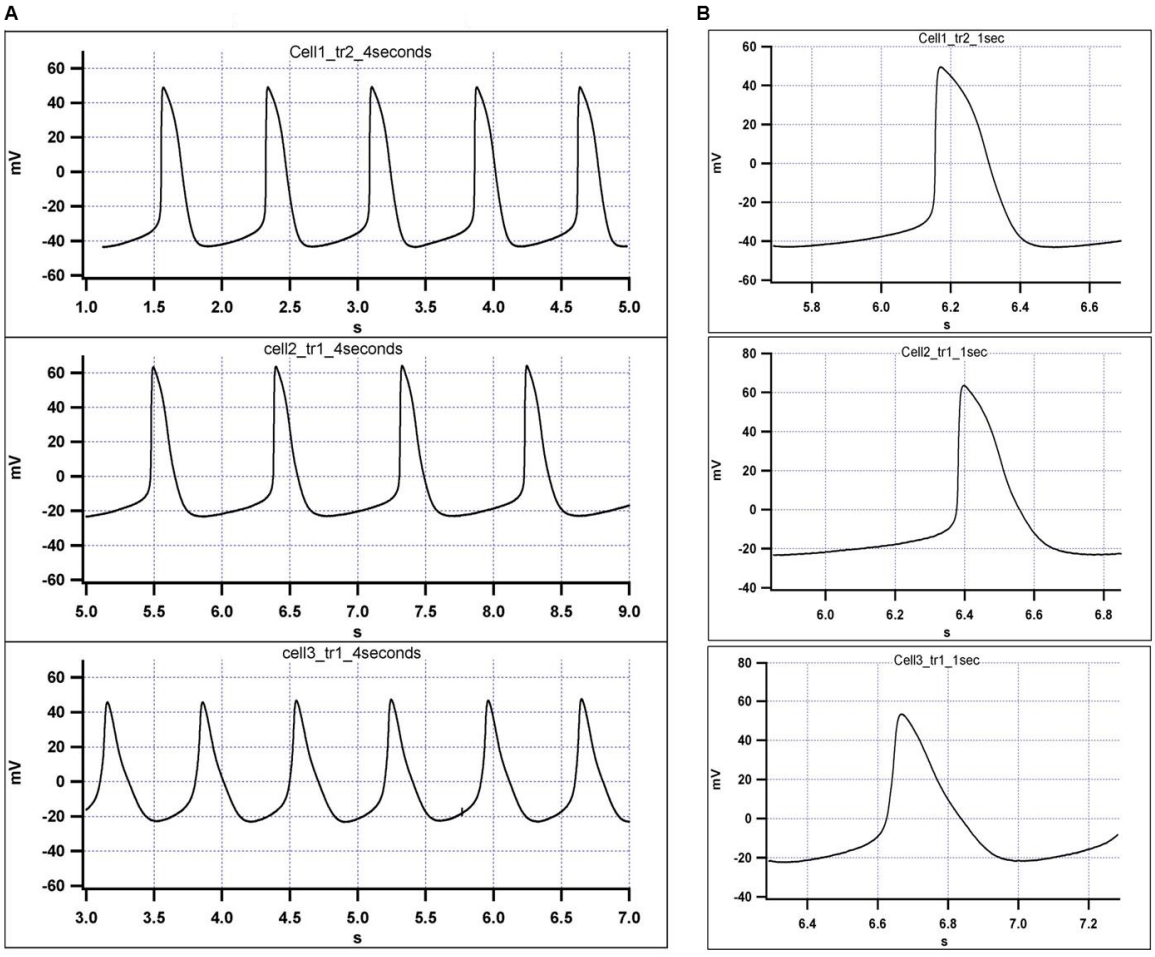

Fig. 32: Action potentials of three contracting cTNT-H9-derived CM at day 15 of differentiation. Spontaneous APs were recorded in the whole-cell configuration of the current clamp technique for several seconds using the I0-current. Four seconds (A) and one second (B) traces of each cell are shown.

3.6.2 Effect of ivabradine on the beat rates of the cardiac clusters

Ivabradine is a specific HCN channel blocker. According to Bucchi et al. (2006) its half-block concentration is 2 µM for HCN4 and 0.94 µM for HCN1. Therefore, starting from 2 µM, increasing concentrations were added to the cardiac cultures at day 15. The beat rates of cardiac clusters derived from sham (Fig. 33 A) and 1 Gy-irradiated cTNT-H9 cells (Fig. 33 B) were decreasing starting from 8 µM. With 40 µM ivabradine, the maximum slowdown was reached and higher concentrations did not lead to a further deceleration.

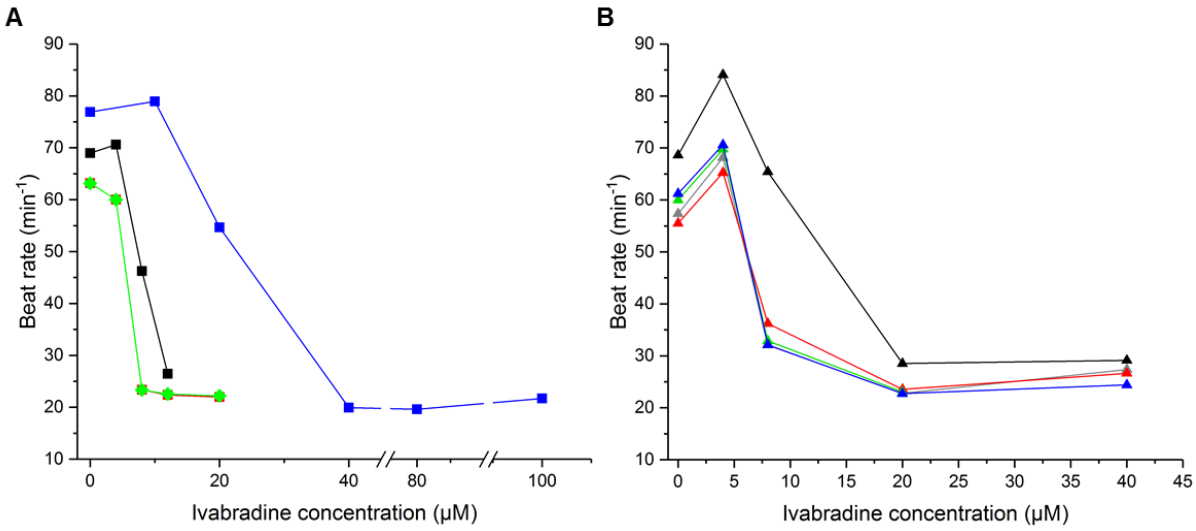

Fig. 33: Effect of ivabradine on the beat rates of cTNT-H9-derived cardiac clusters. At day 15 of differentiation, increasing concentrations of ivabradine between 2 and 100 µM were tested in cultures derived from controls (A, four clusters) and 1 Gy-irradiated cells (B, five clusters). Each color represents one cluster.

3.7 Characterization of the supporting cell layer in cTNT-H9-derived cardiac cultures

Since also non-cardiac cells developed in the cardiac cultures (Fig. 17) and it is known that endothelial cells support CM growth and function (Brutsaert, 2003; Tirziu et al., 2010), endothelial markers, namely CD31 and vWF, were analyzed in the cTNT-H9-derived cardiac cultures on the mRNA and protein level (Fig. 34).

CD31 expression appeared at day 5 of differentiation (Fig. 34 A) and increased until day 15. The 1 and 2 Gy-irradiated samples showed a trend towards decreased levels at day 5, 8 and 15.

In controls, *vWF* expression peaked at day 5 and decreased subsequently (Fig. 34 B). At day 5, its expression was by tendency decreased in samples derived from 0.1 Gy-irradiated cells. Upon 1 and 2 Gy exposure, its amount was markedly decreased in six out of seven experiments. However, at day 8 and 15, *vWF* expression was comparable to controls upon all tested doses.

Immunocytochemical analyses verified the expression of CD31 and vWF protein in non-cardiac cells at day 5 and 8 (Fig. 34 C, D). At day 5, the majority of the non-cardiac cells were vWF-positive and there were more CD31-positive cells compared to day 8. At day 8, the number of vWF- and CD31-positive cells was lower and especially the CD31-signal was mostly detected in apoptotic cells in

controls as well as in irradiated samples, making it difficult to identify specifically positive cells. These mostly occurred in small groups (Fig. 34 C). CD31 was not as finely structured as in HDMEC (positive control, App. Fig. 18 A) and not distributed around the whole cell.

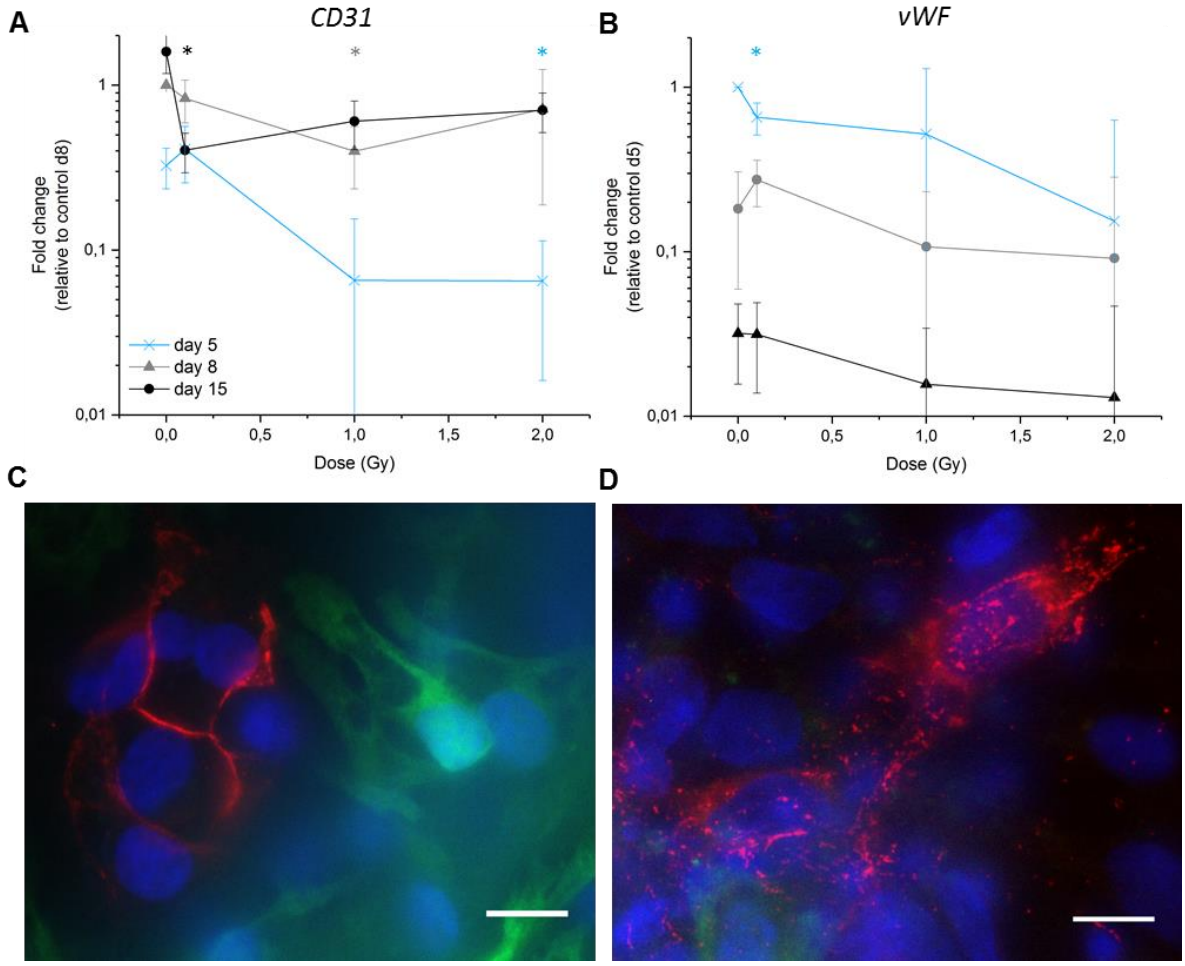

Fig. 34: Expression of CD31 and vWF in cTNT-H9-derived cardiac cultures. A, B) Dose effect-curves of qRT-PCR based analyses of *CD31* (A) and *vWF* (B) gene expression at day 5, 8 and 15 of differentiation of sham controls, 0.1, 1 and 2 Gy-irradiated cTNT-H9 cells. Values were normalized to 18sRNA and to the highest control mRNA level of each target in each experiment. Student's t-test was performed among experiments; * $p < 0.05$. d, day. C, D) Representative pictures of immunocytochemical analyses of CD31 (C, red) and vWF (D, red) in sham controls at day 8. DNA was stained with Hoechst-33342 (blue). Green: cTNT-H9 cells expressing GFP as reporter for cTNT-expression; scale bars: 10 µm.

vWF is stored in Weibel-Palade bodies (Valentijn et al., 2014). These structures were also observed in the supporting cells of the cTNT-H9-derived cardiac cultures (Fig. 34 D). However, their number per cell was lower and their structure was not as pronounced as in HMVEC cells, which were used as positive control (App. Fig. 18 B). In two out of five experiments, the cultures derived from 2 Gy-irradiated cells had a clear increase of vWF-positive cells compared to controls and vWF-positive cells occurred mostly in large non-cardiac clusters (not shown). In one of these two experiments, this increase was also observed on the mRNA level.

In addition to CM and endothelial cells, smooth muscle cells play an important role in the heart *in vivo*, and it was described by Mummery et al. (2003) that *in vitro* also endodermal cells play a synergistic role in cardiac differentiation. Therefore, expression of *MYH11*, encoding the smooth muscle Myosin Heavy Chain 11, and *AFP*, encoding Alpha Fetoprotein, a marker for definitive endoderm, were additionally investigated (App. Fig. 19).

In general, *MYH11* expression level was low and near baseline. Increased CT-values were only detected at day 15. However, the magnitude of expression changes was low and no marked overall IR-induced trend was detected (App. Fig. 19 A). Still, by tendency *MYH11* expression was lower in samples derived from 0.1 and 1 Gy-irradiated cells. For the 2 Gy samples, the variation was high among experiments.

In contrast, *AFP* expression appeared at day 5 and peaked at day 15, clearly distinguishable from baseline levels. No clear changes were detected between controls and irradiated cultures (App. Fig. 19 B).

3.8 Impact of X-ray exposure at specific cardiac differentiation stages

Since the pluripotent state exists only for a very short time *in vivo*, it is statistically more likely that the embryo is exposed to IR at a later stage of development. Therefore, differentiating cTNT-H9 cells were irradiated with 1 Gy at day 5, when cardiac progenitor cells develop, or at day 8, when spontaneous beating occurs, in n = 3 independent experiments.

Spontaneously beating cardiac clusters formed in all conditions and no apparent differences in their number was detected. Gene expression determined via qRT-PCR was compared to sham controls at until day 29 of differentiation. Fig. 35 depicts the gene expression of the cardiac progenitor marker *NKX2.5* and three representative cardiac markers (*TNNT2*, *MYH6* and *MLC2v*) for all three experiments. Medians of each target gene showed by trend no alterations caused by irradiation, however, depending on the experiment, mRNA levels varied.

It is noteworthy that the cTNT-H9 cells used for these experiments were of higher passages and that the resulting cardiac clusters of two out of the three experiments had a different morphology than those in the experiments before. As already described for two experiments in section 3.3, the CM formed thin layers of GFP-positive cells spanning large parts of the culture dishes rather than round compact clusters (App. Fig. 10 A-C). Beat rates of these layers were much higher than in previous experiments and exceeded the physiological range (App. Fig. 20 A, B). However, clusters with the normal round, compact morphology had beat rates comparable to those derived from cells of earlier passages. Since this altered phenotype also appeared in two experiments of section 3.3, it is not a result of the irradiation during differentiation. Comparing the CT-values of various differentiation markers between experiments with early and late passage cells, revealed no differences (data not shown). Hence, only the morphology and beat rates were altered.

In the one experiment with cluster morphologies comparable to those of early-passage-experiments, no differences were observed between the beat rates of all three conditions (App. Fig. 20 C). In addition, in all three experiments clusters of all conditions were able to react to isoproterenol at day 15, 22 and 29 (data not shown).

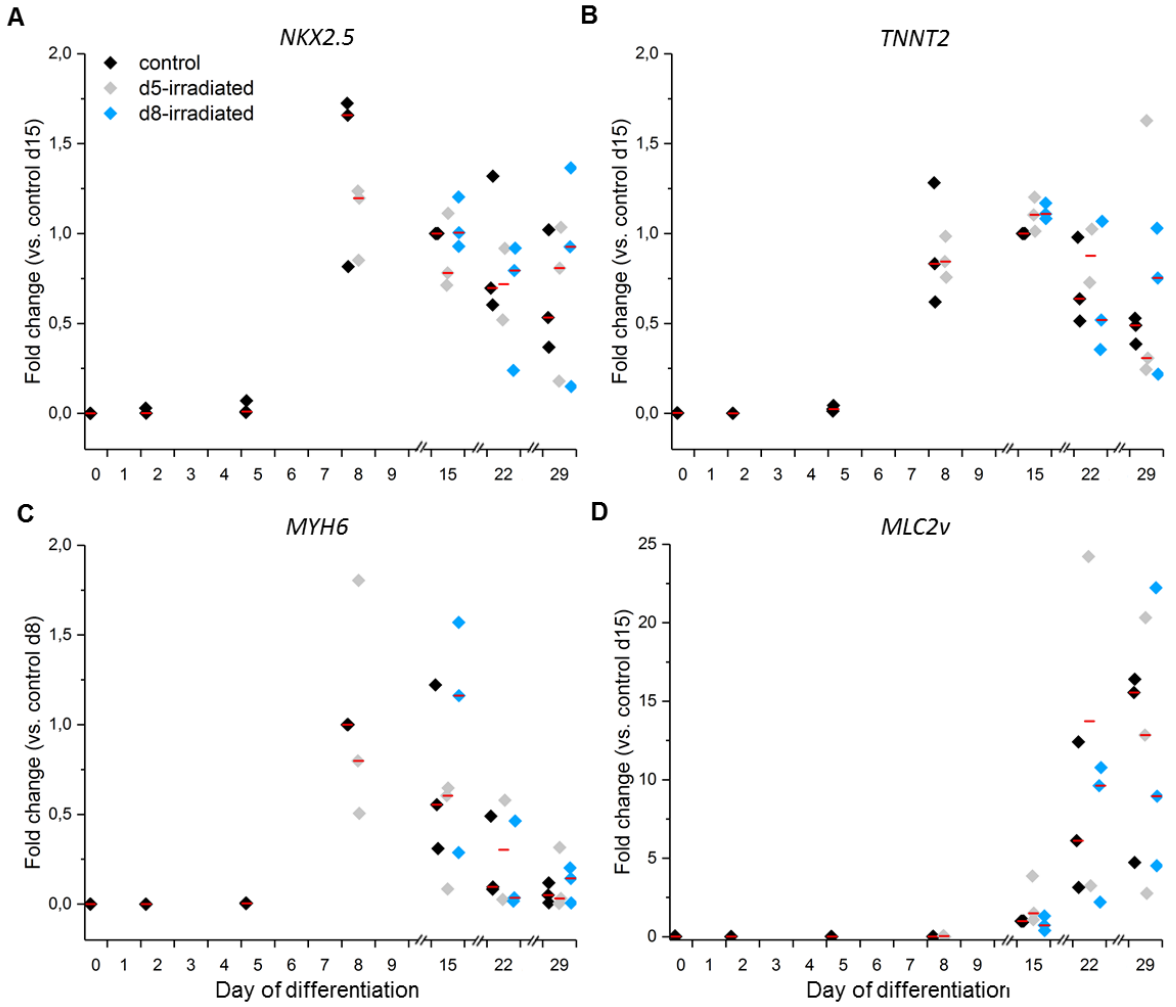

Fig. 35: Expression of cardiac marker genes after irradiation of the cardiac cultures at day 5 or 8 of differentiation. At day 0, differentiation of the cTNT-H9 cells was initiated. Cardiac cultures were irradiated with 0 (sham control, black) or 1 Gy X-rays at day 5 (gray) or day 8 (blue) and expression of *NKX2.5* (A), *TNNT2* (B), *MYH6* (C) and *MLC2v* (D) was analyzed until day 29. Values were normalized to 18sRNA and to control samples with the highest expression level for each target in each experiment. Data of n = 3 independent experiments are shown. Red line, median; d, day.

4 Discussion

The human embryo may be exposed to IR due to medical needs of the mother or by nuclear accidents. The developmental risks depend on the dose of the *in utero* exposure and the stage of gestation, with the most susceptible stages being the preimplantation phase and organogenesis in the first fifteen weeks post conception (Williams and Fletcher, 2010). Since studies on human embryos are ethically unjustifiable and infeasible, hESCs are a suitable model system to evaluate the risks of an *in utero* exposure to diverse noxae and to investigate the underlying molecular mechanisms. The heart is a very radiosensitive organ and its correct formation during development is crucial for all subsequently developing organs to be supplied with oxygen and nutrients. Using specific protocols, hESCs can be differentiated into functional CM by recapitulating all stages of early cardiogenesis. Using this model system, several noxae, like IR or drugs can be analyzed for possible cardiotoxic effects. In addition, hESC-derived CM are of high interest for regenerative medicine, e.g. for the treatment of infarcted hearts. Since the medical use of IR, especially X- and γ-rays, is steadily increasing also for pregnant women (Chen et al., 2008), a detailed risk assessment for the embryo is crucial and the results of this study aim to contribute to it.

4.1 hESC-derived cardiac cultures markedly differ depending on the factors used for differentiation

In our laboratory, cardiac differentiation of hESCs was previously performed according to the GiWi-protocol by Lian et al. (2013a). However, differentiation efficiency was low and effects of IR-exposure were not reproducible (unpublished data). In order to enhance the efficiency, a more recent protocol by Kadari et al. (2015) was established.

4.1.1 Cardiac differentiation efficiency of hESCs is enhanced by stage-dependent modulation of WNT signaling and a higher proliferation rate

Compared to the protocol by Lian et al., the one by Kadari et al. led to a higher cardiac differentiation efficiency of H9 cells (section 3.1). This was evidenced by higher levels of cardiac marker genes and expression of the more mature and ventricular marker MLC2v on gene and protein level. In addition, structural organization of α-Actinin and cTNT of the hESC-derived CM was by tendency higher. These differences can be attributed to only three substances, namely BMP4, XAV939 and ascorbic acid. Supplying the cells with BMP4 in addition to CHIR99021 in the first 24 h of cardiac differentiation, additionally supports canonical WNT signaling leading to an earlier onset of *MESP1* expression (day 1, Fig. 11 B).

As reviewed by Gessert and Kühl (2010), different WNT pathways play crucial roles depending on the phase of cardiac differentiation: whereas mesoderm formation depends on canonical signaling, this pathway needs to be blocked subsequently for the development of cardiac progenitors. In this phase, non-canonical WNT signaling is supportive. Using IWP2 according to Lian et al. (2013a), canonical as well as non-canonical WNT signaling are inhibited since palmitoylation of WNT proteins by Porcn

is prevented (Chen et al., 2009). In contrast, XAV939 used by Kadari et al. (2015) specifically inhibits canonical WNT signaling (Huang et al., 2009), whereas non-canonical signaling can operate to enhance CM development. This was evidenced by a higher expression of *WNT11*, which is involved in non-canonical signaling (Mazzotta et al., 2016; Pandur et al., 2002b), in the cardiac cultures resulting from the Kadari protocol (App. Fig. 1 D). At the same time, *NKX2.5*-positive cardiac progenitor cells developed and reached higher levels compared to the Lian protocol (Fig. 11 D). The increased levels of cardiac progenitor as well as cardiac marker genes with the Kadari protocol can be attributed additionally to the ascorbic acid in the differentiation medium, which enhances proliferation of the progenitors via the MEK-ERK1/2 pathway (Cao et al., 2012).
In summary, the higher cardiac differentiation efficiency using the Kadari protocol is due to enhanced stage-dependent WNT signaling modulation and probably also due to increased proliferation of the cardiac progenitors. However, the latter was not specifically investigated.

Kadari et al. (2015) enhanced CM yield by lactate supplementation. However, in the present study, this did not increase the number of CM at day 15 (not shown) and was thus not applied. One possible explanation for this is that a high number of supporting non-cardiac cells in the cultures disappeared upon replacement of glucose with lactate. This is due to their inability to metabolize lactate, which is in contrast to cardiac cells (Tohyama et al., 2013). Without their supporting signals, cardiac differentiation was probably hampered so that no new cardiac clusters could develop.
Furthermore, the differentiation medium used in this study did not contain insulin throughout the 15 days in contrast to the original protocol by Kadari and colleagues. In the early stages of differentiation, insulin has a negative effect on CM development (Freund et al., 2008) that can be rescued by a stage-dependent modulation of canonical WNT signaling (Lian et al., 2013b). Therefore, no insulin was used at the early stages of differentiation. At later stages, no insulin was added in order to keep the cells in constant conditions and to avoid negative effects of insulin on slower differentiating cells.

4.1.2 Beat rates of the cardiac clusters varied, but beat variability decreased with the time of culture when WNT signaling was modulated precisely

A first sign of the development of functional CM is the onset of spontaneous contractions. Increasing beat rates are linked to an enhanced cardiac output during mouse embryonic development (Keller et al., 1996; Moorman et al., 1998) and are also observed *in vitro* in mESC-derived cardiac EBs (Sauer et al., 2001). However, an *in vitro* study showed decreased beat rates for late hESC-derived CM (26±3 bpm) compared to early ones (36±6 bpm; Sartiani et al., 2007), which is clearly lower than the normal fetal and adult human heart rate.
In two experiments comparing the protocols by Lian et al. and Kadari et al., video-based analyses of the beat rates showed no reproducible protocol-dependent differences since the experiments showed contrary trends (Fig. 15). It was reported that differentiation mediated by addition of FCS led to a

certain variability in the developing cardiac cell types and markedly varying beat rates (i.e. 38 - 106 bpm; He et al., 2003). Despite the more complex modulation of the signaling pathways in the present study, the developing cardiac clusters were still heterogeneous and also the beat rates varied markedly, however, in the same range as described by He et al. (2003). For functional analyses of hESC-derived CM, it is thus necessary to analyze a high number of cardiac clusters to embrace a broad spectrum of the heterogeneous cultures.

Whereas beat variability remained high for the clusters of the Lian protocol throughout differentiation, it was clearly reduced for those generated with the Kadari protocol at day 15. One reason could be differing morphologies: the clusters derived from the Kadari protocol were compact and thus, "isolated" from each other, allowing an individual development. In contrast, the clusters derived from the Lian protocol were strand-like and some were connected with each other. In some cases, these strand-like structures became more compact over time losing their interconnectedness. It is possible that these changes affected the beating features of the Lian protocol-derived clusters, whereas in those of the Kadari protocol only the cell number increased, but the morphology remained the same over time. Another reason might be that due to a higher maturation state evidenced by the expression of MYH7 mRNA as well as MLC2v mRNA and protein, the Kadari protocol-derived clusters had an enhanced intercellular communication leading to a more regular beating.

Cardiac clusters derived from both protocols responded to isoproterenol indicating the presence of functional β-adrenergic receptors and HCN channels. The elevated beat rates are the results of the β-adrenergic receptor-mediated increase of intracellular cAMP levels. This shifts the HCN channel opening potential to more positive values, especially that of HCN2 and HCN4 (Biel et al., 2002), leading to elevated beat rates.

4.2 Cardiac differentiation is more efficient using a feeder-free culture system

hESCs are often cultured on a MEF feeder layer with an exogenous FGF2-supply to maintain their pluripotency via increased levels of Tgfb1 and Activin A secreted by the MEFs (Greber et al., 2007). In the present study, cardiac differentiation of H9 cells grown on MEFs was not efficient and reproducible. Using the feeder-free cTNT-H9 cell line, more cardiac clusters developed and expression levels of cardiac genes were higher compared to the H9-derived cultures (Fig. 20). A possible explanation for the hampered differentiation of H9 cells grown on MEF feeders is that cells were transferred to Matrigel®- or Geltrex®-coated culture plates by using cell scrapers. Thus, the MEF feeders were still present in the culture and hampered differentiation by their pluripotency maintaining signals.

4.3 The wildtype H9 and the transgenic cTNT-H9 cell line have a comparable radiation response

It is well known that ESCs possess unique features to efficiently protect the stem cell pool from genetic aberrations and mutations (see section 1.2.2) and culture conditions markedly influence genomic stability (Draper et al., 2004; Mitalipova et al., 2005; Nguyen et al., 2013). Luft et al. (2017) described that depending on the method of passaging, H9 cells showed a distinct radiation response: Manually passaged cells had a higher percentage of aberrant cells and a higher fraction of apoptosis 24 h after X-ray irradiation compared to enzymatically passaged cells indicating that the manually passaged ones are more sensitive to radiation and more efficient in eliminating aberrant cells from the culture. In order to establish a model system to study radiation impacts on hESC cardiac differentiation, the transgenic cTNT-H9 cells were characterized in terms of their radiation response in comparison to the H9 cells. For this reason, karyotypic and cell death analyses were performed.

4.3.1 cTNT-H9 cells are genetically stable and have a comparable fraction of aberrant cells upon X-ray exposure as the wildtype cell line

There are few publications using the reporter cell line cTNT-H9 (e.g. Garate et al., 2018; Hazeltine et al., 2014; Pallotta et al., 2017). In most of them, the cells were co-cultured with MEF feeders, the methods of passaging were not always described in detail and no cytogenetic data were included. In the study at hand, several passaging methods were tested for the feeder-free cTNT-H9 cell, but only with ReleSR™ a sufficient number of pluripotent colonies was obtained over multiple passages. Since cytogenetic analyses of cTNT-H9 cells passaged with ReleSR™ are not available, the karyotype of high-passage cells was investigated via mFISH. As described in section 3.2.1, no chromosomal aberrations were detected until passage 75 indicating a high efficiency to maintain genetic stability within the cell pool.

One day after exposure to 1 Gy X-rays, the cTNT-H9 cells showed a comparable high fraction of aberrant cells as the wildtype H9 cells analyzed by Luft et al. (2017) and seven days after exposure, the percentage of aberrant cells was reduced (App. Table 8). These results indicate that irradiated H9 and cTNT-H9 cells are comparably efficient in removing aberrant cells from the population.

24 h after irradiation of the cTNT-H9 cells with 2 Gy, hardly any mitotic cells were found. The reason for that could be that most cells underwent cell death already within the first 24 h post irradiation and only very few cells survived. Therefore, the overall amount of cells was probably too low.

4.3.2 Massive cell death occurs upon IR exposure of cTNT-H9 cells

A general observation upon irradiation of ESCs is massive cell death (see section 1.2.3). In the present study, apoptosis and necrosis were quantified upon exposure of the cTNT-H9 cells to 1 Gy X-rays via FACS analyses. By trend, there was a two-fold increase in apoptotic cells at 24 h and 48 h compared to sham controls (Fig. 19). 72 h after exposure, the highest number of apoptotic cTNT-H9 cells was measured (four-fold increased compared to controls), whereas the fraction of necrosis was two-fold

increased compared to controls at all three time points. In a direct comparison (n = 1, data not shown), the wildtype H9 cells showed only a 2.1-fold elevated apoptotic fraction at 24, 48 and 72 h post irradiation and a high fraction of necrotic cells at 24 and 48 h compared to controls (8.5- and 3.7-fold increased, respectively). These results together with those by Luft et al. (2017), who showed an almost five-fold increase in apoptosis 24 h after 1 Gy X-ray exposure compared to controls, indicate that the wildtype H9 cells eliminate most damaged cells within the first 24 h. In contrast, cTNT-H9 cells showed a delayed peak of cell death at 72 h. The reason for this delay could not be clarified yet.

4.4 hESC-derived cardiomyocytes develop functional gap junctions and ion channels

The basis of spontaneous contractions of cardiac cells is electrical activity (i.e. ion currents), which depends on the presence of functional ion channels in the CM and on the propagation of these electrical signals between adjacent CM via gap junctions (see section 1.3.2).

4.4.1 Gap junctions connect adjacent hESC-derived cardiomyocytes

Gap junctions allow the direct communication and propagation of electrical signals between adjacent CM (Gros and Jongsma, 1996; Söhl and Willecke, 2004). Cx43 is the most abundant gap junction protein in the mammalian heart (Gros and Jongsma, 1996) and involved in the communication between pluripotent hESCs (Wong et al., 2008). Immunocytochemistry revealed expression of Cx43 protein at high levels in the pluripotent hESCs (data not shown). Compared to them, Cx43 was expressed at a much lower density in the hESC-derived CM and no difference was detected between controls and irradiated cells. In contrast, for CM derived from mESCs exposed to 5 Gy γ-rays a decreased density of Cx43 was reported and associated with a reduced beat rate (Rebuzzini et al., 2013). The discrepancies to the present study may arise from different cells, doses and differentiation methods.

4.4.2 β-adrenoreceptors are functional, however, develop with a variable pace and density

In the heart, β-adrenergic receptors are responsible for an increased contraction force and heart rate especially via the hormone adrenaline. Isoproterenol is an agonist of these receptors and leads to an increased intracellular level of cAMP. This in turn results in an enhanced calcium release from the SR, thereby increasing the contractility of CM. Cardiac clusters derived from hESCs using the Lian and Kadari protocol responded to isoproterenol, indicating the presence and functionality of β-adrenergic receptors. However, some clusters showed a delayed or no response (App. Fig. 2 and Fig. 27). Still, when these clusters were recorded at day 22 and 29, their response was normal (data not shown). A possible reason is that not all CM developed with the same pace and thus, some might have a more mature phenotype than others. This assumption is supported by a study by Chen et al. (1979) who showed that the responsiveness to isoproterenol depends on the age of murine fetal hearts: at an early stage, the hearts did not respond even though β-adrenergic receptors were already present, but with

ongoing development, the response was more pronounced most likely attributable to a growing receptor density. In addition, He et al. (2003) described a 33+/-27 % increased beat rate upon isoproterenol, indicating a marked variability among hESC-derived EBs. These results and those of the present study point at a varying differentiation pace of the hESC-derived CM. Even with the same protocol and in the same petri dish there might be cells with less (and/or less mature) β-adrenergic receptors and thus, have a lower chronotropic response to isoproterenol than others at one defined time point. For this reason, the CM derived from the 2 Gy-irradiated hESCs are likely to have a more immature phenotype and a lower density of β-adrenoreceptors compared to controls (Fig. 27). In a previous study, a delayed cardiac differentiation of mESCs upon irradiation was reported (Helm et al., 2016). Hence, it was analyzed whether the isoproterenol responsiveness of the 2 Gy-irradiated clusters reached control levels after a prolonged culture time. However, due to the low amount of surviving cells after the 2 Gy irradiation, their cardiac development could only be monitored in two out of five experiments until day 29. Yet, in these experiments, their responsiveness did not reach the day 15-levels of controls (data not shown), suggesting that hESCs are more sensitive to X-ray irradiation than mESCs since they keep their immature phenotype for a prolonged time upon a 2 Gy exposure.

4.4.3 HCN4 channels are functional in cTNT-H9-derived cardiac clusters

One of the three main currents of the cardiac pacemaker, namely the funny current (I_f), is generated by HCN channels and in the adult SAN, HCN4 is the main isoform (Stieber et al., 2003). Compared to the SAN, HCN4 expression is downregulated in the working myocardium (Weisbrod et al., 2016). Whereas early ventricular myocytes express HCN4 and beat spontaneously, they lose their ability to beat with ongoing development and switch to HCN2 expression (Yasui et al., 2001). Furthermore, I_f currents are downregulated in the chambers compared to the conduction system (Abi-Gerges et al., 2000). Since atrial and ventricular I_f currents activate with slower kinetics and at lower activation potentials than those of the SAN, they do not play a functional role at physiological conditions (Biel et al., 2002). Therefore, analyses of HCN4 can give hints regarding the cardiac cell types generated by *in vitro* differentiation of hESCs.

Even though the presence and functionality of HCN channels was already evidenced by the increased beat rates upon addition of isoproterenol, their contribution to the spontaneously beating cardiac clusters was further investigated. In line with the results of Sartiani et al. (2007), HCN4 was detected on the mRNA level in the pluripotent H9 and cTNT-H9 cells (Fig. 12 D and Fig. 22 B). After initiation of differentiation, its gene expression was decreased, but with the onset of spontaneous beating, it was elevated again. However, its protein expression was not clearly detected (App. Fig. 8). Therefore, the presence of the I_f current was investigated in the whole-cell configuration of the current clamp technique. Since it was impossible to singularize the hESC-derived clusters with trypsin or Accutase®, the measurements were hampered in the normal cardiac cultures resulting from the Kadari protocol. Only three cells could be measured and thus, the results are not statistically significant. Still,

one out of the three measured cells appeared to be pacemaker-like (Fig. 31, cell 3), since the shape of its AP showed a steady diastolic depolarization, which is characteristic for the SAN AP (Baruscotti et al., 2005; compare section 1.3.2). The AP of the other two cells rather resembled ventricular-like ones according to He et al. (2003) and Mummery et al. (2003). The AP amplitudes were in a comparable range to the literature, but their maximum diastolic potentials and the AP peaks were shifted to more positive values compared to adult CM. This was also observed in other studies and is probably due to the immature ion currents in the hESC-derived CM (Keung et al., 2014; Yang et al., 2014).

To increase the number of measured cells, the conditions need to be improved for future experiments. First of all, cardiac clusters should be dissociated into single cells, for example by using collagenase (Mummery et al., 2003). Compared to trypsin, this is a much milder reagent preserving the integrity of the cell membrane lipids (Kirkpatrick et al., 1985), thereby allowing the reattachment of functional CM. In addition, the Port-a-patch system (Nanion Technologies) is a valuable surrogate technique since single cells are automatically captured and sealed by suction with a computer-controlled pump, thereby increasing the output.

Furthermore, ivabradine was used in this study to specifically inhibit HCN channels to analyze their contribution to the spontaneous contraction of the hESC-derived cardiac clusters. Ivabradine decreases the slope of the diastolic depolarization curve, leading to prolonged intervals between two APs and thereby, reduces the beat rate (Thollon et al., 1997). Increasing concentrations of ivabradine in the day 15-cardiac cultures led to decreased beat rates (Fig. 33), indicating the presence of HCN4 and HCN1 channels. However, between 40 and 100 µM no further slowing down was detected, hinting at compensating mechanisms within the clusters. Upon addition of 100 µM ivabradine, Niehoff et al. (2016) detected a reduction to 45 % of the initial beat rate of mESC-derived cardiac EBs. In contrast, the beat rate was reduced to about 27 % in the present study suggesting that the hESC-derived CM are more sensitive to this drug than mESCs.

All these results indicate that pacemaker-like cells are present in the hESC-derived cardiac clusters. They might, however, not all express HCN4, since a distinct HCN4 signal was only detected in some clusters, and like in the adult heart, their number is lower compared to atrial and ventricular CM.

4.5 Cardiac differentiation of hESCs is impaired by IR

Studies of atomic bomb survivors that were exposed to radiation *in utero*, revealed no significantly increased number of cardiovascular disease cases up to now compared to an unexposed control group and controversial results were reported for their risk of hypertension (Tatsukawa et al., 2008). However, exposure of adults leads to an increased risk for cardiovascular diseases in atomic bomb survivors and breast cancer patients (see section 1.3.4, Puukila et al., 2017; Taylor and Kirby, 2015). Up to date, there are only few studies dealing directly with the influence of a radiation exposure of ESCs on cardiac differentiation (Helm et al., 2016; Rebuzzini et al., 2013) reporting that gene expression of differentiating mESC-derived CM and their functionality are impaired. The present

study provides additional information that cardiac differentiation also of hESCs is impaired by an X-ray exposure. During differentiation of the hESCs, also non-cardiac cell types developed that typically co-exist and support each other in the living heart (Fig. 34 and App. Fig. 19), resulting in a suitable *in vitro* model system for studying cardiotoxic effects. qRT-PCR arrays were performed with irradiated hESCs to shed light on possibly altered molecular mechanisms that could influence differentiation. However, for these arrays, samples before initiation of differentiation were used and each array was performed only once for each time point. Therefore, no statistical significance was achieved and the results only served to gain a first impression of IR-induced alterations in gene expression of pluripotent hESCs.

Exposure of the cTNT-H9 cells to IR did not markedly affect expression of pluripotency markers, namely OCT4 and NANOG, neither on mRNA nor on protein level. Upon initiation of differentiation, also mesoderm formation indicated by *T* expression was not impaired by all tested doses (Fig. 21) and in line with this, *NOTCH1* expression, which was described to negatively impact on mesodermal differentiation (Schroeder et al., 2006; Nemir et al., 2006), did not differ from controls (App. Fig. 12 C).

Following this stage of differentiation, cardiac mesoderm is formed, which is marked by *MESP1*, one of the key regulators of cardiac development (Bondue et al., 2008; Islas et al., 2012; Saga et al., 2000). Whereas 0.1 Gy did not have a general effect on its expression, it was clearly reduced following the 1 and 2 Gy exposure indicating an impaired cardiac mesoderm formation. Possible underlying mechanisms could not be identified in this study. MESP1 is regulated among others by Brachyury (David et al., 2011) and SP1 (Beketaev et al., 2016) . However, since no IR-induced alterations in their gene expression were found, other mechanisms must be responsible for *MESP1* downregulation. One possible candidate revealed by the qRT-PCR arrays is LEF1. Binding of Oct4 and Tcf/Lef to the Mesp1 promoter leads to its expression in differentiating mESCs (Li et al., 2013). In the present study, LEF1 expression was increased in the first days of differentiation of the 2 Gy-irradiated cells compared to controls. This hints at dysregulated gene expression that could lead to carcinogenesis since high levels of LEF1 are associated with leukemia (Metzeler et al., 2012). In combination with upregulated active β-catenin, it leads to elevated expression of target genes of canonical WNT signaling. Indeed, according to the results of the SCS-array, also *CTNNB1* (encoding β-catenin) was upregulated. However, whether LEF1 and β-catenin are also increased on the protein level remains to be investigated.

NKX2.5, a marker of cardiac precursor cells, was dose-dependently decreased (Fig. 22 A). It was suggested to be one of the earliest targets of FGFR1 (Dell'Era et al., 2003). However, since no IR-induced alterations in FGFR1 expression were detected, this pathway does not seem to be impaired upon an exposure of the hESCs. In mouse cells, Nkx2.5, Tbx5 and Gata4 were found to be direct targets of Stat3 (Snyder et al., 2010). Glycoprotein-130 (gp130) is a receptor, which is encoded by the

gene *IL6ST* and is upstream of STAT3-signaling involved in cardiac development (Fischer and Hilfiker-Kleiner, 2008). In the differentiating cardiac cultures derived from irradiated cTNT-H9 cells, *IL6ST* expression was reduced compared to controls (Fig. 28) suggesting that CM formation is impaired due to impaired gp130/ STAT3 signaling. This should be investigated in more detail and on the protein level in future studies.

All subsequently emerging cardiac marker genes (e.g. *TNNT2, MYH6/7, MLC2a/v*) were likewise dose-dependently decreased (Fig. 22 and Fig. 23). Possible reasons are the reduced amount of *NKX2.5*-positive cardiac precursor cells and the reduction of *WNT11* (Fig. 30 A). The supportive function of WNT11-mediated non-canonical WNT signaling in differentiation of cardiac progenitors was described by Mazzotta et al. (2016; see Fig. 4). These results suggest that cardiac differentiation is hampered upon irradiation by impaired WNT-11 mediated non-canonical WNT signaling, whereas the WNT5B mediated non-canonical signaling, which is more important in early differentiation steps, was not affected (Fig. 30 B). However, this requires further verification on the protein level.

Additionally, miR-1 is expressed in cardiac muscle and its overexpression in murine cardiac progenitor cells has a negative impact on their proliferation (Zhao et al., 2005). The same authors showed that miR-1 functions in cardiac progenitor cells, is involved in ventricular development and targets Hand2, which is a central cardiac transcription factor involved in myocyte expansion. In addition, miR-1 is involved in cardiac cell cycle regulation (Zhao et al., 2007). miR-1 first appeared at day 8 and was markedly expressed at day 15 of differentiation (Fig. 31). In three out of six experiments, its expression was decreased upon irradiation with all three doses. However, in the other three experiments, a reduction was only detected in the 1 Gy samples, but following the 0.1 and 2 Gy exposure, *miR-1* was several fold increased compared to controls (Fig. 31). Despite these unexpected results, which cannot be explained at the moment, irradiation seems to reduce *miR-1* expression. Since Hand2 is among its downstream targets, CM expansion might be affected leading to a lower amount of CM and thus, to lower levels of cardiac genes.

On the protein level, MLC2v expression and structural organization was impaired following the 2 Gy exposure (Fig. 24) and CM functionality (beat rates and response to isoproterenol) was affected (see sections 3.3.3 and 3.3.4) suggesting an even more immature phenotype than the control CM (discussed in section 4.4.2). In contrast to the study by Rebuzzini et al. (2013) who described a decreased beat rate of mESC-derived CM following a 5 Gy γ-ray exposure, the CM derived from 2 Gy-irradiated hESCs of the present study were rather beating faster than controls.

Furthermore, *NOTCH1* expression was increased at day 15 in the cardiac cultures derived from 2 Gy-irradiated cTNT-H9 cells. According to Kwon et al. (2009) cardiac progenitor cells exit from expansion into the differentiation state via NOTCH1 signaling suggesting that differentiation of the progenitor cells derived from 2 Gy-irradiated hESCs is delayed. This assumption is further supported by an increased number of very small, newly developed cardiac clusters at day 15 in current

experiments (data not shown) and also Helm et al. (2016) reported a delayed cardiac differentiation of irradiated mESCs.
Analysis of the GFP-positive CM separated from non-cardiac cells by Fluorescence-Activated Cell Sorting (FACS) would give information on the mechanisms underlying the IR-induced impairment of cardiac differentiation. However, sorting the cells was not successful (data not shown) since only a very low cell number remained afterwards even though cardiac cultures of day 29 with a high GFP-intensity were used. For this reason, the question remains whether the observed effects are due to a lower number of developing CM or due to altered (lower) cardiac gene expression within the CM.

To verify the results on RNA-level, quantitative protein analyses should be performed in future experiments. Currently, samples are prepared for proteomic analyses in collaboration with the Helmholtz Centre Munich. Preliminary results (n = 1) suggest that cardiac cultures derived from 1 Gy-irradiated hESCs have impaired metabolism, enhanced ROS production and alterations in energy production pathways, among others.

The results of the DDR- as well as SCS-array were mostly not confirmed by individual qRT-PCR of several genes. For example, an upregulation of *ATM* and *CDKN1A* (encoding p21) was detected seven days post irradiation via the DDR-array with pooled samples. When these were analyzed individually for these two genes, no upregulation was detected at that time point. The reason for the apparent discrepancy between the array results and those of individual qRT-PCR is not clear. One possible reason is the use of different primer sequences leading to amplification of unspecific target genes in either the arrays or the individual qRT-PCR. Another reason might be outliers in the pooled samples that tamper with the array-results. Mechanical problems were excluded.
However, it should be mentioned that ATM and p21 were also analyzed on the protein level and both were not detected. This is in line with previous studies that did not find an increase of un-phosphorylated ATM upon DNA damaging treatments (Momcilovic et al., 2009, Mujoo et al., 2017) and of p21, which is due to microRNA-mediated degradation of its RNA (Dolezalova et al., 2012). This suggests that there was rather a problem with the arrays than with the individual qRT-PCRs.

Nevertheless, the results of the SCS-array revealed many development-associated signaling pathways to be affected by an X-ray exposure. The results of the 24 h samples mainly confirm those published by Luft et al. (2017) who used the same array with samples of irradiated H9 cells. The authors reported further a reduced expression of *ACVR1B* and *ACVR2B* in manually passaged H9 cells (1.7-fold) four days after irradiation with 1 Gy X-rays. This low magnitude decrease was confirmed with the individual qRT-PCR of the present study since both genes were decreased (2.0- and 3.0-fold) in two out of six samples seven days after irradiation. However, in contrast, the results of the SCS-array revealed an upregulation of both genes. It has to be mentioned that only low *ACVR1B* levels were

detected in the cTNT-H9 cells (controls and irradiated samples) in the present study as well as in the study by Luft and colleagues. In contrast, *ACVR2B* was clearly expressed. In the present study, expression changes among the individual samples were nearly identical for *ACVR1B* and *ACVR2B*, which is due to almost unchanged CT-values for all samples. The alterations upon normalization were almost exclusively due to changes in 18sRNA levels. Since activin signaling plays an important role in cardiac mesoderm formation (Kattman et al., 2011), future studies should address the role of these two activin receptor genes in cardiac differentiation upon irradiation.

4.6 High passage cTNT-H9 cells were culture-adapted

At early passages, cTNT-H9 cells were split 1:5 to 1:8 to allow passage once a week. However, around passage 70, the cells started to grow faster and more robustly, thus higher splitting ratios (up to 1:15) were needed to keep the normal passaging rhythm. The same phenomenon was described by Baker et al. (2007) who used H1, H7 and H14 hESCs grown on MEF feeders and reported that at later passages, "cells grew more robustly and were split at 1:5 to 1:10 split ratios", whereas early passage cells were split 1:2 or 1:3. The authors assumed that there was an adaptation to the culture conditions by mutations or selection. In the present study, the cTNT-H9 cells were analyzed for karyotypic abnormalities via mFISH, but also at the highest passage used for this study (p75) no aberrations were found (see sections 3.2.1 and 4.3.1). Still, mutations of single genes, which may lead to a selection advantage, cannot be ruled out. Genome analyses were, however, beyond the scope of this study.

Cardiac differentiation with higher passage cTNT-H9 cells led to an altered cluster morphology: Whereas at day 8 the clusters were small and separated and their beat rates were in a physiological range, they showed a higher degree of interconnectedness starting from day 10 and some of them were beating very quickly (exceeding 300 bpm). However, beat rates of clusters with the normal round, compact morphology were in a physiological range. The thinner the clusters, the higher was their beat rate. Altogether, this altered morphology was observed in four out of five experiments using high passage cells. An altered differentiation efficiency between early and late passage cells was excluded by comparing the CT-values of several differentiation markers among the respective experiments (data not shown), indicating that only the cluster-morphology and beat rates were altered. Anyway, it is reasonable to re-investigate the impact of an IR exposure at specific differentiation stages with early passage cells.

4.7 Exposure to IR at specific stages of differentiation does not markedly impair further cardiac development

Cardiac cultures were exposed to IR at day 5 or 8. At day 5, there should be predominantly cardiac progenitor cells, which are still dividing and expanding, and at day 8, when spontaneous beating established, it is possible that a certain number of the developing CM already stopped cell cycling.

Irradiation at these days did not lead to marked overall alterations in cardiac gene expression and CM functionality until day 29. In a previous study, no altered beat rates of primary chicken CM were observed upon 0.5 and 1 Gy X-rays (Frieß et al., 2015). Similarly, Heselich et al. (2018) did not observe altered beat rates upon titanium or carbon ion irradiation of primary chicken CM especially with low doses suggesting a high functional robustness of CM against radiation. In addition, *in vitro*-cultured primary beating rat CM were irradiated with very high γ-ray doses (Lampidis et al., 1975), showing that below 100 Gy (10,000 rad) neither beat rate nor beating rhythmicity were affected, suggesting that post-mitotic cells are radio-resistant. This confirms the results of the present study, which further suggest that also cardiac progenitor cells (day 5 hESC-derived CM) do not show immediate effects upon IR exposure.

However, these results do not exclude radiation-induced long-term effects on the CM and their functionality. The heart is considered to be a late-responding organ (Boerma et al., 2016) probably due to the post-mitotic state of the CM. This is in line with the observation that upon radiotherapy, breast cancer patients rarely show immediate cardiac effects, but have a higher risk of cardiovascular diseases years or decades after radiotherapy (Boerma et al., 2016). The same observation was made for atomic bomb survivors. For this purpose, long-term *in vitro* studies are needed to investigate the molecular mechanisms of these late effects.

4.8 Conclusions and outlook

hESCs show massive cell death as a first reaction to X-ray exposure in order to eliminate damaged cells from the population. The surviving cells continue to express pluripotency markers on the gene and protein level. They were differentiated into CM under optimized culture and differentiation conditions, which have a great impact on differentiation efficiency. Whereas mesoderm formation was not affected by the exposure, a decreased expression of *MESP1* indicating impaired cardiac mesoderm formation was detected upon the 1 and 2 Gy exposure. Markers of the following differentiation stages, comprising precursor cells as well as CM, showed a dose-dependent decrease. Even an exposure to the lowest dose tested (0.1 Gy) impaired gene expression, which was even more pronounced upon 1 and 2 Gy. Effects on the protein and functional level were only detected upon a high dose (2 Gy). This suggests that these CM were more immature than those resulting from control hESCs and as evidenced by a lower response to isoproterenol even upon prolonged culture time (day 29), they seem to keep their immature phenotype and do not reach the maturity level of day 15-control CM. Pathway analyses did not yet clarify the mechanisms underlying the impaired cardiac mesoderm differentiation. However, data obtained so far indicate that the specification of the cardiac progenitors is hampered by impaired miR-1, WNT11-mediated non-canonical WNT and gp130-mediated STAT3 signaling.

In addition, it was shown in three experiments that an exposure to 1 Gy at the cardiac progenitor-stage and during the onset of spontaneous beating has no general effect on cardiac gene expression as well

as on the functionality of the CM until day 29. These experiments should be repeated with low passage hESCs and cardiac cultures should be observed for a prolonged time to investigate the mechanisms of possible long-term effects. Furthermore, the impact of irradiation at an earlier time point (e.g. during mesoderm formation at day 1 or 2 of differentiation), as well as a radiation impact on the maturation capability of the hESC-derived CM needs to be investigated in future.

According to the *DGMP*- and *DRG*-report (2002), 0.1 Gy sparsely IR is the threshold dose of an *in utero* exposure, above which the risk for malformations and mental retardation is increased. In the present study, 0.1 Gy exposure led to alterations on the molecular level during cardiac differentiation, but with high standard errors and CM functionality was not affected. Functional effects only occurred after exposure to a high dose. In combination with a study of atomic bomb survivors exposed *in utero* showing no increased numbers of non-fatal cardiac diseases so far (Tatsukawa et al., 2008), these results suggest that the risk of cardiac effects upon an *in utero* exposure to doses below 0.1 Gy, which are typically used in medical diagnostics, is negligible. However, higher doses might lead to severe effects due to dysregulated developmental processes. hESC-derived cardiac cultures are thus a suitable model system to evaluate the risk of an *in utero* IR-exposure, also because the typical cell types that co-exist in the heart *in vivo* develop during differentiation, thereby mimicking the heart as closely as possible. However, this model system might not be sensitive enough to study effects of even lower doses since already the results of the 0.1 Gy exposure showed high standard errors. For this, a more sensitive approach should be selected, for example on the basis of single cells. In addition, to verify the observations of this study protein analyses are needed. Furthermore, various cardiac ion channels, especially those involved in calcium fluxes leading to the cardiac contraction should be investigated since they are crucial for the correct functionality of CM.

Literature

Abdul-Ghani, M., Dufort, D., Stiles, R., De Repentigny, Y., Kothary, R., Megeney, L.A., 2011. Wnt11 Promotes Cardiomyocyte Development by Caspase-Mediated Suppression of Canonical Wnt Signals. Mol. Cell. Biol. 31, 163–178.

Abi-Gerges, N., Ji, G.J., Lu, Z.J., Fischmeister, R., Hescheler, J., Fleischmann, B.K., 2000. Functional expression and regulation of the hyperpolarization activated non-selective cation current in embryonic stem cell-derived cardiomyocytes. J Physiol 523.2, 377–389.

Adams, B.R., Golding, S.E., Rao, R.R., Valerie, K., 2010a. Dynamic dependence on ATR and ATM for double-Strand break repair in human embryonic stem cells and neural descendants. PLoS One 5. e10001

Adams, B.R., Hawkins, A.J., Povirk, L.F., Valerie, K., 2010b. ATM-independent, high-fidelity nonhomologous end joining predominates in human embryonic stem cells. Aging (Albany. NY). 2, 582–596.

Alberts, B., Bray, D., Hopkin, K., Johnson, A., Lewis, J., Raff, M., Roberts, K., Walter, P., 2009. Essential Cell Biology (3rd edition). Garl. Sci.

Amino, M., Yoshioka, K., Tanabe, T., Tanaka, E., Mori, H., Furusawa, Y., Zareba, W., Yamazaki, M., Nakagawa, H., Honjo, H., Yasui, K., Kamiya, K., Kodama, I., 2006. Heavy ion radiation up-regulates Cx43 and ameliorates arrhythmogenic substrates in hearts after myocardial infarction. Cardiovasc. Res. 72, 412–421.

Baker, D.E.C., Harrison, N.J., Maltby, E., Smith, K., Moore, H.D., Shaw, P.J., Heath, P.R., Holden, H., Andrews, P.W., 2007. Adaptation to culture of human embryonic stem cells and oncogenesis in vivo. Nat. Biotechnol. 25, 207–215.

Baker, J.E., Fish, B.L., Su, J., Haworth, S.T., Strande, J.L., Komorowski, R.A., Migrino, R.Q., Doppalapudi, A., Harmann, L., Allen Li, X., Hopewell, J.W., Moulder, J.E., 2009. 10 Gy total body irradiation increases risk of coronary sclerosis, degeneration of heart structure and function in a rat model. Int. J. Radiat. Biol. 85, 1089–1100.

Bakshi, M. V., Barjaktarovic, Z., Azimzadeh, O., Kempf, S.J., Merl, J., Hauck, S.M., Eriksson, P., Buratovic, S., Atkinson, M.J., Tapio, S., 2013. Long-term effects of acute low-dose ionizing radiation on the neonatal mouse heart: A proteomic study. Radiat. Environ. Biophys. 52, 451–461.

Baljinnyam, E., Venkatesh, S., Gordan, R., Mareedu, S., Zhang, J., Xie, L.H., Azzam, E.I., Suzuki, C.K., Fraidenraich, D., 2017. Effect of densely ionizing radiation on cardiomyocyte differentiation from human-induced pluripotent stem cells. Physiol. Rep. 5, 1–13.

Bao, Z.-Z., Bruneau, B.G., Seidman, J.G., Seidman, C.E., Cepko, C.L., 1999. Regulation of chamber-specific gene expression in the developing heart by Irx4. Science. 283, 1161–1164.

Barker, D.J.P., 1999. Fetal origins of cardiovascular disease. Ann. Med. 31, 3–6.

Baruscotti, M., Bucchi, A., DiFrancesco, D., 2005. Physiology and pharmacology of the cardiac pacemaker (“funny”) current. Pharmacol. Ther. 107, 59–79.

Becker, K.A., Ghule, P.N., Therrien, J.A., Lian, J.B., Stein, J.L., Van Wijnen, A.J., Stein, G.S., 2006. Self-Renewal of Human Embryonic Stem Cells is Supported by a Shortened G1 Cell Cycle Phase. J. Cell. Physiol. 209, 883–893.

Becker, K.A., Stein, J.L., Lian, J.B., Van Wijnen, A.J., Stein, G.S., 2007. Establishment of histone gene regulation and cell cycle checkpoint control in human embryonic stem cells. J. Cell. Physiol. 210, 517–526.

Beeler, G.W., Reuter, H., 1977. Reconstruction of the action potential of ventricular myocardial fibers. J. Physiol. 268, 177–210.

Beketaev, I., Zhang, Y., Weng, K.C., Rhee, S., Yu, W., Liu, Y., Mager, J., Wang, J., 2016. cis-regulatory control of Mesp1 expression by YY1 and SP1 during mouse embryogenesis. Dev. Dyn. 245, 379–387.

Biel, M., Schneider, A., Wahl, C., 2002. Cardiac HCN Channels : Structure, Function, and Modulation. Trends Cardiovasc. Med. 12, 206–213.

Blauwkamp, T.A., Nigam, S., Ardehali, R., Weissman, I.L., Nusse, R., 2012. Endogenous Wnt signalling in human embryonic stem cells generates an equilibrium of distinct lineage-specified progenitors. Nat. Commun. 3, 1070.

Boerma, M., Kruse, J.J.C.M., van Loenen, M.M., Klein, H.R., Bart, C.I., Zurcher, C., Wondergem, J., 2004. Increased deposition of von Willebrand factor in the rat heart after local ionizing irradiation. Strahlenther Onkol 180, 109–116.

Boerma, M., Sridharan, V., Mao, X.-W., Nelson, G.A., Cheema, A.K., Koturbash, I., Singh, S.P., Tackett, A.J., Hauer-Jensen, M., 2016. Effects of ionizing radiation on the heart. Mutat. Res. 770, 319–327.

Boheler, K.R., Czyz, J., Tweedie, D., Yang, H.T., Anisimov, S. V., Wobus, A.M., 2002. Differentiation of pluripotent embryonic stem cells into cardiomyocytes. Circ. Res. 91, 189–201.

Bondue, A., Blanpain, C., 2010. Mesp1: A key regulator of cardiovascular lineage commitment. Circ. Res. 107, 1414–1427.

Bondue, A., Lapouge, G., Paulissen, C., Semeraro, C., Iacovino, M., Kyba, M., Blanpain, C., 2008. Mesp1 acts as a master regulator of multipotent cardiovascular progenitor specification. Cell Stem Cell 3, 69–84.

Bouillon, K., Haddy, N., Delaloge, S., Garbay, J.R., Garsi, J.P., Brindel, P., Mousannif, A., Lê, M.G., Labbe, M., Arriagada, R., Jougla, E., Chavaudra, J., Diallo, I., Rubino, C., De Vathaire, F., 2011. Long-term cardiovascular mortality after radiotherapy for breast cancer. J. Am. Coll. Cardiol. 57, 445–452.

Boyer, L.A., Tong, I.L., Cole, M.F., Johnstone, S.E., Levine, S.S., Zucker, J.P., Guenther, M.G., Kumar, R.M., Murray, H.L., Jenner, R.G., Gifford, D.K., Melton, D.A., Jaenisch, R., Young, R.A., 2005. Core transcriptional regulatory circuitry in human embryonic stem cells. Cell 122, 947–956.

Brade, T., Pane, L.S., Moretti, A., Chien, K.R., Laugwitz, K.-L., 2013. Embryonic heart progenitors and cardiogenesis. Cold Spring Harb. Perspect. Med. 3, 1–18.

Brutsaert, D.L., 2003. Cardiac Endothelial-Myocardial Signaling: Its Role in Cardiac Growth, Contractile Performance, and Rhythmicity. Physiol. Rev. 83, 59–115.

Bucchi, A., Tognati, A., Milanesi, R., Baruscotti, M., DiFrancesco, D., 2006. Properties of ivabradine-induced block of HCN1 and HCN4 pacemaker channels. J. Physiol. 572, 335–346.

Burridge, P.W., Keller, G., Gold, J.D., Wu, J.C., 2012. Production of de novo cardiomyocytes: Human pluripotent stem cell differentiation and direct reprogramming. Cell Stem Cell 10, 16–28.

Cao, N., Liu, Z., Chen, Z., Wang, J., Chen, T., Zhao, X., Ma, Y., Qin, L., Kang, J., Wei, B., Wang, L., Jin, Y., Yang, H.-T., 2012. Ascorbic acid enhances the cardiac differentiation of induced pluripotent stem cells through promoting the proliferation of cardiac progenitor cells. Cell Res. 22, 219–236.

Cervantes, R.B., Stringer, J.R., Shao, C., Tischfield, J.A., Stambrook, P.J., 2002. Embryonic stem cells and somatic cells differ in mutation frequency and type. Proc. Natl. Acad. Sci. 99, 3586–3590.

Chen, B., Dodge, M.E., Tang, W., Lu, J., Ma, Z., Fan, C.W., Wei, S., Hao, W., Kilgore, J., Williams, N.S., Roth, M.G., Amatruda, J.F., Chen, C., Lum, L., 2009. Small molecule-mediated disruption of Wnt-dependent signaling in tissue regeneration and cancer. Nat. Chem. Biol. 5, 100–107.

Chen, C., Kaimal, A., Laros, R., 2008. Guidelines for computed tomography and magnetic resonance imaging use during pregnancy and lactation. Obs. Gynecol 112, 333–340.

Chen, F.C.M., Yamamura, H.I., Roeske, W.R., 1979. Ontogeny of mammalian myocardial β-adrenergic receptors. Eur. J. Pharmacol. 58, 255–264.

Cho, Y.M., Kwon, S., Pak, Y.K., Seol, H.W., Choi, Y.M., Park, D.J., Park, K.S., Lee, H.K., 2006. Dynamic changes in mitochondrial biogenesis and antioxidant enzymes during the spontaneous differentiation of human embryonic stem cells. Biochem. Biophys. Res. Commun. 348, 1472–1478.

Chong, J.J.H., Yang, X., Don, C.W., Minami, E., Liu, Y.W., Weyers, J.J., Mahoney, W.M., Van Biber, B., Cook, S.M., Palpant, N.J., Gantz, J.A., Fugate, J.A., Muskheli, V., Gough, G.M., Vogel, K.W., Astley, C.A., Hotchkiss, C.E., Baldessari, A., Pabon, L., Reinecke, H., Gill, E.A., Nelson, V., Kiem, H.P., Laflamme, M.A., Murry, C.E., 2014. Human embryonic-stem-cell-derived cardiomyocytes regenerate non-human primate hearts. Nature 510, 273–277.

Coleman, M.A., Sasi, S.P., Onufrak, J., Natarajan, M., Manickam, K., Schwab, J., Muralidharan, S., Peterson, L.E., Alekseyev, Y.O., Yan, X., Goukassian, D.A., 2015. Low-dose radiation affects cardiac physiology: gene networks and molecular signaling in cardiomyocytes. Am. J. Physiol. Circ. Physiol. 309, H1947–H1963.

Cyganek, L., Chen, S., Borchert, T., Guan, K., 2013. Cardiac Progenitor Cells and their Therapeutic Application for Cardiac Repair. J. Clin. Exp. Cardiolog. S11.

David, R., Brenner, C., Stieber, J., Schwarz, F., Brunner, S., Vollmer, M., Mentele, E., Müller-Höcker, J., Kitajima, S., Lickert, H., Rupp, R., Franz, W.M., 2008. MesP1 drives vertebrate cardiovascular differentiation through Dkk-1-mediated blockade of Wnt-signalling. Nat. Cell Biol. 10, 338–345.

David, R., Jarsch, V.B., Schwarz, F., Nathan, P., Gegg, M., Lickert, H., Franz, W.M., 2011. Induction of MesP1 by Brachyury (T) generates the common multipotent cardiovascular stem cell. Cardiovasc. Res. 92, 115–122.

Davidson, K.C., Adams, A.M., Goodson, J.M., McDonald, C.E., Potter, J.C., Berndt, J.D., Biechele, T.L., Taylor, R.J., Moon, R.T., 2012. Wnt/beta-catenin signaling promotes differentiation, not self-renewal, of human embryonic stem cells and is repressed by Oct4. Proc. Natl. Acad. Sci. 109, 4485–4490.

De la Pompa, J.L., Epstein, J.A., 2012. Coordinating Tissue Interactions: Notch Signaling in Cardiac Development and Disease. Dev. Cell 22, 244–254.

De Santis, M., Cesari, E., Nobili, E., Straface, G., Cavaliere, A.F., Caruso, A., 2007. Radiation effects on development. Birth Defects Res. Part C - Embryo Today Rev. 81, 177–182.

Dell'Era, P., Ronca, R., Coco, L., Nicoli, S., Metra, M., Presta, M., 2003. Fibroblast growth factor receptor-1 is essential for in vitro cardiomyocyte development. Circ. Res. 93, 414–420.

Devalla, H.D., Schwach, V., Ford, J.W., Milnes, J.T., El-Haou, S., Jackson, C., Gkatzis, K., Elliott, D.A., Chuva de Sousa Lopes, S.M., Mummery, C.L., Verkerk, A.O., Passier, R., 2015. Atrial-like cardiomyocytes from human pluripotent stem cells are a robust preclinical model for assessing atrial-selective pharmacology. EMBO Mol. Med. 7, 394–410.

DGMP- und DRG-Bericht. Pränatale Strahlenexposition aus medizinischer Indikation, 2002.

Dolezalova, D., Mraz, M., Barta, T., Plevova, K., Vinarsky, V., Holubcova, Z., Jaros, J., Dvorak, P., Pospisilova, S., Hampl, A., 2012. MicroRNAs regulate p21Waf1/Cip1 protein expression and the DNA damage response in human embryonic stem cells. Stem Cells 30, 1362–1372.

Draper, J.S., Smith, K., Gokhale, P., Moore, H.D., Maltby, E., Johnson, J., Meisner, L., Zwaka, T.P., Thomson, J.A., Andrews, P.W., 2004. Recurrent gain of chromosomes 17q and 12 in cultured human embryonic stem cells. Nat. Biotechnol. 22, 53–54.

Dumitru, R., Gama, V., Fagan, B.M., Bower, J.J., Swahari, V., Pevny, L.H., Deshmukh, M., 2012. Human Embryonic Stem Cells Have Constitutively Active Bax at the Golgi and Are Primed to Undergo Rapid Apoptosis. Mol. Cell 46, 573–583.

Dunwoodie, S.L., 2007. Combinatorial signaling in the heart orchestrates cardiac induction, lineage specification and chamber formation. Semin. Cell Dev. Biol. 18, 54–66.

England, J., Loughna, S., 2013. Heavy and light roles: Myosin in the morphogenesis of the heart. Cell. Mol. Life Sci. 70, 1221–1239.

Evans, M.J., Kaufman, M.H., 1981. Establishment in culture of pluripotent cells from mouse embryos. Nature 292, 154–156.

Evans, S.M., Yelon, D., Conlon, F.L., Kirby, M.L., 2010. Myocardial lineage development. Circ. Res. 107, 1428–1444.

Ezashi, T., Das, P., Roberts, R.M., 2005. Low O2 tensions and the prevention of differentiation of hES cells. Nat. Methods 102, 4783–4788.

Fan, J., Robert, C., Jang, Y.Y., Liu, H., Sharkis, S., Baylin, S.B., Rassool, F.V., 2011. Human induced pluripotent cells resemble embryonic stem cells demonstrating enhanced levels of DNA repair and efficacy of nonhomologous end-joining. Mutat. Res. - Fundam. Mol. Mech. Mutagen. 713, 8–17.

Filion, T.M., Qiao, M., Ghule, P.N., Mandeville, M., Van Wijnen, A.J., Stein, J.L., Lian, J.B., Altieri, D.C., Stein, G.S., 2009. Survival responses of human embryonic stem cells to DNA damage. J. Cell. Physiol. 220, 586–592.

Fischer, B., Bavister, B.D., 1993. Oxygen tension in the oviduct and uterus of rhesus monkeys, hamsters and rabbits. J. Reprod. Fertil. 99, 673–679.

Fischer, P., Hilfiker-Kleiner, D., 2008. Role of gp130-mediated signalling pathways in the heart and its impact on potential therapeutic aspects. Br. J. Pharmacol. 153, 414–427.

Freund, C., Ward-van Oostwaard, D., Monshouwer-Kloots, J., van den Brink, S., van Rooijen, M., Xu, X., Zweigerdt, R., Mummery, C., Passier, R., 2008. Insulin redirects differentiation from cardiogenic mesoderm and endoderm to neuroectoderm in differentiating human embryonic stem cells. Stem Cells 26, 724–733.

Frieß, J.L., Heselich, A., Ritter, S., Haber, A., Kaiser, N., Layer, P.G., Thielemann, C., 2015. Electrophysiologic and cellular characteristics of cardiomyocytes after X-ray irradiation. Mutat. Res. - Fundam. Mol. Mech. Mutagen. 777, 1–10.

Fu, J.-D., Rushing, S.N., Lieu, D.K., Chan, C.W., Kong, C.-W., Geng, L., Wilson, K.D., Chiamvimonvat, N., Boheler, K.R., Wu, J.C., Keller, G., Hajjar, R.J., Li, R.A., 2011. Distinct Roles of MicroRNA-1 and -499 in Ventricular Specification and Functional Maturation of Human Embryonic Stem Cell-Derived Cardiomyocytes. PLoS One 6, e27417.

Garate, X., La Greca, A., Neiman, G., Blüguermann, C., Santín Velazque, N.L., Moro, L.N., Luzzani, C., Scassa, M.E., Sevlever, G.E., Romorini, L., Miriuka, S.G., 2018. Identification of the miRNAome of early mesoderm progenitor cells and cardiomyocytes derived from human pluripotent stem cells. Sci. Rep. 8, 1–14.

Gessert, S., Kühl, M., 2010. The multiple phases and faces of Wnt signaling during cardiac differentiation and development. Circ. Res. 107, 186–199.

Greber, B., Lehrach, H., Adjaye, J., 2007. Fibroblast Growth Factor 2 Modulates Transforming Growth Factor β Signaling in Mouse Embryonic Fibroblasts and Human ESCs (hESCs) to Support hESC Self-Renewal. Stem Cells 25, 455–464.

Gros, D.B., Jongsma, H.J., 1996. Connexins in mammalian heart function. BioEssays 18, 719–730.

Gudmundsdottir, K., Ashworth, A., 2006. The roles of BRCA1 and BRCA2 and associated proteins in the maintenance of genomic stability. Oncogene 25, 5864–5874.

Hailstones, D., Barton, P., Chan-Thomas, P., Sasse, S., Sutherland, C., Hardeman, E., Gunning, P., 1992. Differential regulation of the atrial isoforms of the myosin light chains during striated muscle development. J. Biol. Chem. 267, 23295–300.

Hall, E.J., Giaccia, A.J., 2006. Radiobiology for the Radiologist (Sixth Edition). Lippincott Williams & Wilkins.

Hatch, M., Little, M.P., Brenner, A. V., Cahoon, E.K., Tereshchenko, V., Chaikovska, L., Pasteur, I., Likhtarov, I., Bouville, A., Shpak, V., Bolshova, O., Zamotayeva, G., Grantz, K., Sun, L., Mabuchi, K., Albert, P., Tronko, M., 2017. Neonatal outcomes following exposure in utero to fallout from Chernobyl. Eur. J. Epidemiol. 32, 1075–1088.

Hayashi, T., Kusunoki, Y., Hakoda, M., Morishita, Y., Kubo, Y., Maki, M., Kasagi, F., Kodama, K., MacPhee, D.G., Kyoizumi, S., 2003. Radiation dose-dependent increases in inflammatory response markers in A-bomb survivors. Int. J. Radiat. Biol. 79, 129–136.

Hazeltine, L.B., Badur, M.G., Lian, X., Das, A., Han, W., Palecek, S.P., 2014. Temporal impact of substrate mechanics on differentiation of human embryonic stem cells to cardiomyocytes. Acta Biomater. 10, 604–612.

He, C., Chen, F., Li, B., Hu, Z., 2014. Neurophysiology of HCN channels: From cellular functions to multiple regulations. Prog. Neurobiol. 112, 1–23.

He, J.-Q., Ma, Y., Lee, Y., Thomson, J.A., Kamp, T.J., 2003. Human Embryonic Stem Cells Develop Into Multiple Types of Cardiac Myocytes: Action Potential Characterization. Circ. Res. 93, 32–39.

Helm, A., Arrizabalaga, O., Pignalosa, D., Schroeder, I.S., Durante, M., Ritter, S., 2016. Ionizing Radiation Impacts on Cardiac Differentiation of Mouse Embryonic Stem Cells. Stem Cells Dev. 25, 178–188.

Heselich, A., Frieß, J.L., Ritter, S., Benz, N.P., Layer, P.G., Thielemann, C., 2018. High LET radiation shows no major cellular and functional effects on primary cardiomyocytes in vitro. Life Sci. Sp. Res. 16, 93–100.

Houweling, A.C., Van Borren, M.M., Moorman, A.F.M., Christoffels, V.M., 2005. Expression and regulation of the atrial natriuretic factor encoding gene Nppa during development and disease. Cardiovasc. Res. 67, 583–593.

Huang, S.M.A., Mishina, Y.M., Liu, S., Cheung, A., Stegmeier, F., Michaud, G.A., Charlat, O., Wiellette, E., Zhang, Y., Wiessner, S., Hild, M., Shi, X., Wilson, C.J., Mickanin, C., Myer, V., Fazal, A., Tomlinson, R., Serluca, F., Shao, W., Cheng, H., Shultz, M., Rau, C., Schirle, M., Schlegl, J., Ghidelli, S., Fawell, S., Lu, C., Curtis, D., Kirschner, M.W., Lengauer, C., Finan, P.M., Tallarico, J.A., Bouwmeester, T., Porter, J.A., Bauer, A., Cong, F., 2009. Tankyrase inhibition stabilizes axin and antagonizes Wnt signalling. Nature 461, 614–620.

Islas, J.F., Liu, Y., Weng, K.-C., Robertson, M.J., Zhang, S., Prejusa, A., Harger, J., Tikhomirova, D., Chopra, M., Iyer, D., Mercola, M., Oshima, R.G., Willerson, J.T., Potaman, V.N., Schwartz, R.J., 2012. Transcription factors ETS2 and MESP1 transdifferentiate human dermal fibroblasts into cardiac progenitors. Proc. Natl. Acad. Sci. 109, 13016–13021.

Jang, J., Ku, S.Y., Kim, J.E., Choi, K., Kim, Y.Y., Kim, H.S., Oh, S.K., Lee, E.J., Cho, H.-J., Song, Y.H., Lee, S.H., Lee, S.H., Suh, C.S., Kim, S.H., Moon, S.Y., Choi, Y.M., 2008. Notch Inhibition Promotes Human Embryonic Stem Cell-Derived Cardiac Mesoderm Differentiation. Stem Cells 26, 2782–2790.

John, J.C. St., Ramalho-Santos, J., Gray, H.L., Petrosko, P., Rawe, V.Y., Navara, C.S., Simerly, C.R., Schatten, G.P., 2005. The Expression of Mitochondrial DNA Transcription Factors during Early Cardiomyocyte In Vitro Differentiation from Human Embryonic Stem Cells. Cloning Stem Cells 7, 141–153.

Kadari, A., Mekala, S., Wagner, N., Malan, D., Köth, J., Doll, K., Stappert, L., Eckert, D., Peitz, M., Matthes, J., Sasse, P., Herzig, S., Brüstle, O., Ergün, S., Edenhofer, F., 2015. Robust generation of cardiomyocytes from human iPS cells requires precise modulation of BMP and WNT signaling. Stem Cell Rev. Reports 11, 560–569.

Kattman, S.J., Witty, A.D., Gagliardi, M., Dubois, N.C., Niapour, M., Hotta, A., Ellis, J., Keller, G., 2011. Stage-specific optimization of activin/nodal and BMP signaling promotes cardiac differentiation of mouse and human pluripotent stem cell lines. Cell Stem Cell 8, 228–240.

Keller, B.B., MacLennan, M.J., Tinney, J.P., Masaaki, Y., 1996. In Vivo Assessment of Embryonic Cardiovascular Dimensions and Function in Day-10.5 to -14.5 Mouse Embryos. Circ. Res. 79, 247–255.

Kelly, R.G., 2012. The Second Heart Field, Current Topics in Developmental Biology. Elsevier Inc.

Kelly, R.G., Buckingham, M.E., Moorman, A.F., 2014. Heart fields and cardiac morphogenesis. Cold Spring Harb. Perspect. Med. 4:a015750

Keung, W., Boheler, K.R., Li, R.A., 2014. Developmental cues for the maturation of metabolic, electrophysiological and calcium handling properties of human pluripotent stem cell-derived cardiomyocytes. Stem Cell Res. Ther. 5.

Kimler, B.F., Norton, S., 1988. Behavioral changes and structural defects in rats irradiated in utero. Int. J. Radiat. Oncol. Biol. Phys. 15, 1171–1177.

Kirkpatrick, C.J., Melzner, I., Goller, T., 1985. Comparative Effects of Trypsin, Collagenase and Mechanical Harvesting on Cell-Membrane Lipids Studied in Monolayer-Cultured Endothelial-Cells and a Green Monkey Kidney-Cell Line. Biochim. Biophys. Acta 846, 120–126.

Kodama, K., Mabuchi, K., Shigematsu, I., 1996. A Long-Term Cohort Study of the Atomic-Bomb Survivors. J. Epidemiol. 6. S95-S105

Kolanowski, T.J., Antos, C.L., Guan, K., 2017. Making human cardiomyocytes up to date: Derivation, maturation state and perspectives. Int. J. Cardiol. 241, 379–386.

Kopan, R., 2012. Notch Signaling. Cold Spring Harb. Perspect. Biol. 4, 1–5.

Koyanagi, M., Bushoven, P., Iwasaki, M., Urbich, C., Zeiher, A.M., Dimmeler, S., 2007. Notch signaling contributes to the expression of cardiac markers in human circulating progenitor cells. Circ. Res. 101, 1139–1145.

Kwon, C., Qian, L., Cheng, P., Nigam, V., Arnold, J., Srivastava, D., 2009. A regulatory pathway involving Notch1/β-catenin/Isl1 determines cardiac progenitor cell fate. Nat. Cell Biol. 11, 951–957.

Lampidis, T.J., Weichselbaum, R.R., Little, J.B., 1975. Gamma-irradiation of Mammalian Beating Heart Cells in Vitro Effects on Cellular Function. Int. J. Radiat. Biol. Relat. Stud. Physics, Chem. Med. 28, 99–102.

Lee, S., Otake, M., Schull, W.J., 1999. Changes in the pattern of growth in stature related to prenatal exposure to ionizing radiation. Int. J. Radiat. Biol. 75, 1449–1458.

Li, Y., Yu, W., Cooney, A.J., Schwartz, R.J., Liu, Y., 2013. Oct4 and canonical Wnt signaling regulate the cardiac lineage factor Mesp1 through a Tcf/Lef-Oct4 composite element, Stem Cells.

Lian, X., Zhang, J., Azarin, S.M., Zhu, K., Hazeltine, L.B., Bao, X., Hsiao, C., Kamp, T.J., Palecek, S.P., 2013a. Directed cardiomyocyte differentiation from human pluripotent stem cells by modulating Wnt/b-catenin signaling under fully defined conditions. Nat. Protoc. 8, 162–175.

Lian, X., Zhang, J., Zhu, K., Kamp, T.J., Palecek, S.P., 2013b. Insulin inhibits cardiac mesoderm, not mesendoderm, formation during cardiac differentiation of human pluripotent stem cells and modulation of canonical wnt signaling can rescue this inhibition. Stem Cells 31, 447–457.

Lie, R.T., Moster, D., Strand, P., Wilcox, A.J., 2017. Prenatal exposure to Chernobyl fallout in Norway: neurological and developmental outcomes in a 25-year follow-up. Eur. J. Epidemiol. 32, 1065–1073.

Liu, J., Laksman, Z., Backx, P.H., 2016. The electrophysiological development of cardiomyocytes. Adv. Drug Deliv. Rev. 96, 253–273.

Liu, Y.-W., Chen, B., Yang, X., Fugate, J.A., Kalucki, F.A., Futakuchi-Tsuchida, A., Couture, L.,

Vogel, K.W., Astley, C.A., Baldessari, A., Ogle, J., Don, C.W., Steinberg, Z.L., Seslar, S.P., Tuck, S.A., Tsuchida, H., Naumova, A. V, Dupras, S.K., Lyu, M.S., Lee, J., Hailey, D.W., Reinecke, H., Pabon, L., Fryer, B.H., Robb MacLellan, W., Scott Thies, R., Murry, C.E., 2018. Human embryonic stem cell–derived cardiomyocytes restore function in infarcted hearts of non-human primates. Nat. Biotechnol. 36, 597–605.

Luft, S., Arrizabalaga, O., Kulish, I., Nasonova, E., Durante, M., Ritter, S., Schroeder, I.S., 2017. Ionizing Radiation Alters Human Embryonic Stem Cell Properties and Differentiation Capacity by Diminishing the Expression of Activin Receptors. Stem Cells Dev. 26, 341–352.

Luft, S., Pignalosa, D., Nasonova, E., Arrizabalaga, O., Helm, A., Durante, M., Ritter, S., 2014. Fate of D3 mouse embryonic stem cells exposed to X-rays or carbon ions. Mutat. Res. - Genet. Toxicol. Environ. Mutagen. 760, 56–63.

MacDonald, B.T., Tamai, K., He, X., 2009. Wnt/β-Catenin Signaling: Components, Mechanisms, and Diseases. Dev. Cell 17, 9–26.

Martin, G.R., 1981. Isolation of a pluripotent cell line from early mouse embryos cultured in medium conditioned by teratocarcinoma stem cells. Proc. Natl. Acad. Sci. 78, 7634–7638.

Mazzotta, S., Neves, C., Bonner, R.J., Bernardo, A.S., Docherty, K., Hoppler, S., 2016. Distinctive Roles of Canonical and Noncanonical Wnt Signaling in Human Embryonic Cardiomyocyte Development. Stem Cell Reports 7, 764–776.

Menasché, P., Vanneaux, V., Hagège, A., Bel, A., Cholley, B., Cacciapuoti, I., Parouchev, A., Benhamouda, N., Tachdjian, G., Tosca, L., Trouvin, J.H., Fabreguettes, J.-R., Bellamy, V., Guillemain, R., Suberbielle Boissel, C., Tartour, E., Desnos, M., Larghero, J., 2015. Human embryonic stem cell-derived cardiac progenitors for severe heart failure treatment: First clinical case report. Eur. Heart J. 36, 2011–2017.

Menasché, P., Vanneaux, V., Hagège, A., Cholley, B., Tachdjian, G., Tosca, L., Trouvin, J.-H., Fabreguettes, J.-R., Blons, H., Al-Daccak, R., Agbulut, O., Tartour, E., Desnos, M., Larghero, J., 2017. Abstract 14798: Human Embryonic Stem Cell-derived Cardiac Progenitors for Heart Failure. One-year Results of the ESCORT Trial. Circulation 136.

Metzeler, K.H., Heilmeier, B., Edmaier, K.E., Rawat, V.P.S., Dufour, A., Döhner, K., Feuring-Buske, M., Braess, J., Spiekermann, K., Büchner, T., Sauerland, M.C., Döhner, H., Hiddemann, W., Bohlander, S.K., Schlenk, R.F., Bullinger, L., Buske, C., 2012. High expression of lymphoid enhancer-binding factor-1 (LEF1) is a novel favorable prognostic factor in cytogenetically normal acute myeloid leukemia. Blood 120, 2118–2126.

Mitalipova, M.M., Rao, R.R., Hoyer, D.M., Johnson, J.A., Meisner, L.F., Jones, K.L., Dalton, S., Stice, S.L., 2005. Preserving the genetic integrity of human embryonic stem cells. Nat. Biotechnol. 23, 19–20.

Momcilovic, O., Choi, S., Varum, S., Bakkenist, C., Schatten, G., Navara, C., 2009. Ionizing radioation induces ATM dependent checkpoint signaling and G2 but not G1 cell cycle arrest in pluripotent human embryonic stem cells. Stem Cells 27, 1822–1835.

Mone, S.M., Gillman, M.W., Miller, T.L., Herman, E.H., Lipshultz, S.E., 2004. Effects of Environmental Exposures on the Cardiovascular System: Prenatal Period Through Adolescence. Pediatrics 113, 1058–1069.

Moorman, A.F.M., Jong, F. de, Denyn, M.M.F.J., Lamers, W.H., 1998. Mini Review Development of the Cardiac Conduction System. Circ. Res. 82, 629–644.

Morgani, S., Nichols, J., Hadjantonakis, A.K., 2017. The many faces of Pluripotency: In vitro adaptations of a continuum of in vivo states. BMC Dev. Biol. 17, 10–12.

Mummery, C., Ward-van Oostwaard, D., Doevendans, P., Spijker, R., van den Brink, S., Hassink, R., van der Heyden, M., Opthof, T., Pera, M., de la Riviere, A.B., Passier, R., Tertoolen, L., 2003. Differentiation of human embryonic stem cells to cardiomyocytes: role of coculture with visceral endoderm-like cells. Circulation 107, 2733–40.

Nagaria, P., Robert, C., Rassool, F. V., 2013. DNA double-strand break response in stem cells: Mechanisms to maintain genomic integrity. Biochim. Biophys. Acta - Gen. Subj. 1830, 2345–2353.

Naito, A.T., Shiojima, I., Akazawa, H., Hidaka, K., Morisaki, T., Kikuchi, A., Komuro, I., 2006. Developmental stage-specific biphasic roles of Wnt/beta-catenin signaling in cardiomyogenesis and hematopoiesis. Proc. Natl. Acad. Sci. 103, 19812–19817.

Nelson, D.O., Lalit, P.A., Biermann, M., Markandeya, Y.S., Capes, D.L., Addesso, L., Patel, G., Han, T., John, M.C., Powers, P.A., Downs, K.M., Kamp, T.J., Lyons, G.E., 2016. Irx4 marks a multipotent, ventricular-specific progenitor cell. Stem Cells 34, 2875–2888.

Nguyen, H.T., Geens, M., Spits, C., 2013. Genetic and epigenetic instability in human pluripotent stem cells. Hum. Reprod. Update 19, 187–205.

Nichols, J., Smith, A., 2009. Naive and Primed Pluripotent States. Cell Stem Cell 4, 487–492.

Niehoff, J., Matzkies, M., Nguemo, F., Hescheler, J., Reppel, M., 2016. Beat rate variability in murine embryonic stem cell-derived cardiomyocytes: Effect of antiarrhythmic drugs. Cell. Physiol. Biochem. 38, 646–658.

Nitsch, S., Braun, F., Ritter, S., Scholz, M., Schroeder, I.S., 2018. Functional video-based analysis of 3D cardiac structures generated from human embryonic stem cells. Stem Cell Res. 29, 115–124.

Niwa, H., Miyazaki, J., Smith, A.G., 2000. Quantitative expression of OCT3/4 defines differentiation, dedifferentiation or self-renewal of ES cells. Nat Genet 24, 372–376.

Pallotta, I., Sun, B., Wrona, E.A., Freytes, D.O., 2017. BMP protein-mediated crosstalk between inflammatory cells and human pluripotent stem cell-derived cardiomyocytes. J. Tissue Eng. Regen. Med. 11, 1466–1478.

Pampfer, S., Streffer, C., 1988. Prenatal death and malformations after irradiation of mouse zygotes with neutrons or X-rays. Teratology 37, 599–607.

Pandur, P., Läsche, M., Eisenberg, L.M., Kühl, M., 2002a. Wnt-11 activation of a non-canonical Wnt signalling pathway is required for cardiogenesis. Nature 418, 636–641.

Pandur, P., Läsche, M., Eisenberg, L.M., Kühl, M., 2002b. American men of letters: their nature and nurture. Nature 418.

Pannunzio, N.R., Watanabe, G., Lieber, M.R., 2018. Nonhomologous DNA end-joining for repair of DNA double-strand breaks. J. Biol. Chem. 293, 10512–10523.

Pauklin, S., Vallier, L., 2013. Erratum: The cell-cycle state of stem cells determines cell fate propensity. Cell 155, 135–147.

Puukila, S., Lemon, J.A., Lees, S.J., Tai, T.C., Boreham, D.R., Khaper, N., 2017. Impact of Ionizing Radiation on the Cardiovascular System: A Review. Radiat. Res. 188, 539–546.

Rebuzzini, P., Fassina, L., Mulas, F., Bellazzi, R., Redi, C.A., Di Liberto, R., Magenes, G., Adjaye, J., Zuccotti, M., Garagna, S., 2013. Mouse embryonic stem cells irradiated with γ-rays differentiate into cardiomyocytes but with altered contractile properties. Mutat. Res. - Genet. Toxicol. Environ. Mutagen. 756, 37–45.

Rebuzzini, P., Pignalosa, D., Mazzini, G., Di Liberto, R., Coppola, A., Terranova, N., Magni, P., Redi, C.A., Zuccotti, M., Garagna, S., 2012. Mouse embryonic stem cells that survive gamma-rays exposure maintain pluripotent differentiation potential and genome stability. J. Cell. Physiol. 227, 1242–1249.

Reiser, P.J., Portman, M.A., Ning, X.H., Schomisch Moravec, C., 2001. Human cardiac myosin heavy chain isoforms in fetal and failing adult atria and ventricles. Am. J. Physiol. Heart Circ. Physiol. 280, H1814–H1820.

Rones, M.S., McLaughlin, K.A., Raffin, M., Mercola, M., 2000. Serrate and Notch specify cell fates in the heart field by suppressing cardiomyogenesis. Development 127, 3865–3876.

Saga, Y., Kitajima, S., Miyagawa-Tomita, S., 2000. Mesp1 Expression Is the Earliest Sign of Cardiovascular Development. Trends Cardiovasc Med. 10, 345–52.

Saito, S., Sawada, K., Mori, Y., Yoshioka, Y., Murase, K., 2015. Brain and arterial abnormalities following prenatal X-ray irradiation in mice assessed by magnetic resonance imaging and angiography. Congenit. Anom. 55, 103–106.

San Filippo, J., Sung, P., Klein, H., 2008. Mechanism of Eukaryotic Homologous Recombination. Annu. Rev. Biochem. 77, 229–257.

Saretzki, G., Armstrong, L., Leake, A., Lako, M., von Zglinicki, T., 2004. Stress Defense in Murine Embryonic Stem Cells is Superior to That of Various Differentiated Murine Cells. Stem Cells 22, 962–971.

Sartiani, L., Bettiol, E., Stillitano, F., Mugelli, A., Cerbai, E., Jaconi, M.E., 2007. Developmental Changes in Cardiomyocytes Differentiated from Human Embryonic Stem Cells: A Molecular and Electrophysiological Approach. Stem Cells 25, 1136–1144.

Sauer, H., Theben, T., Hescheler, J., Lindner, M., Brandt, M.C., Wartenberg, M., 2001. Characteristics of calcium sparks in cardiomyocytes derived from embryonic stem cells. Am. J. Physiol. Heart Circ. Physiol. 281, H411–H421.

Schroeder, T., Meier-Stiegen, F., Schwanbeck, R., Eilken, H., Nishikawa, S., Häsler, R., Schreiber, S., Bornkamm, G.W., Nishikawa, S.I., Just, U., 2006. Activated Notch1 alters differentiation of embryonic stem cells into mesodermal cell lineages at multiple stages of development. Mech. Dev. 123, 570–579.

Schull, W., Otake, M., 1999. Cognitive function and prenatal exposure to ionizing radiation. Teratology 59, 222–226.

Seemann, I., Gabriels, K., Visser, N.L., Hoving, S., Te Poele, J.A., Pol, J.F., Gijbels, M.J., Janssen, B.J., Van Leeuwen, F.W., Daemen, M.J., Heeneman, S., Stewart, F.A., 2012. Irradiation induced modest changes in murine cardiac function despite progressive structural damage to the myocardium and microvasculature. Radiother. Oncol. 103, 143–150.

Sehnert, A.J., Huq, A., Weinstein, B.M., Walker, C., Fishman, M., Stainier, D.Y.R., 2002. Cardiac troponin T is essential in sarcomere assembly and cardiac contractility. Nat. Genet. 31, 106–110.

Seidman, J.G., Seidman, C., 2001. The Genetic Basis for Cardiomyopathy. Cell 104, 557–567.

Sela, Y., Molotski, N., Golan, S., Itskovitz-Eldor, J., Soen, Y., 2012. Human embryonic stem cells exhibit increased propensity to differentiate during the G1 phase prior to phosphorylation of retinoblastoma protein. Stem Cells 30, 1097–1108.

Semenov, M. V., Habas, R., MacDonald, B.T., He, X., 2007. SnapShot: Noncanonical Wnt Signaling Pathways. Cell 131, 11–12.

Shenoy, S., Rockman, H.A., 2011. Heart fails without pump partner. Nature 477, 546–547.

Shimizu, Y., Kodama, K., Nishi, N., Kasagi, F., Suyama, A., Soda, M., Grant, E.J., Sugiyama, H., Sakata, R., Moriwaki, H., Hayashi, M., Konda, M., Shore, R.E., 2010. Radiation exposure and circulatory disease risk: Hiroshima and Nagasaki atomic bomb survivor data, 1950-2003. BMJ 340.

Showell, C., Binder, O., Conlon, F.L., 2004. T-box Genes in Early Embryogenesis. Dev. Dyn. 229, 201–218.

Singh, A.M., Reynolds, D., Cliff, T., Ohtsuka, S., Mattheyses, A.L., Sun, Y., Menendez, L., Kulik, M., Dalton, S., 2012. Signaling network crosstalk in human pluripotent cells: A Smad2/3-regulated switch that controls the balance between self-renewal and differentiation. Cell Stem Cell 10, 312–326.

Snyder, M., Huang, X.Y., Zhang, J.J., 2010. Stat3 directly controls the expression of Tbx5, Nkx2.5, and GATA4 and is essential for cardiomyocyte differentiation of P19CL6 cells. J. Biol. Chem. 285, 23639–23646.

Söhl, G., Willecke, K., 2004. Gap junctions and the connexin protein family. Cardiovasc. Res. 62, 228–232.

Sokolov, M., Nguyen, V., Neumann, R., 2015. Comparative Analysis of Whole-Genome Gene Expression Changes in Cultured Human Embryonic Stem Cells in Response to Low, Clinical Diagnostic Relevant, and High Doses of Ionizing Radiation Exposure. Int. J. Mol. Sci. 16, 14737–14748.

Sokolov, M. V., Panyutin, I. V., Onyshchenko, M.I., Panyutin, I.G., Neumann, R.D., 2010. Expression of pluripotency-associated genes in the surviving fraction of cultured human embryonic stem cells is not significantly affected by ionizing radiation. Gene 455, 8–15.

Sokolov, M. V., Panyutin, I. V., Panyutin, I.G., Neumann, R.D., 2011. Dynamics of the transcriptome response of cultured human embryonic stem cells to ionizing radiation exposure. Mutat. Res. - Fundam. Mol. Mech. Mutagen. 709–710, 40–48.

Spencer, C.I., Baba, S., Nakamura, K., Hua, E.A., Sears, M.A.F., Fu, C.C., Zhang, J., Balijepalli, S., Tomoda, K., Hayashi, Y., Lizarraga, P., Wojciak, J., Scheinman, M.M., Aalto-Setälä, K., Makielski, J.C., January, C.T., Healy, K.E., Kamp, T.J., Yamanaka, S., Conklin, B.R., 2014. Calcium transients closely reflect prolonged action potentials in iPSC models of inherited cardiac arrhythmia. Stem Cell Reports 3, 269–281.

Stammzellgesetz - StZG, 2002.

Stieber, J., Herrmann, S., Feil, S., Loster, J., Feil, R., Biel, M., Hofmann, F., Ludwig, A., 2003. The hyperpolarization-activated channel HCN4 is required for the generation of pacemaker action potentials in the embryonic heart. Proc. Natl. Acad. Sci. 100, 15235–15240.

Tatsukawa, Y., Nakashima, E., Yamada, M., Funamoto, S., Hida, A., Akahoshi, M., Sakata, R., Ross, N.P., Kasagi, F., Fujiwara, S., Shore, R.E., 2008. Cardiovascular disease risk among atomic bomb survivors exposed in utero, 1978-2003. Radiat. Res. 170, 269–274.

Taylor, C.W., Kirby, A.M., 2015. Cardiac Side-effects From Breast Cancer Radiotherapy. Clin. Oncol. 27, 621–629.

Terami, H., Hidaka, K., Katsumata, T., Iio, A., Morisaki, T., 2004. Wnt11 facilitates embryonic stem cell differentiation to Nkx2.5-positive cardiomyocytes. Biochem. Biophys. Res. Commun. 325, 968–975.

Thollon, C., Bidouard, J.P., Cambarrat, C., Lesage, L., Reure, H., Delescluse, I., Vian, J., Peglion, J.L., Vilaine, J.P., 1997. Stereospecific in vitro and in vivo effects of the new sinus node inhibitor (+)-S 16257. Eur. J. Pharmacol. 339, 43–51.

Thomson, J.A., Itskovitz-Eldor, J., Shapiro, S.S., Waknitz, M.A., Swiergiel, J.J., Marshall, V.S., Jones, J.M., 1998. Embryonic Stem Cell Lines Derived from Human Blastocysts. Science. 282, 1145–1147.

Tichy, E.D., Pillai, R., Deng, L., Liang, L., Tischfield, J., Schwemberger, S.J., Babcock, G.F., Stambrook, P.J., 2010. Mouse embryonic stem cells, but not somatic cells, predominantly use homologous recombination to repair double-strand DNA breaks. Stem Cells Dev. 19, 1699–1711.

Tirziu, D., Giordano, F.J., Simons, M., 2010. Cell communications in the heart. Circulation 122, 928–937.

Tohyama, S., Hattori, F., Sano, M., Hishiki, T., Nagahata, Y., Matsuura, T., Hashimoto, H., Suzuki, T., Yamashita, H., Satoh, Y., Egashira, T., Seki, T., Muraoka, N., Yamakawa, H., Ohgino, Y., Tanaka, T., Yoichi, M., Yuasa, S., Murata, M., Suematsu, M., Fukuda, K., 2013. Distinct metabolic flow enables large-scale purification of mouse and human pluripotent stem cell-derived cardiomyocytes. Cell Stem Cell 12, 127–137.

Valentijn, K.M., Sadler, J.E., Valentijn, J.A., Voorberg, J., Eikenboom, J., 2014. Functional architecture of Weibel-Palade bodies. Blood 117, 5033–5043.

Varum, S., Rodrigues, A.S., Moura, M.B., Momcilovic, O., Easley IV, C.A., Ramalho-Santos, J., van Houten, B., Schatten, G., 2011. Energy metabolism in human pluripotent stem cells and their differentiated counterparts. PLoS One 6, e20914.

Wagner, M., Siddiqui, M.A.Q., 2007. Signal transduction in early heart development (I): cardiogenic induction and heart tube formation. Exp. Biol. Med. (Maywood). 232, 852–865.

Wang, Z., Oron, E., Nelson, B., Razis, S., Ivanova, N., 2012. Distinct lineage specification roles for NANOG, OCT4, and SOX2 in human embryonic stem cells. Cell Stem Cell 10, 440–454.

Weisbrod, D., Khun, S.H., Bueno, H., Peretz, A., Attali, B., 2016. Mechanisms underlying the cardiac pacemaker: The role of SK4 calcium-activated potassium channels. Acta Pharmacol. Sin. 37, 82–97.

Williams, P.M., Fletcher, S., 2010. Health effects of prenatal radiation exposure. Am Fam Physician 82, 488–493.

Wilson, K.D., Sun, N., Huang, M., Zhang, W.Y., Lee, A.S., Li, Z., Wang, S.X., Wu, J.C., 2010. Effects of ionizing radiation on self-renewal and pluripotency of human embryonic stem cells. Cancer Res. 70, 5539–5548.

Wong, R.C.B., Pera, M.F., Pébay, A., 2008. Role of gap junctions in embryonic and somatic stem cells. Stem Cell Rev. 4, 283–292.

Wrighton, P.J., Klim, J.R., Hernandez, B.A., Koonce, C.H., Kamp, T.J., 2014. Signals from the surface modulate differentiation of human pluripotent stem cells through glycosaminoglycans and integrins. PNAS 111, 18126–18131.

Wu, S., Cheng, C.M., Lanz, R.B., Wang, T., Respress, J.L., Ather, S., Chen, W., Tsai, S.J., Wehrens, X.H.T., Tsai, M.J., Tsai, S.Y., 2013. Atrial Identity Is Determined by a COUP-TFII Regulatory Network. Dev. Cell 25, 417–426.

Yamada, M., Lennie Wong, F., Fujiwara, S., Akahoshi, M., Suzuki, G., 2004. Noncancer Disease Incidence in Atomic Bomb Survivors, 1958–1998. Radiat. Res. 161, 622–632.

Yan, X., Sasi, S.P., Gee, H., Lee, J., Yang, Y., Mehrzad, R., Onufrak, J., Song, J., Enderling, H., Agarwal, A., Rahimi, L., Morgan, J., Wilson, P.F., Carrozza, J., Walsh, K., Kishore, R., Goukassian, D.A., 2014. Cardiovascular Risks Associated with Low Dose Ionizing Particle Radiation. PLoS One 9, e110269.

Yang, X., Pabon, L., Murry, C.E., 2014. Engineering adolescence: Maturation of human pluripotent stem cell-derived cardiomyocytes. Circ. Res. 114, 511–523.

Yasui, K., Liu, W., Opthof, T., Kada, K., Lee, J., Kamiya, K., Kodama, I., 2001. If Current and Spontaneous Activity in Mouse Embryonic Ventricular Myocytes. Circ. Res. 88, 536–542.

Yeo, J.C., Ng, H.H., 2013. The transcriptional regulation of pluripotency. Cell Res. 23, 20–32.

Zhang, Q., Jiang, J., Han, P., Yuan, Q., Zhang, J., Zhang, X., Xu, Y., Cao, H., Meng, Q., Chen, L., Tian, T., Wang, X., Li, P., Hescheler, J., Ji, G., Ma, Y., 2011. Direct differentiation of atrial and ventricular myocytes from human embryonic stem cells by alternating retinoid signals. Cell Res. 21, 579–587.

Zhao, Y., Ransom, J.F., Li, A., Vedantham, V., von Drehle, M., Muth, A.N., Tsuchihashi, T., McManus, M.T., Schwartz, R.J., Srivastava, D., 2007. Dysregulation of Cardiogenesis, Cardiac Conduction, and Cell Cycle in Mice Lacking miRNA-1-2. Cell 129, 303–317.

Zhao, Y., Samal, E., Srivastava, D., 2005. Serum response factor regulates a muscle-specific microRNA that targets Hand2 during cardiogenesis. Nature 436, 214–220.

Zhou, C., Yang, X., Sun, Y., Yu, H., Zhang, Y., Jin, Y., 2016. Comprehensive profiling reveals mechanisms of SOX2-mediated cell fate specification in human ESCs and NPCs. Cell Res. 26, 171–189.

Appendix

App. Table 1: Kits.

Kit	Manufacturer	Catalog number
24xCyte Human Multicolor FISH Probe Kit	Metasystems	D-0125060
CellEvent™ Caspase-3/7 Green Flow Cytometry Assay Kit	Invitrogen/Thermo Fisher Scientific	C10427
HOT FIREPol® EvaGreen® qPCR Mix Plus	Solis Biodyne	083600001
miScript II RT Kit	QIAGEN	218161
miScript SYBR Green PCR Kit	QIAGEN	218075
RevertAid RT Reverse Transcription Kit	Thermo Scientific	K1691
RNase-free DNase Set	QIAGEN	79254
RNeasy Mini Kit	QIAGEN	74106
RT² First Strand Kit	QIAGEN	330404
RT² SYBR® Green ROX qPCR Mastermix	QIAGEN	330523

App. Table 2: Media and supplements

Substance	Source	Catalog number
Ascorbic Acid	Sigma Aldrich/Merck	A-4034
B-27™ minus insulin	Life technologies	A18956-01
FGF2	PeproTech	100-18B
β-Mercaptoethanol	Carl Roth	4227.3
BMP-4	PeproTech	120-05
CHIR99021	BioVision	1991-1
DMEM	Biochrom	FG0445
FCS	Biochrom/Merck	S0115
IWP2	Tocris Bioscience	3533
Knockout DMEM	Invitrogen	10829-018
Knockout Serum Replacer	Invitrogen	10828-028
L-Alanyl-L-Glutamine	Merck	K0302
mTeSR1™ Medium	STEMCELL Technologies	85851
mTeSR1™ 5x supplement	STEMCELL Technologies	85852
Non-essential amino acids	Biochrom/Merck	K0293
Penicillin/Streptomycin	Biochrom/Merck	A2212
RPMI 1640 (with stable glutamine)	Biochrom/Merck	FG1215
StemBeads® FGF2	StemCultures	SB500
XAV 939	Tocris Bioscience	3748
Y-27632 ROCK-Inhibitor	Enzo Life Sciences	ALX-270-333

App. Table 3: Chemicals

Substance	Source	Catalog number
Accutase®	Life Technologies	A11105-01
Acetic Acid	Carl Roth	3738.4
β-Mercaptoethanol	Carl Roth	4227.3
BSA (Albumin Fraction V)	Carl Roth	8076.3
Chloroform	Carl Roth	6340.1
Citric Acid Monohydrate	Carl Roth	5110.1
Colcemide	Biochrom/Merck	L6231
DMSO	Carl Roth	A994.1
Ethanol (> 99.8 %)	Carl Roth	9065.3
Fluorescent Mounting Medium	Dako	S3023
Formaldehyde (37 %)	Carl Roth	CP10-1
Gelatine powder	NeoLab	9475.0500
Geltrex™	Life Technologies	A15696-01
Hoechst-33342	Thermo Scientific	62249
5x HOT FIREPol®	Solis Biodyne	083600001
Isoproterenol hydrochloride	Sigma Aldrich/Merck	I6504
Ivabradine hydrochloride	Sigma Aldrich/Merck	SML0281
Laminin-521	BioLamina	600962
Matrigel	Corning	354234
Methanol	Carl Roth	8388.5
Nuclease free water	Acros Organics	HV-88295-49
$PBS^{-/-}$	Merck	L1825
$PBS^{+/+}$	Life Technologies	14040091
QIAzol® Lysis Reagent	QIAGEN	79306
ReleSR™	STEMCELL Technologies	05872
Triton X-100	Sigma Aldrich/Merck	T8787
Trypsin	PAN-Biotech	P10-027500

App. Table 4: Devices.

Type	Manufacturer
Axio Imager Z2 microscope	Zeiss
Automatic Cell Counter TC20	BioRad
Dry Bath Incubator FB15103	Thermo Fisher Scientific
Leica DMI 4000B microscope	Leica
Leica DM IRBE microscope	Leica
Nanophotometer Colibri	Titertek Berthold
PCR Thermal Cycler Peqstar	Peqlab/VWR
Quant Studio 3	Thermo Fisher Scientific
SN4 dosimeter	PTW
StepOnePlus Real-Time PCR Systems	Thermo Fisher Scientific
UI-3140CP-M-GL Rev. 2 camera	IDS
X-ray Tube Isovolt DS1	Seifert

App. Table 5: Softwares.

Name	Manufacturer
ABI StepOne Software v2.3	ABI/Thermo Fisher Scientific
cardiac Beat Rate Analyzer (cBRA)	F. Braun/M. Scholz
FACSDiva v7.0	BD Biosciences
Fiji	Open source, contributors: https://imagej.net/Contributors
ISIS Software	MetaSystems
Metafer 4 Software	MetaSystems
Origin	OriginLab
Quant Studio™ Design & Analysis Software v1.4	ABI/Thermo Fisher Scientific

App. Table 6: RNA used for standard curves for different markers.

Primers	RNA used for Standard Curve	Manufacturer
cardiac markers	total RNA of human fetal heart tissue total RNA of human adult heart tissue	Clontech BioChain
endothelial markers	total RNA of human adult lung tissue	BioChain
endodermal markers	total RNA of human fetal liver	Clontech
pluripotency markers	pluripotent hESCs	-
mesodermal markers	differentiating hESCs at day 2 of cardiac differentiation	-

App. Table 7: qRT-PCR-primers for human target genes. All primers were manufactured by the company *biomers.net.*

Target	Sequence (5‘ … 3‘)
18sRNA (s)	ACT CAA CAC GGG AAA CCT CAC C
18sRNA (as)	CGC TCC ACC AAC TAA GAA CGG
NANOG (s)	AAA TCT AAG AGG TGG CAG AAA AAC A
NANOG (as)	CTT CTG CGT CAC ACC ATT GC
OCT4 (s)	ACC CAC ACT GCA GCA GAT CA
OCT4 (as)	CAC ACT CGG ACC ACA TCC TTC T
Brachyury (T) (s)	TGC TGC AAT CCC ATG ACA
Brachyury (T) (as)	CGT TGC TCA CAG ACC ACA
MESP1 (s)	TGA GGA GCC CAA GTG ACA AG
MESP1 (as)	GTC TGC CAA GGA ACC ACT TC
HCN4 (s)	TGA TGG TGG GAA ACC TGA TTA
HCN4 (as)	GTT GAG GAC CAA GTC GAT GAG
alpha MHC (s)	GAC TGT TGT GGC CCT GTA CCA
alpha MHC (as)	TTT TAC CAC TGC CCC AGT ATC G
beta MHC (s)	CTG CAC AGG GAA AAT CTG AAC A
beta MHC (as)	GTC CAT CAC CCC TGG AGA CTT
MLC2a (s)	CTG AGT GCC TTC CGC ATG T
MLC2a (as)	CCA CCT CAG CTG GAG AGA ACT T
MLC2v (s)	CTC TGT CCC TAC CTT GTC TGT TAG C
MLC2v (as)	GCC ACC CAG GCT GCA A
NKX2.5 (s)	CCT GCG GAG ACC TAG GAA CTT
NKX2.5 (as)	CTC ATT GCA CGC TGC ATA ATC
GATA4 (s)	CCT GAA GCT CTC CCC ACA AG
GATA4 (as)	CCA AGA CCA GGC TGT TCC AA
TNNT2 (s)	AGT TCA AGC AGC AGA AAT ATG AGA TC

TNNT2 (as)	GTG AAG GAG GCC AGG CTC TA
TBX5 (s)	GAA CCA CAA GAT CAC GCA ATT A
TBX5 (as)	ACA CCA TTC TCA CAC TGG TAT
NPPA (s)	TGA TCG ATC TGC CCT CCT A
NPPA (as)	TGT CCT CCC TGG CTG TTA TC
NR2F2 (s)	GCC CGG GTA GCG ACA AG
NR2F2 (as)	CAC GTG AAC TGG CCG TAG TG
KCNA5 (s)	TAC CAC CGG GAA ACG GAT CA
KCNA5 (as)	CTT CGG GCA CTG TCT GCA TT
CD31 (s)	TGC CGT GGA AAG CAG ATA CTC
CD31 (as)	AGC CTG AGG AAT TGC TGT GTT
vWF (s)	TGT CCA GCA GCT GAG TTT CC
vWF (as)	AAG GGT CCC TGG CAA AAT GA
IRX4 (s)	CTC TGG GCC AGT ACC CCT AT
IRX4 (as)	GAG AGG TCC AGG CCA ATT CC
IL6ST (s)	ACT GGA GTG ACT GGA GTG AAG
IL6ST (as)	AGC CTT GAG TAT GGG ATG GA
WNT11 (s)	AGC GCT ATG TCT GCA AGT GA
WNT11 (as)	CCT GGT GGC TTC CAA GTG AA
AFP (s)	CTG CAA ACT GAC CAC GCT
AFP (as)	TGA GAC AGC AAG CTG AGG AT
MYH11 (s)	AGC CGG GAA AAC CGA AAA CA
MYH11 (as)	GCT CTC CGT AGG CAA AAG ATG

App. Table 8: mFISH-based cytogenetic analyses of cTNT-H9 after exposure to 1 or 2 Gy X-rays.

	analyzed cells	**aberrant cells**	**breaks per 100 cells**	**translocations per 100 cells**	**dic. per 100 cells**	**complex aberr. per 100 cells**	**other aberr. per 100 cells**
24 h after 1 Gy	95	15	9.5	5.3	1	0	2.1
7 d after 1 Gy	183	6	3.8	0.5	0	0	0
7 d after 2 Gy	57	4	3.5	1.75	0	1.75	0

dic. = dicentric chromosomes; aberr. = aberrations

App. Table 9: Fraction of necrotic cTNT-H9 cells at 24, 48 and 72 h after exposure to 1 Gy X-rays.

Experiment #	24 h (%)	48 h (%)	72 h (%)
1	2,21	1,23	1,65
2	1,80	1,45	1,64
3	1,02	1,47	2,02
mean	1,68	1,39	1,77

App. Table 10: Fraction of apoptotic cTNT-H9 cells at 24, 48 and 72 h after exposure to 1 Gy X-rays.

Experiment #	24 h (%)	48 h (%)	72 h (%)
1	2,15	2,64	6,03
2	3,62	1,12	1,72
3	1,97	2,64	4,18
mean	2,58	2,13	3,98

App. Table 11: Intensity measurement in average-intensity projections of ATM protein in cTNT-H9 seven days after exposure to 0 and 1 Gy X-rays with the Fiji-Software.

	Control	1 Gy
1	78,81	97,38
2	91,77	104,48
3	81,60	81,68
4	90,78	100,05
5	81,25	68,04
6	97,44	123,86
7	73,04	100,94
8	97,38	87,99
9	96,61	77,12
10	69,78	85,31
11	81,66	91,92
12	90,47	76,85
13	77,35	86,37
14	87,03	79,81
15	72,54	102,01
16	69,29	101,34
17	84,35	103,43
18	73,81	90,75
19	76,82	80,15
20	97,79	74,46
Median	81,6	89,4
Mean	83,5	90,7

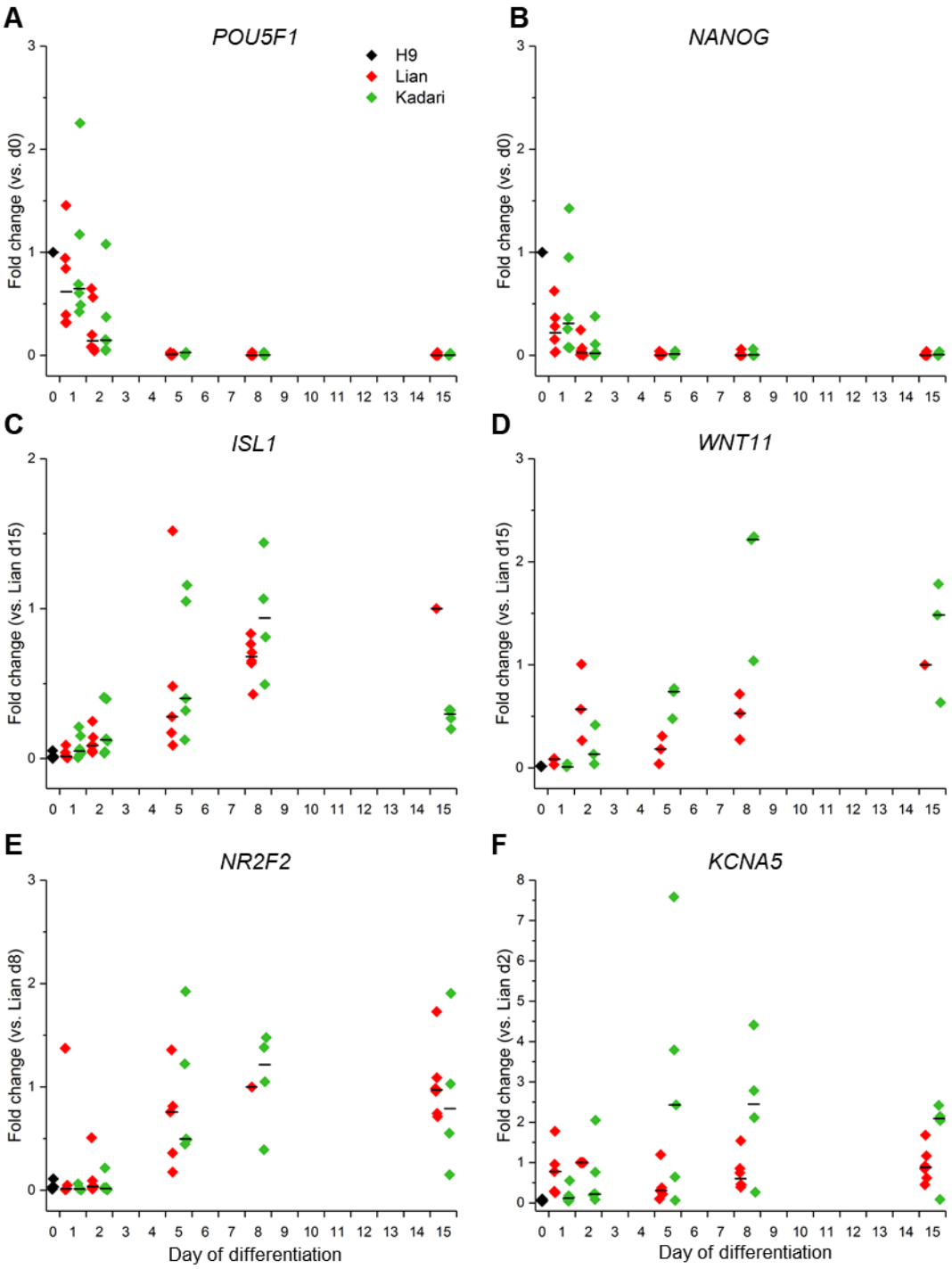

App. Fig. 1: Marker gene expression during cardiac differentiation of H9 wildtype cells according to Lian et al., 2013a (red) and Kadari et al., 2015 (green). At various days during differentiation of H9 cells (black), RNA samples were analyzed for the expression of pluripotency genes (A, B), *ISL1* (C), *WNT11* (D) and atrial markers (E, F). Values were normalized to 18sRNA and to the highest mRNA level of each target. *WNT11* was analyzed in only n = 3 independent experiments. d, day.

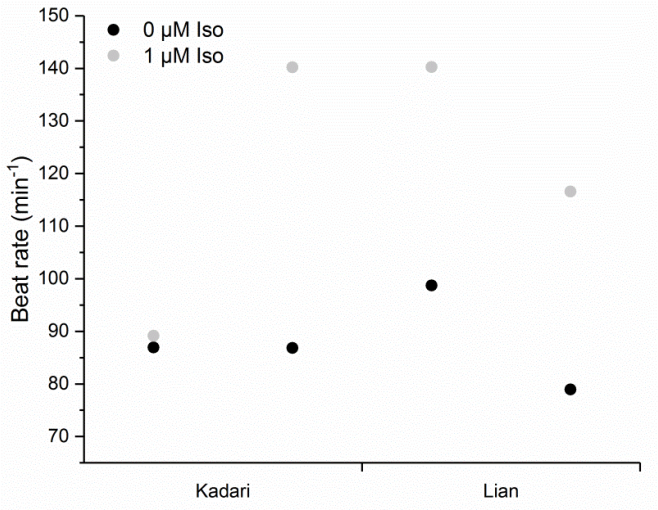

App. Fig. 2: Increased beat rates of cardiac clusters derived from the Lian et al. and Kadari et al. protocol upon addition of isoproterenol. Data of one experiment with two recorded clusters per protocol at day 15 of cardiac differentiation before (black) and after addition of 1 µM isoproterenol (gray).

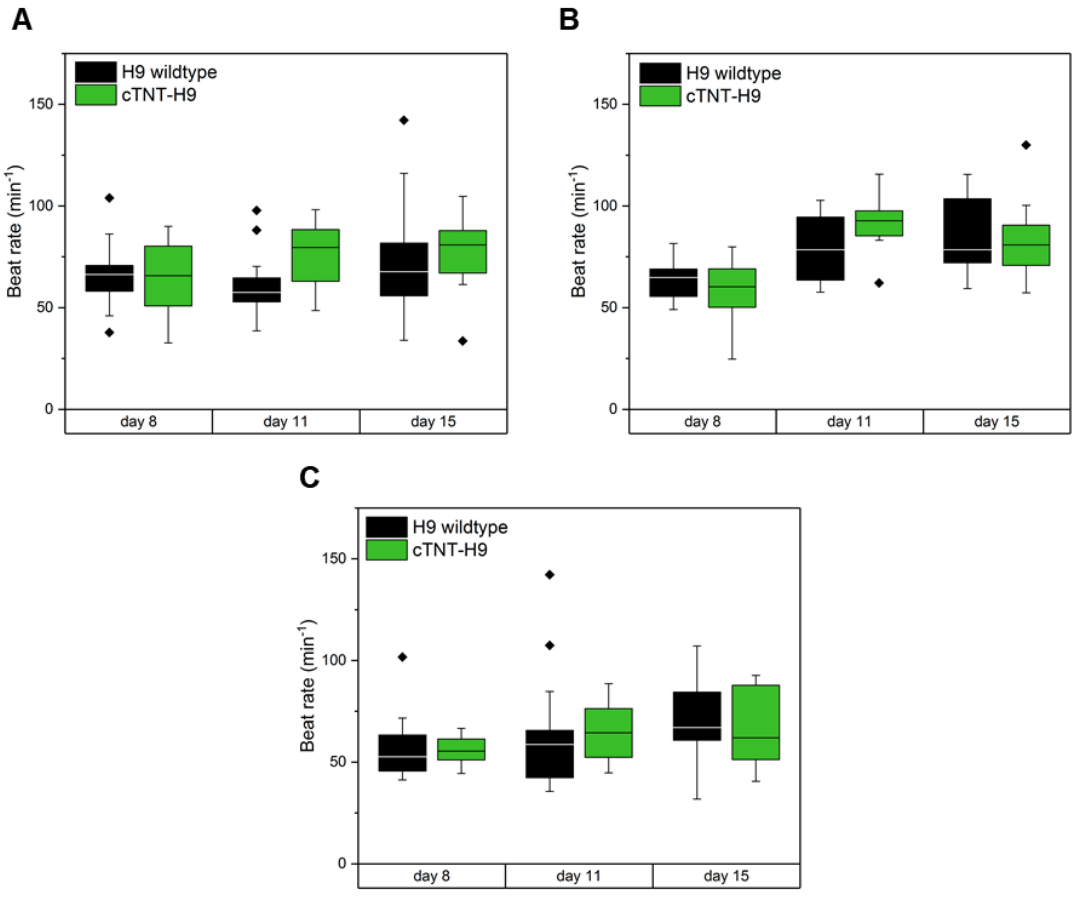

App. Fig. 3: Beat rates of H9- and cTNT-H9-derived cardiac clusters. Videos of at least 20 clusters were recorded at day 8, 11 and 15 of differentiation for H9 wildtype (black boxes) and cTNT-H9 (green boxes) cells of n = 3 independent experiments. Beat rates were determined with the software cBRA.

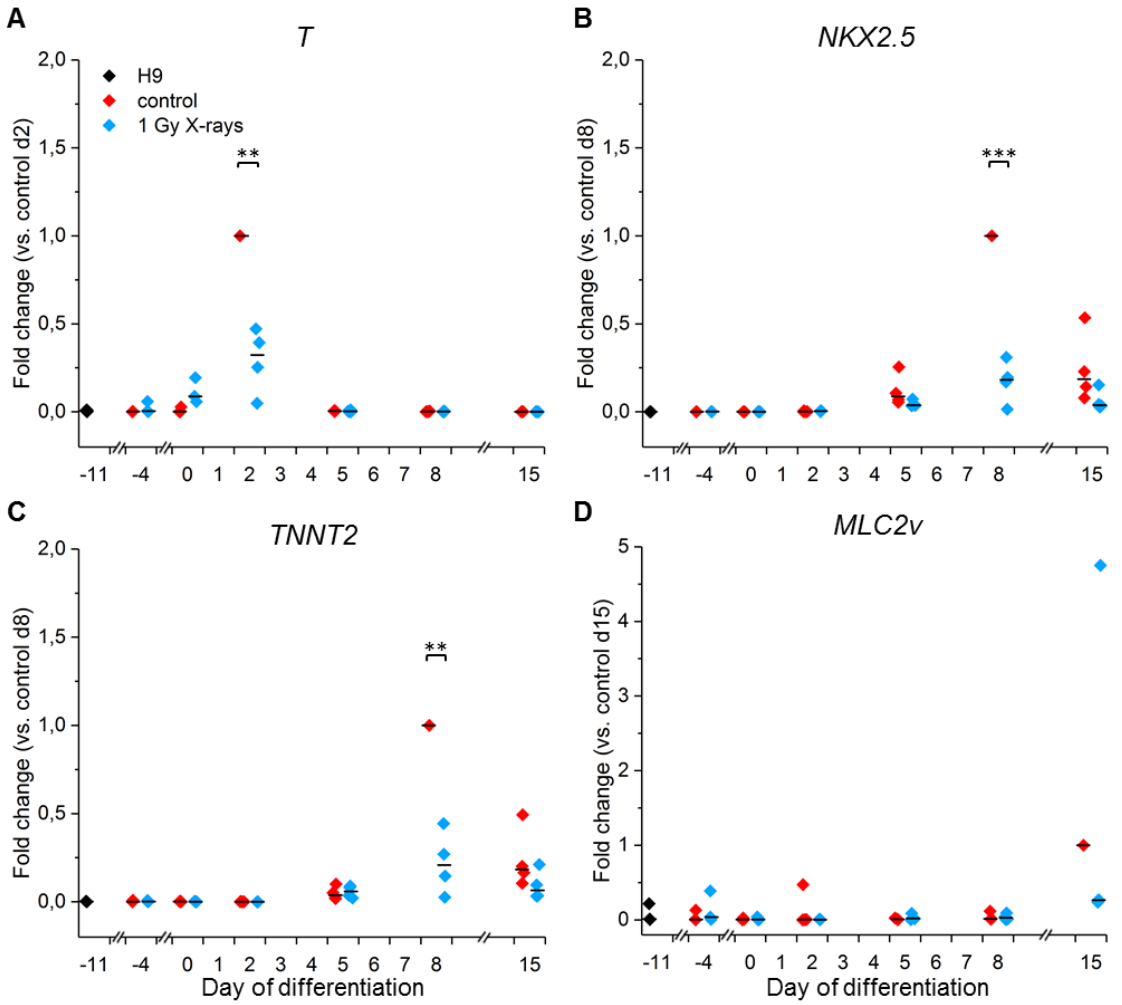

App. Fig. 4: Gene expression analyses of differentiating H9 cells upon exposure to 1 Gy X-rays. *T* (A), *NKX2.5* (B), *TNNT2* (C) and *MLC2v* (D) expression was reduced in irradiated samples (blue) compared to controls (red). Student's t-test was performed among experiments. ** $p < 0.01$; *** $p < 0.001$; d, day. Black symbols, target gene expression in H9 cells before irradiation.

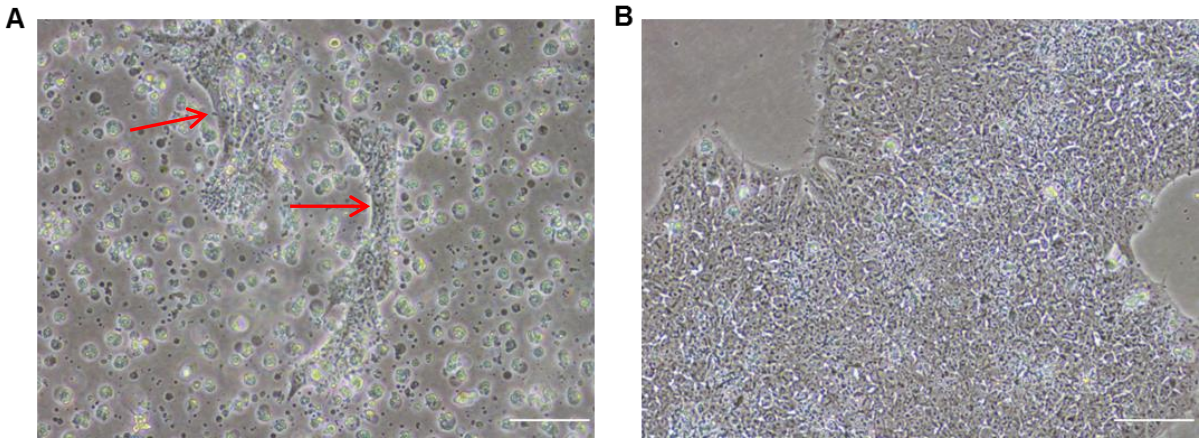

App. Fig. 5: Decreased colony size of cTNT-H9 cells upon exposure to 2 Gy X-rays. A) 24 h after irradiation with 2 Gy X-rays, the number of dying cells was very high (round, floating cells) and the colonies of the surviving cells were very small (red arrows) compared to sham control (B). Scale bar: 100 µm.

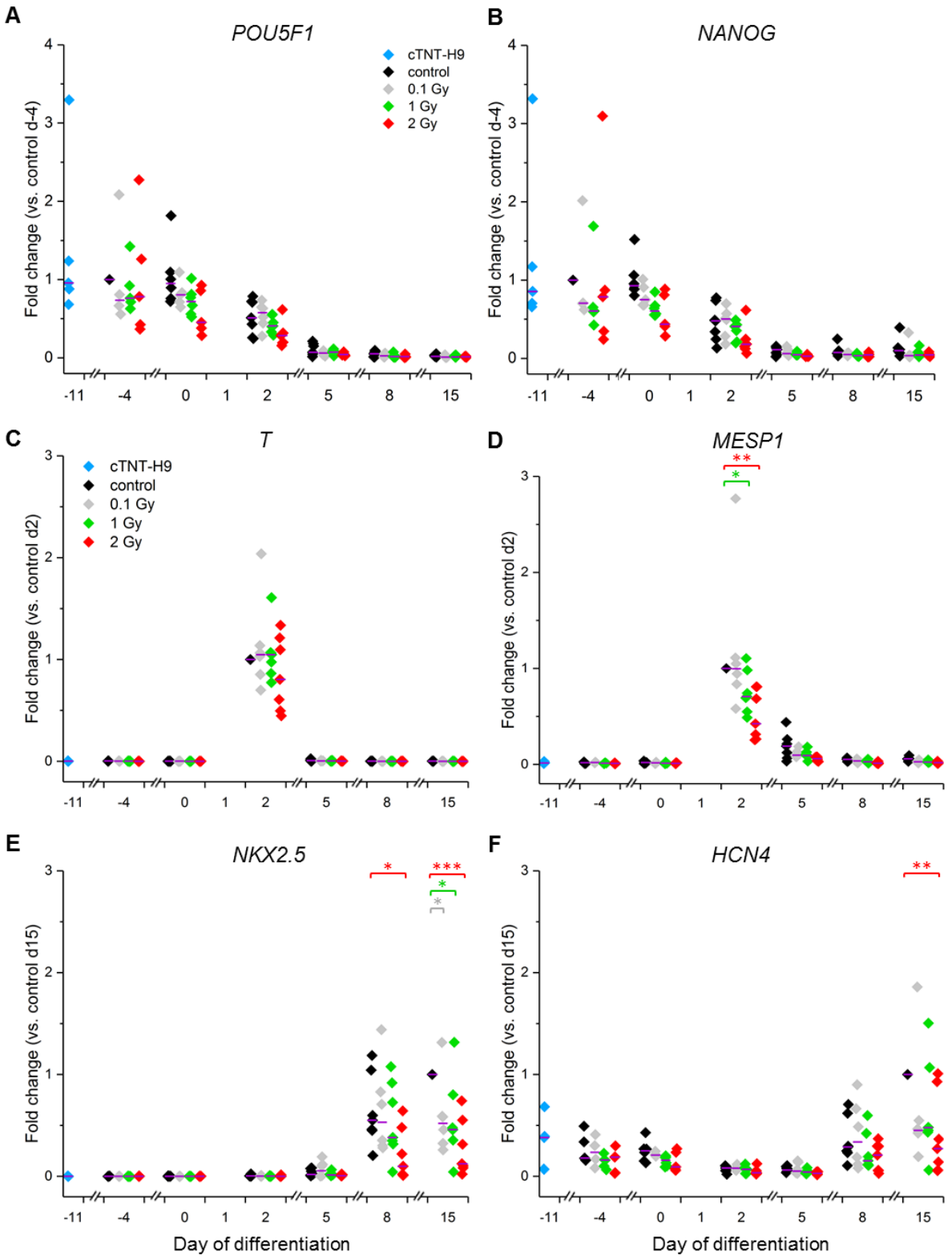

App. Fig. 6: qRT-PCR based analyses of pluripotency and early cardiac marker genes in irradiated differentiating cTNT-H9 cells. The cells were irradiated with 0 (control, black), 0.1 (gray), 1 (green) or 2 Gy (red) X-rays at day -7 and cardiac differentiation was initiated at day 0. RNA samples were taken at the indicated time points and analyzed for *POU5F1* (A), *NANOG* (B), *T* (C), *MESP1* (D), *NKX2.5* (E) and *HCN4* (F) expression. Student's t-test was performed among experiments, * $p < 0.05$; ** $p < 0.01$; *** $p < 0.001$. Blue symbols, expression levels in pluripotent cells before irradiation; violet line, median; d, day.

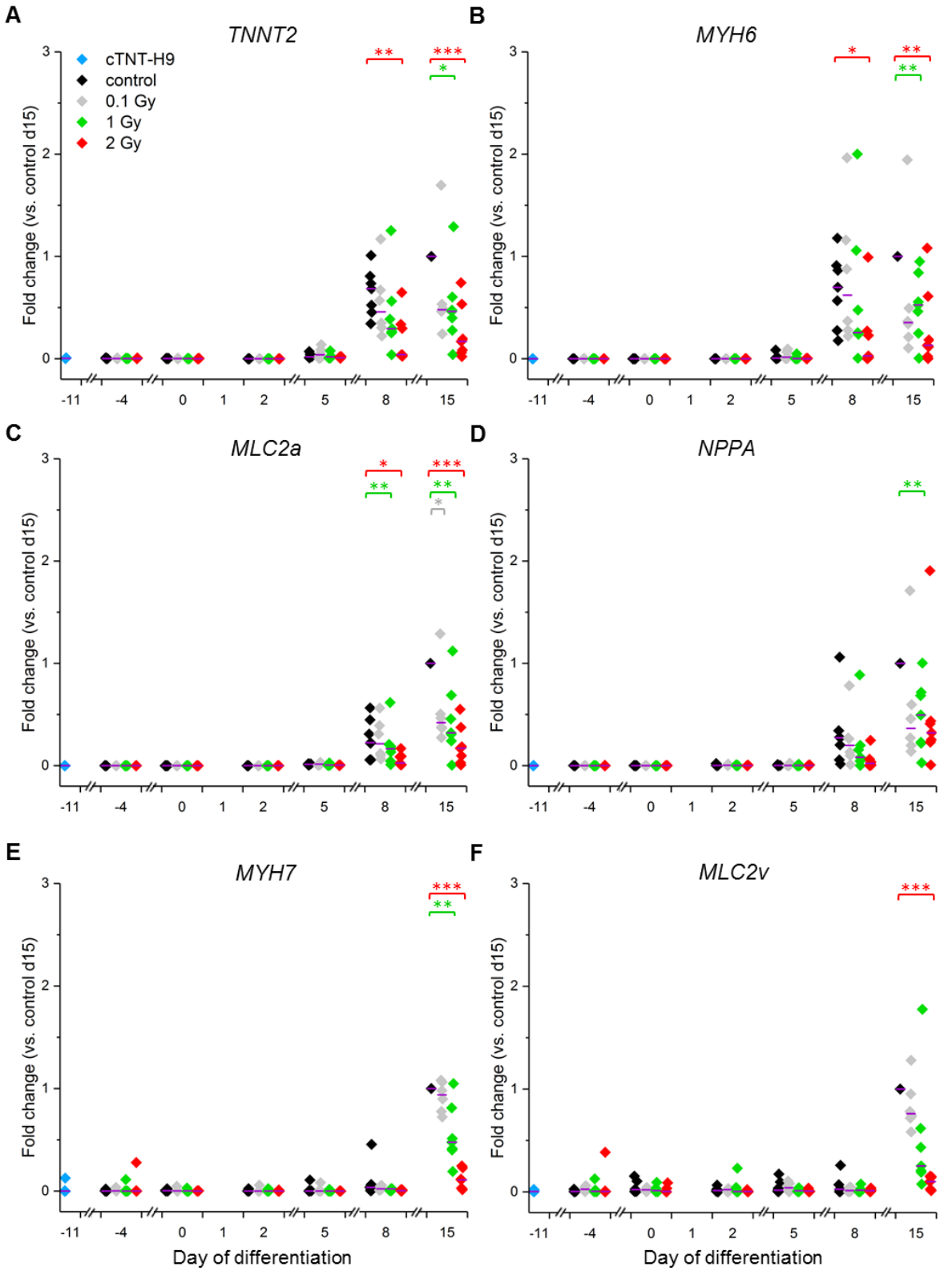

App. Fig. 7: Cardiac marker gene expression of differentiating cTNT-H9 cells exposed to various X-ray doses. Pluripotent cells (blue) were irradiated with 0 (control; black), 0.1 (gray), 1 (green) or 2 Gy (red) and seven days later, cardiac differentiation was initiated. RNA samples were collected at several days and analyzed for *TNNT2* (A), *MYH6* (B), *MLC2a* (C), *NPPA* (D), *MYH7* (E) and *MLC2v* (F) expression via qRT-PCR. Student's t-test was performed among experiments, * $p < 0.05$; ** $p < 0.01$; *** $p < 0.001$. Violet line, median; d, day.

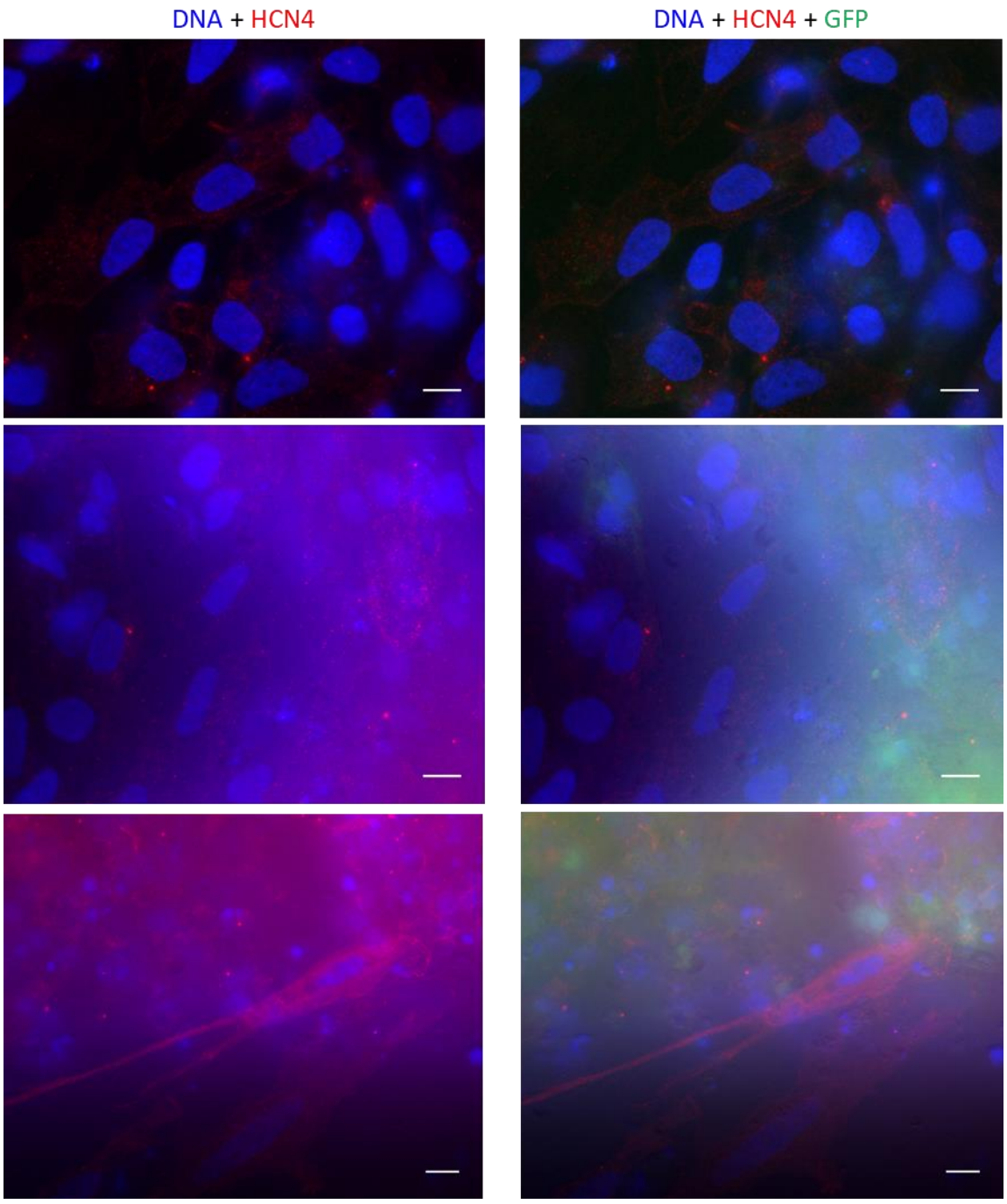

App. Fig. 8: Immunocytochemical detection of HCN4 in cTNT-H9-derived cardiac cultures at day 15. Top: non-GFP cells showing a weak signal in the red (HCN4) channel. Middle: Some cells near GFP-positive clusters had a higher signal in the HCN4 channel. Bottom: HCN4-positive cell with a distinct morphology and no GFP-expression. DNA was stained with Hoechst-33342 (blue). Scale bars: 10 µm.

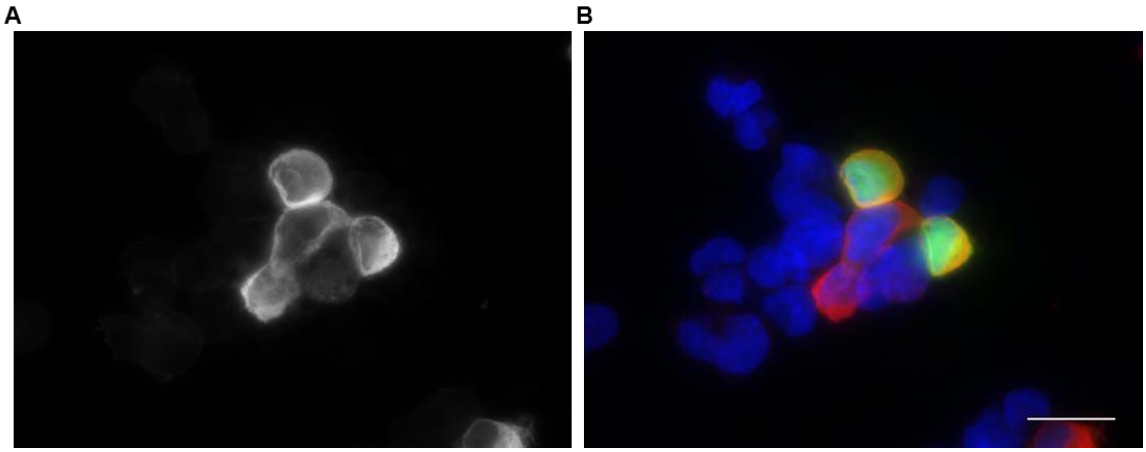

App. Fig. 9: HEK-293 cells transfected with human HCN4 as positive controls for detection of HCN4. Transfected cells were kindly provided by Paolo Zuccholini/Technical University of Darmstadt. HEK293-cells were transfected with plasmids containing the hHCN4 gene and a GFP-reporter gene (green). Fixed cells were stained for HCN4 (red). DNA was stained with Hoechst-33342 (blue). Scale bar: 20 µm.

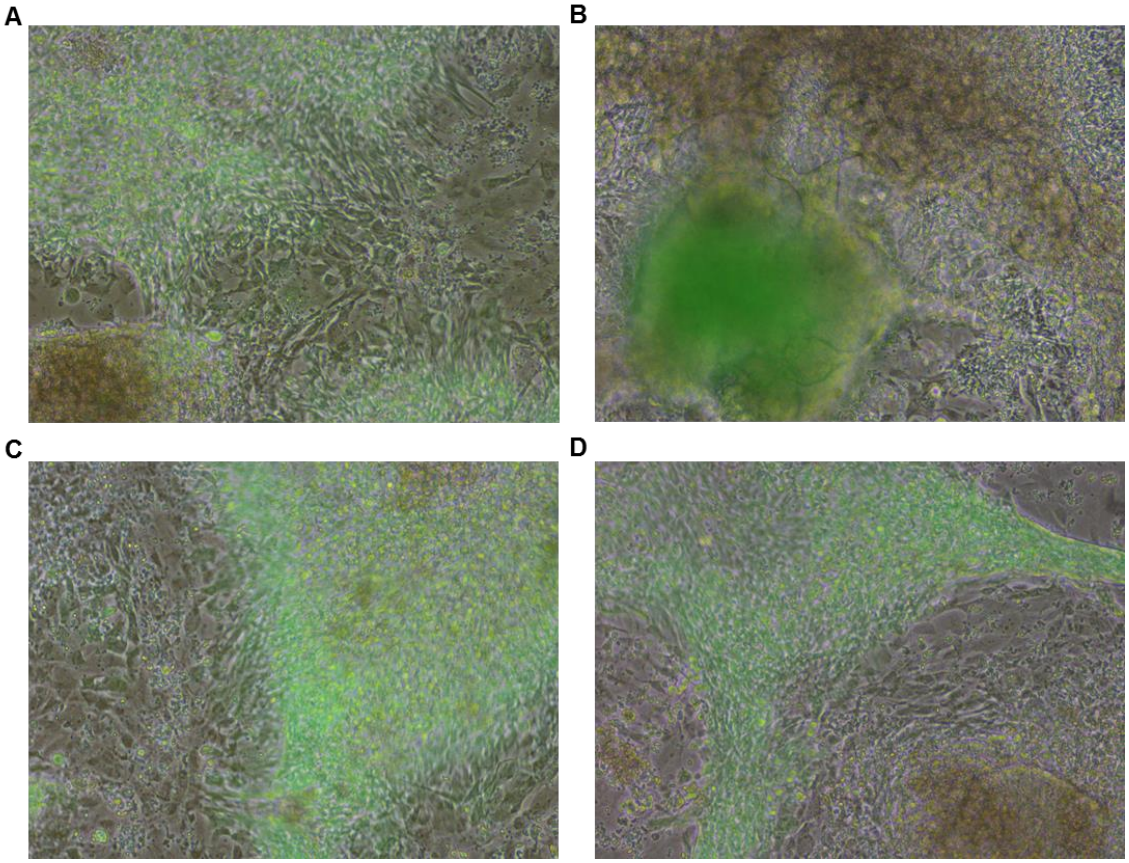

App. Fig. 10: Altered morphology of the cardiac clusters derived from high-passage cTNT-H9. Thin, green-fluorescing layers of contracting CM formed starting from day 10 of differentiation in samples derived from sham controls (A), 1 Gy (C) and 2 Gy (C) X-ray irradiated cTNT-H9. Clusters derived from 0.1 Gy irradiated cTNT-H9 had the usually observed compact, round morphology (D), however, only few cardiac clusters had formed in this sample.

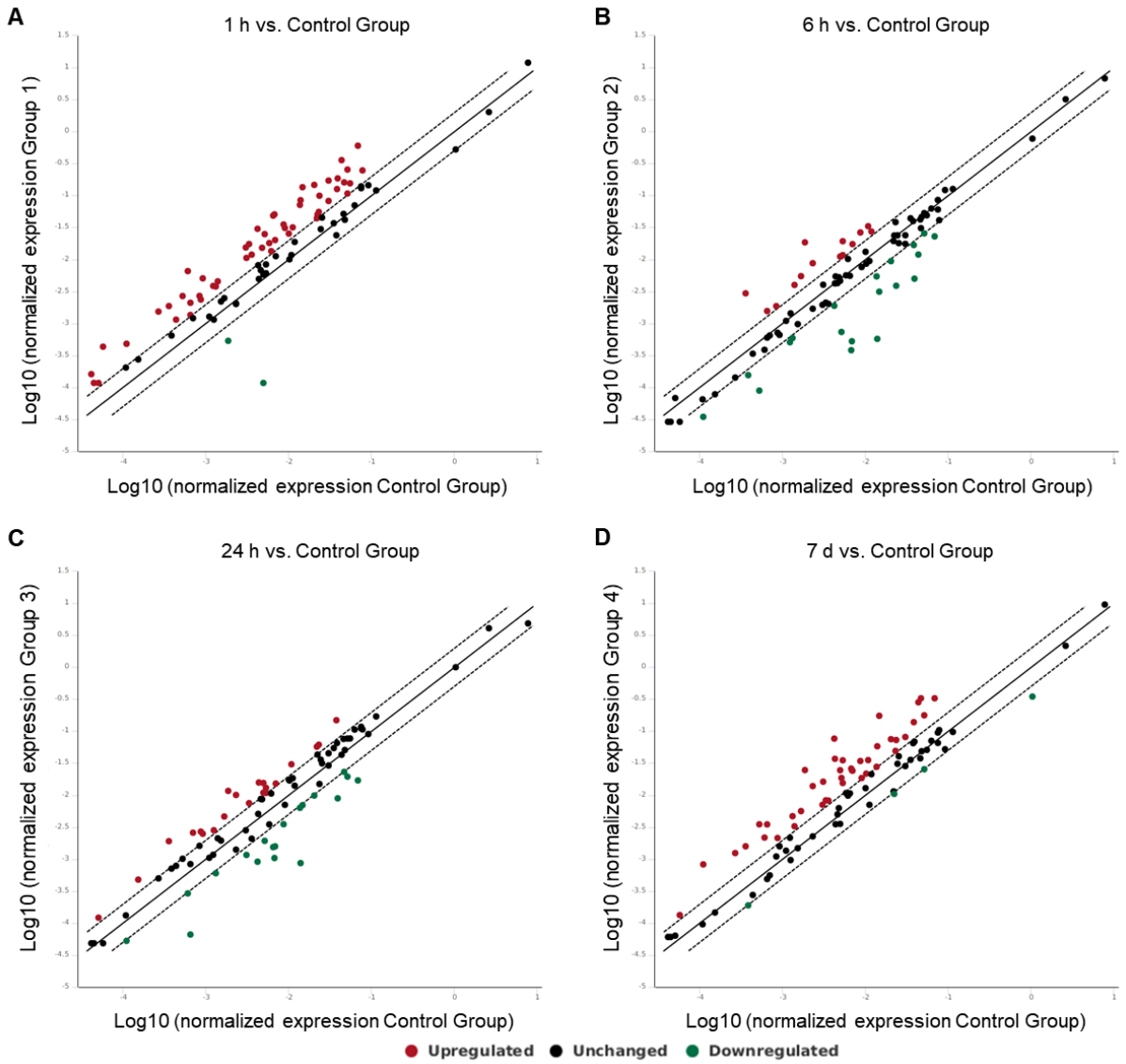

App. Fig. 11: Scatter plots of gene expression changes in Stem Cell Signaling upon exposure of cTNT-H9 cells to 1 Gy X-rays. RNA-samples of sham and 1 Gy X-ray irradiated cTNT-H9 cells were collected at 1 h (A), 6 h (B), 24 h (C) and 7 d (D) after exposure (n = 6 independent experiments). Samples were pooled for each time point and compared to controls using the ΔΔCT-method. All controls were set as one control group automatically. For normalization, *GAPDH*, *HPRT1*, *RPLP0* were used. Results are depicted in scatter plots with significantly (more than 2-fold) up- (red) or downregulated (green) genes. Genes whose expression is not altered compared to controls (less than 2-fold), are depicted with black dots.

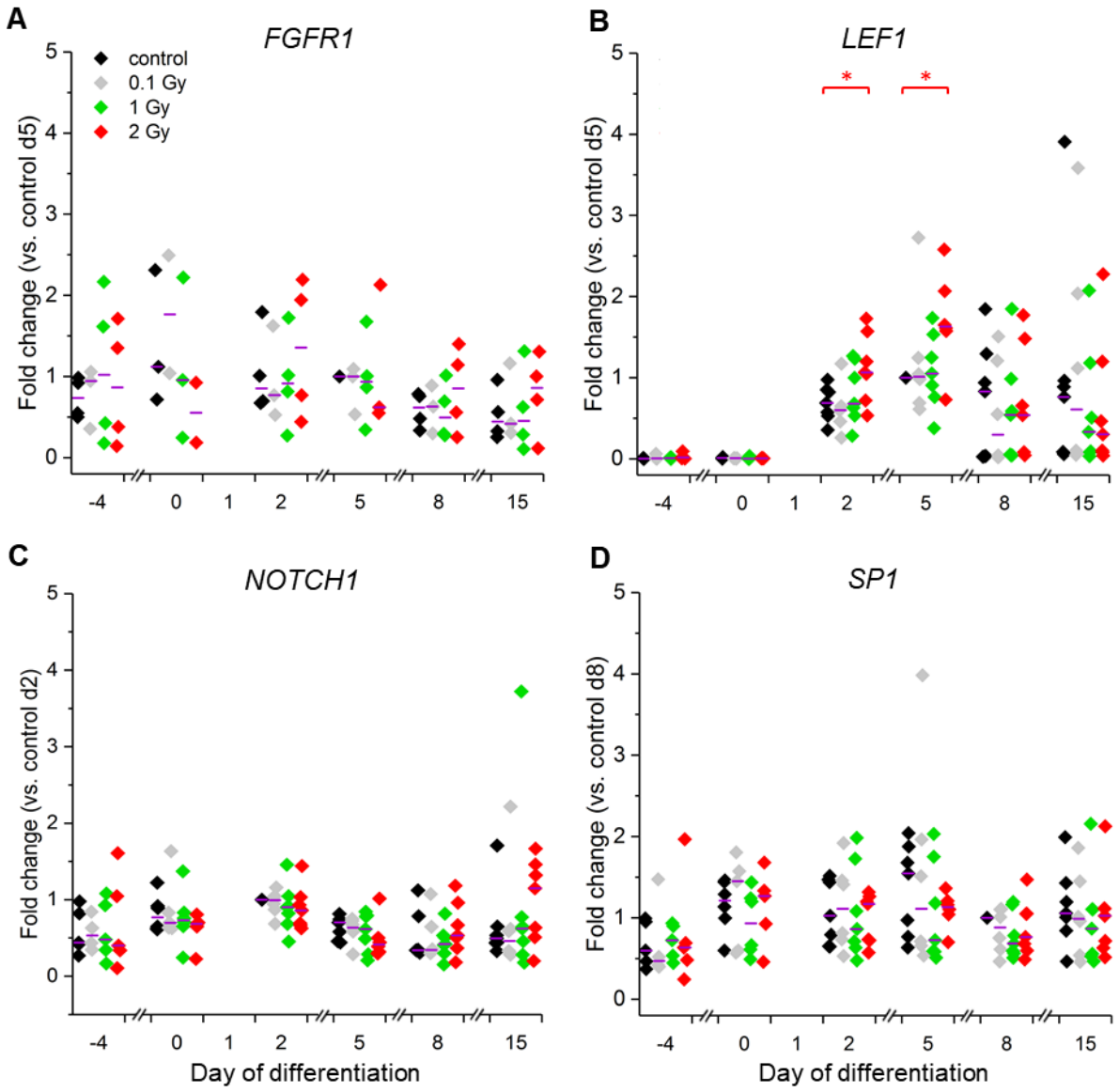

App. Fig. 12: Expression of FGFR1, LEF1, NOTCH1 and SP1 during cardiac differentiation of irradiated cTNT-H9 cells. Cells were irradiated with 0 Gy (sham control, black), 0.1 Gy (gray), 1 Gy (green) and 2 Gy (red) X-rays and cardiac differentiation was initiated seven days later. Expression of FGFR1 was analyzed in n = 4 experiments (A), LEF1 (B), NOTCH1 (C) and SP1 (D) was analyzed in n = 7 experiments via qRT-PCR. Values were normalized to 18sRNA and to the control samples with the highest expression level of each gene. The violet line represents the median. Student's t-test was performed among experiments; * $p < 0.05$; d, day

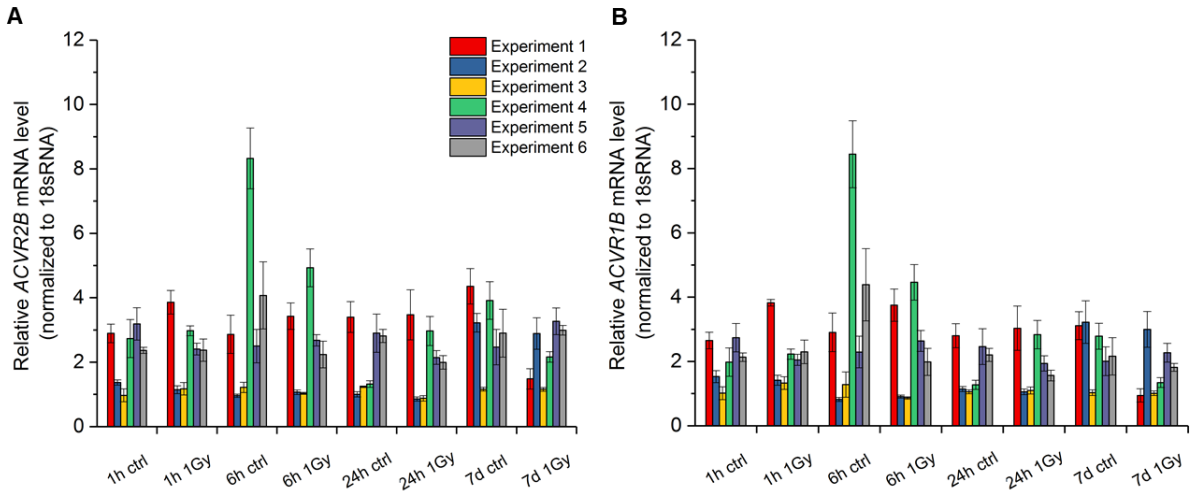

App. Fig. 13: qRT-PCR based analyses of the expression of activin receptors in the samples that were pooled for the arrays. cTNT-H9 cells were irradiated with 1 Gy X-rays and after 1 h, 6 h, 24 h and 7 d RNA samples were taken (n = 6) and analyzed for *ACVR2B* (A) and *ACVR1B* (B) expression via qRT-PCR. Values were normalized to 18sRNA.

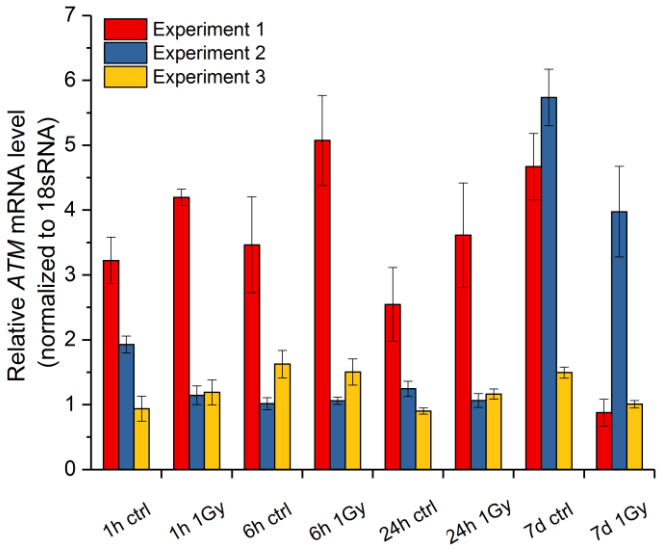

App. Fig. 14: Gene expression of *ATM* upon exposure to 1 Gy X-rays in the samples pooled for the arrays. cTNT-H9 cells were irradiated with 1 Gy X-rays and after 1 h, 6 h, 24 h and 7 d RNA samples were taken. In 3 out of 6 experiments, *ATM* expression was investigated. 18sRNA was used for normalization.

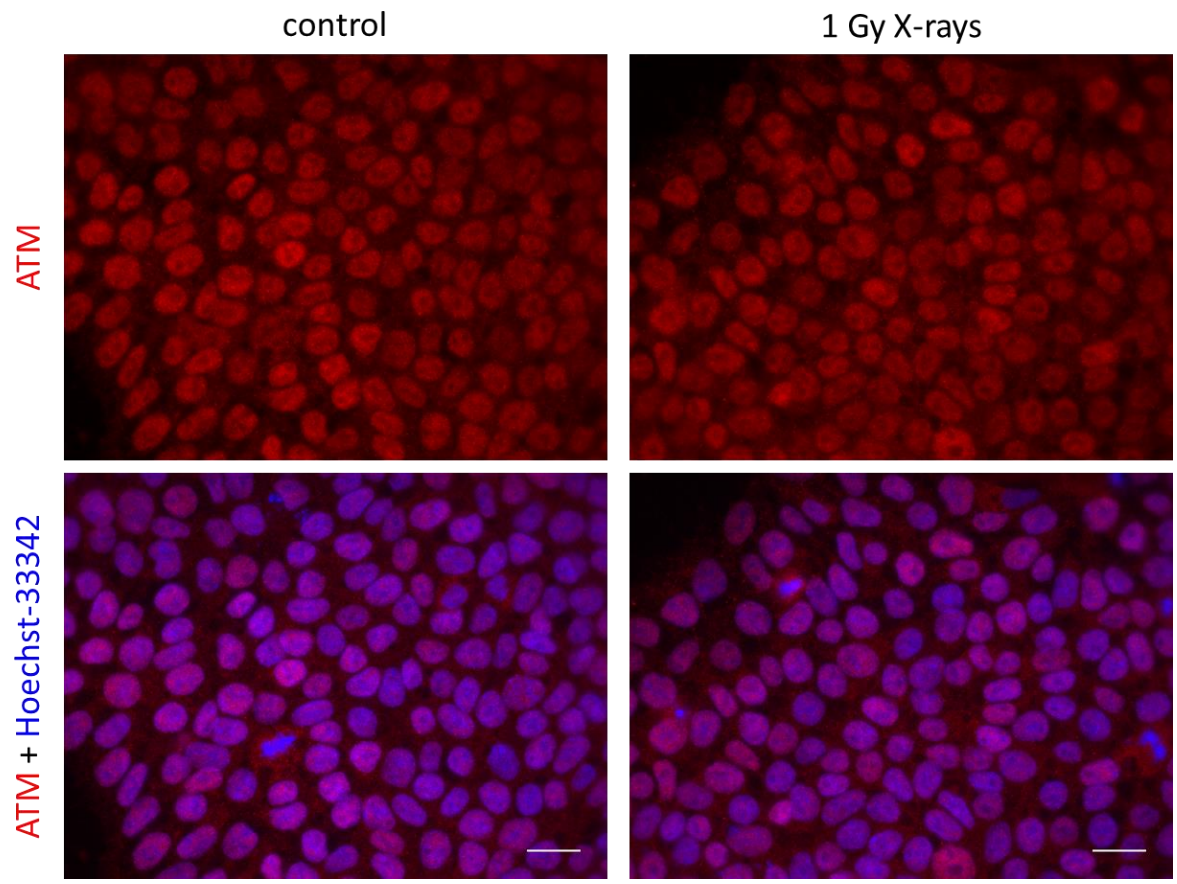

App. Fig. 15: ATM expression in sham and 1 Gy irradiated cTNT-H9 cells seven days after exposure. One week after irradiation with 1 Gy X-rays, cTNT-H9 cells were fixed, permeabilized, blocked and stained against ATM. DNA was stained with Hoechst-33342 (blue). Scale bars: 20 µm.

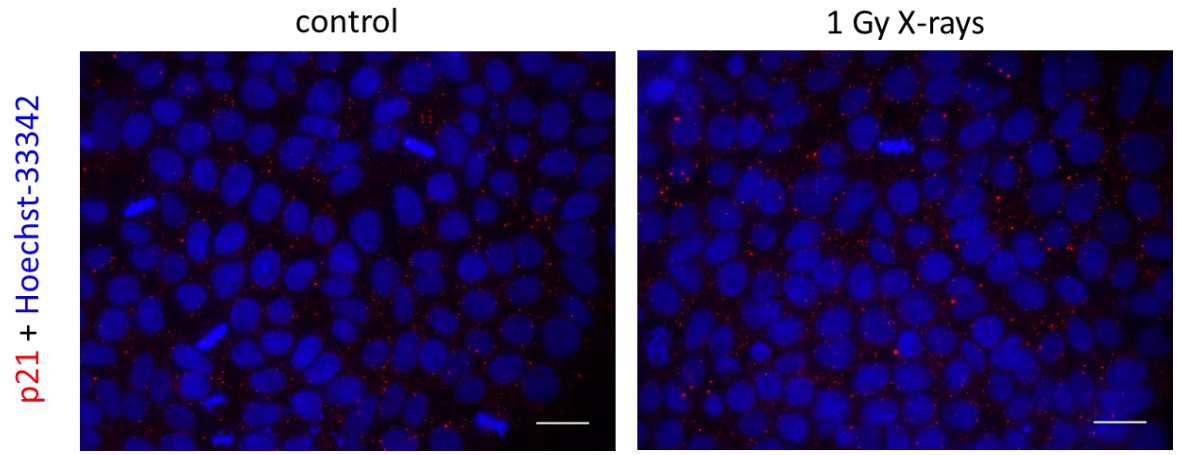

App. Fig. 16: p21 detection in sham and 1 Gy irradiated cTNT-H9 cells seven days after exposure. cTNT-H9 cells were irradiated with 1 Gy X-rays and one week later, they were fixed, permeabilized, blocked and stained against p21 (red). DNA was stained with Hoechst-33342 (blue). Scale bars: 20 µm.

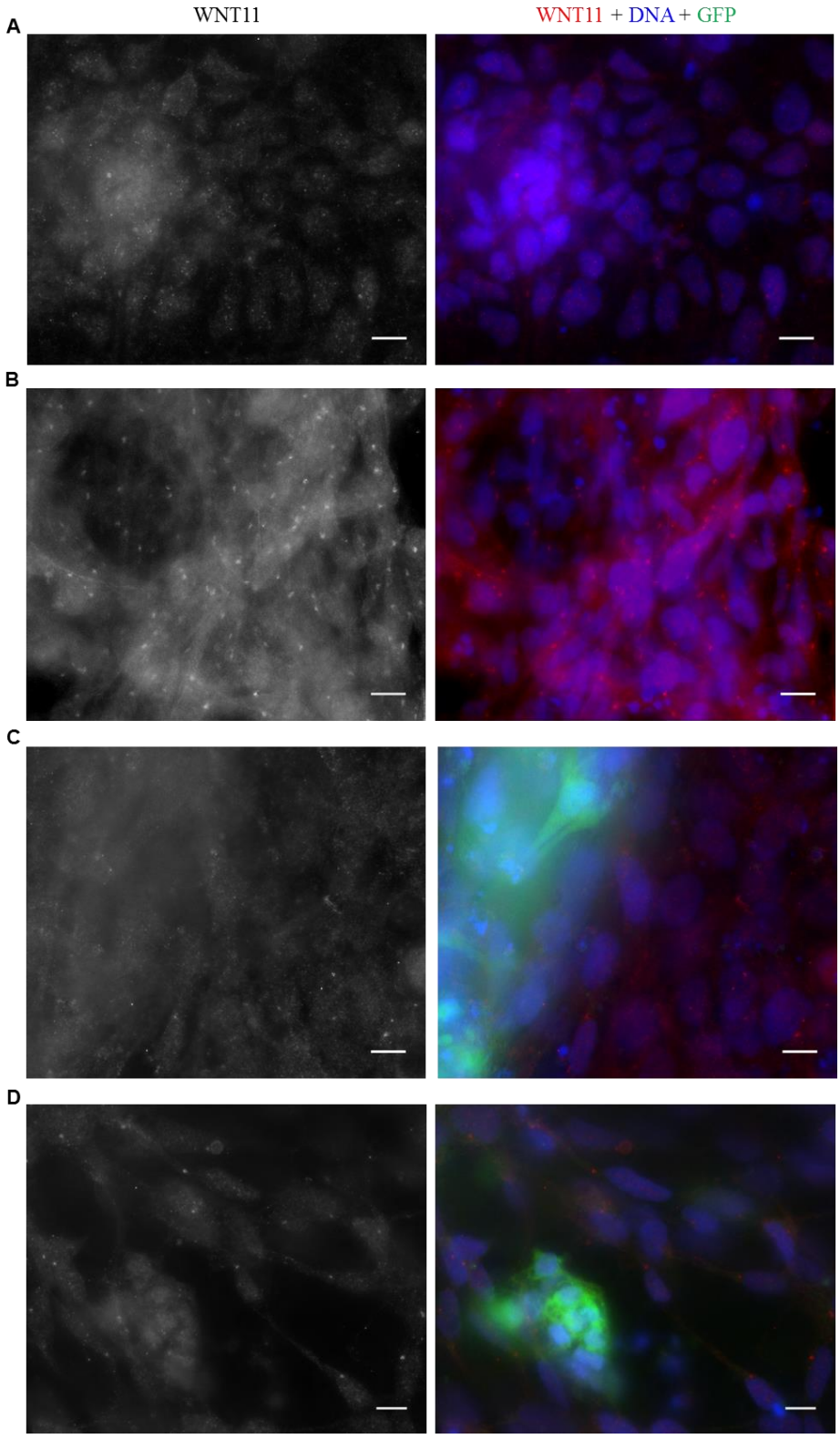

App. Fig. 17: Immunocytochemical detection of WNT11. cTNT-H9 cells (controls) were differentiated and at day 5 (A), 8 (B, C) and 15 (D) WNT11 protein was analyzed. Since expression of GFP was very low at day 5 (A, in the small cluster of cells on the left side) and also at day 8 in those clusters that did not start to beat yet (B, cells on the right and lower part of the picture), the green channel is not shown since the signal could not be distinguished from noise in the pictures. C, D) GFP-expressing clusters with WNT11-signal all over the nucleus and non-GFP-cells showing one big spot per cell near the nucleus. DNA was stained with Hoechst-33342. Scale bars: 10 µm.

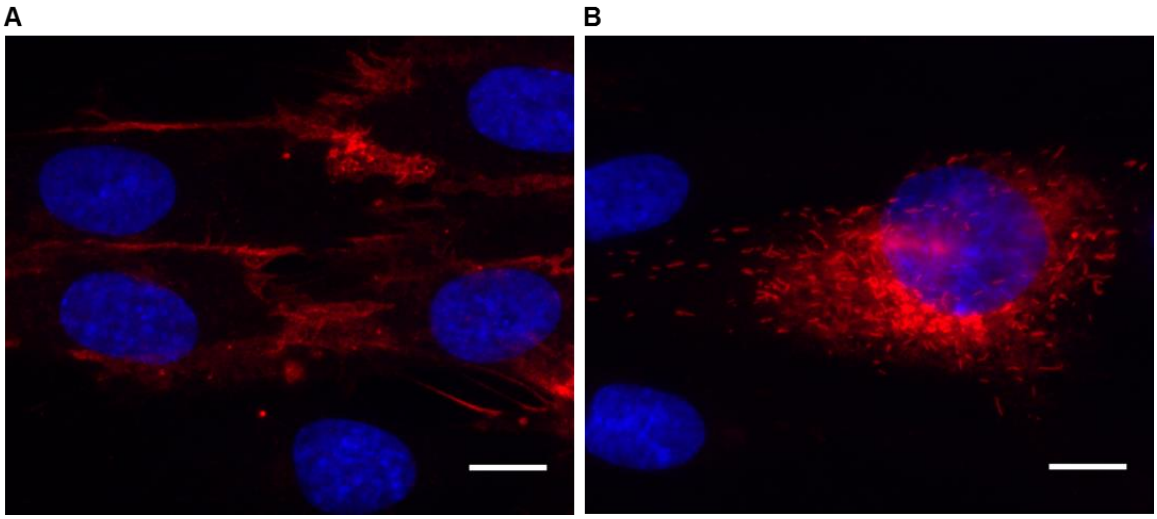

App. Fig. 18: Positive controls for immunocytochemical staining of endothelial markers. A) HDMEC stained for CD31. B) HMVEC stained for vWF. DNA was stained with Hoechst33342. Scale bars: 10 µm.

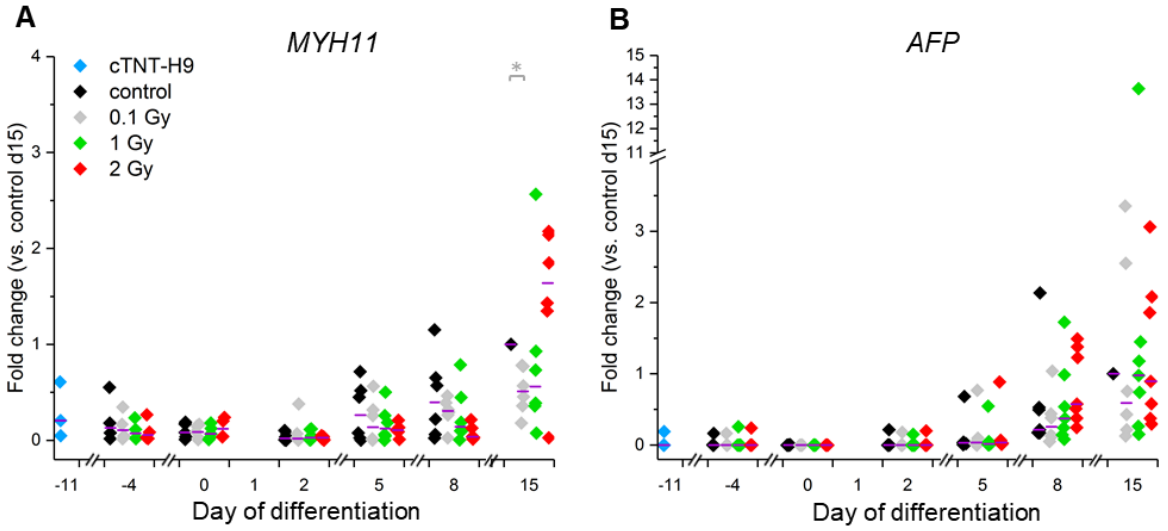

App. Fig. 19: Gene expression of *MYH11* and *AFP* during cardiac differentiation of irradiated cTNT-H9 cells. Expression of *MYH11* (A) and *AFP* (B) in cardiac cultures derived from sham controls (black) or 0.1 Gy (gray), 1 Gy (green) or 2 Gy (red) irradiated cells was analyzed via qRT-PCR. Values were normalized to 18sRNA and to day 15-control mRNA levels for each experiment. Student's t-test was performed among experiments. * $p < 0.05$; blue symbols, gene expression level before irradiation; d, day.

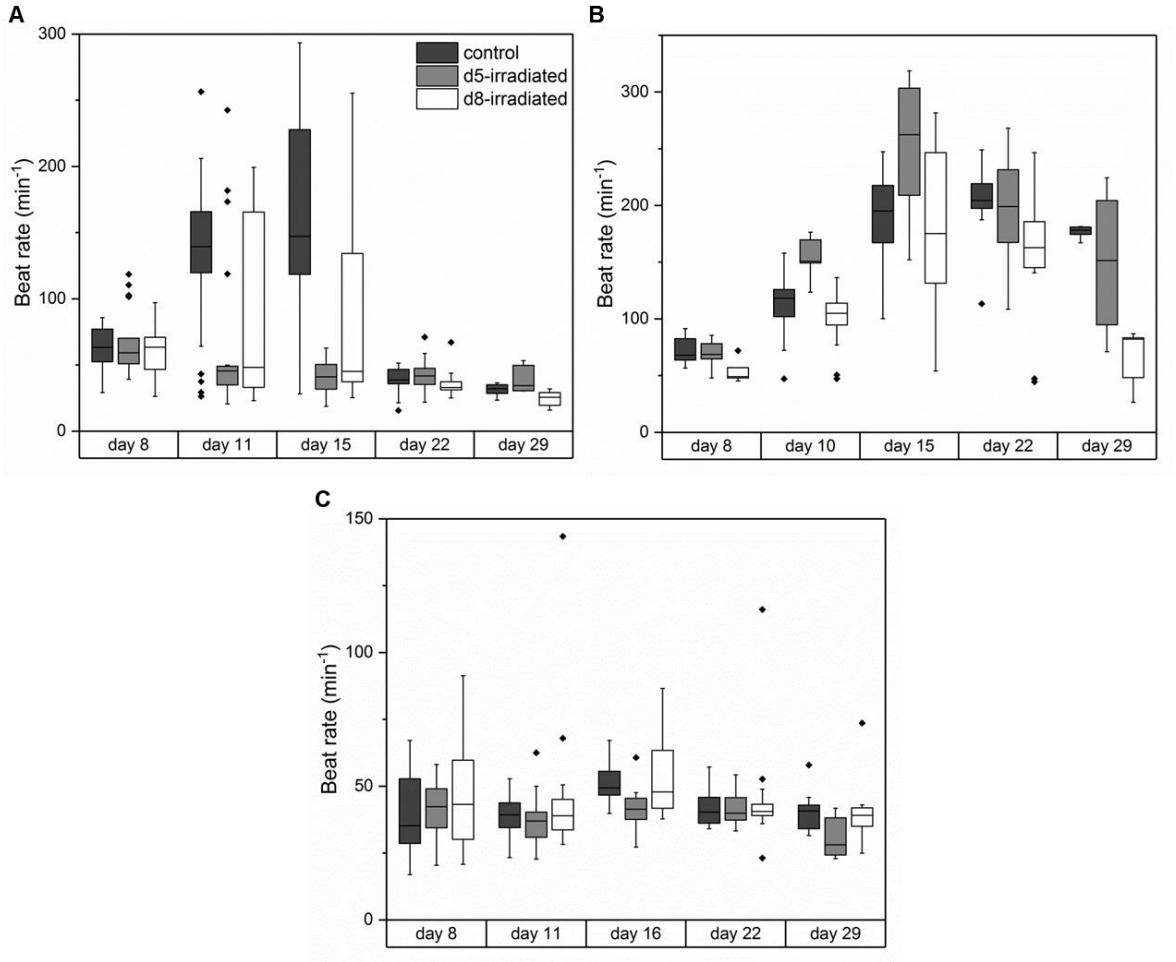

App. Fig. 20: Beat rates of cardiac clusters derived from cTNT-H9 cells that were irradiated at day 5 or 8 of cardiac differentiation. cTNT-H9 cells were differentiated according to Kadari et al., 2015 and irradiated at day 5 (gray boxes) or day 8 (white boxes) with 1 Gy X-rays. Controls (black boxes) were sham irradiated. Videos of at least 20 clusters were recorded at day 8, 10 (or 11), 15 (or 16), 22 and 29.

Publications

Peer reviewed publications

Nitsch, S., Braun, F., Ritter, S., Scholz, M., Schroeder, I.S. 2018. Functional video-based analysis of 3D cardiac structures generated from human embryonic stem cells. Stem Cell Res. 29, 115–124

Ibrahim, A.A., Schmithals, C., Kowarz, E., Köberle, V., Kakoschky, B., Pleli, T., Kollmar, O., Nitsch, S., Waidmann, O., Finkelmeier, F., Zeuzem, S., Korf, H.W., Schmid, T., Weigert, A., Kronenberger, B., Marschalek, R., Piiper, A., 2017. Hypoxia causes down-regulation of Dicer in hepatocellular carcinoma, which is required for up-regulation of hypoxia inducible factor 1α and epithelial-mesenchymal transition. Clin Cancer Res. 23, 3896-3905.

Scientific reports

Nitsch, S., Braun, F., Kunz, J., Scholz, M., Taucher-Scholz, G., Ritter, S., Schroeder, I. Characterization of the cardiac cultures generated from human embryonic stem cells with distinct differentiation protocols. GSI Scientific Report 2017

Nitsch, S., Braun, F., Kunz, J., Ritter, S., Scholz, M., Schroeder, I. Impact of ionizing radiation on cardiac differentiation – an update. GSI Scientific Report 2016

Schroeder, I., Nitsch, S., Braun, F., Scholz, M., Ritter, S. Cardiomyocytes derived from human embryonic stem cells respond with functional and transcriptional alterations to chemical stress and ionizing radiation. GSI Scientific Report 2015

Conference Poster Contributions

S. Nitsch, I.S. Schroeder, S. Ritter. Cardiac differentiation of human embryonic stem cells is hampered upon exposure to ionizing radiation. German Stem Cell Network, Heidelberg/Germany, 2018.

S. Nitsch, F. Braun, J. Kunz, S. Ritter, I.S. Schroeder. Cardiac differentiation of human embryonic stem cells is dysregulated upon exposure to ionizing radiation. GBS 21st Annual Meeting/Frankfurt 2018.

S. Nitsch, F. Braun, I. S. Schroeder, S. Ritter. Ionizing irradiation impairs the cardiac differentiation of human embryonic stem cells. Kompetenznetzwerk Stammzellforschung NRW, Münster/Germany, 2017.

S. Nitsch, F. Braun, I. S. Schroeder, S. Ritter. Impact of cardiac differentiation methods on human embryonic stem cells and their response to ionizing irradiation. German Stem Cell Network, Hannover/Germany, 2016.

S. Nitsch, F. Braun, I.S. Schroeder, S. Ritter. Impact of ionizing radiation on human embryonic stem cells and their cardiac differentiation capability. European Radiation Research Society, Amsterdam/Netherlands, 2016.

Curriculum Vitae

Personal Data

Name:	Scarlett Nitsch
Date and Place of Birth:	13th April 1990
	Offenbach am Main/Germany

Education and Work Experience

Since 10/2015	PhD student at GSI Helmholtz Centre for Heavy Ion Research, Department of Biophysics/enrolled at Technical University Darmstadt
09/2014 – 08/2015	Medical Technical Assistant at University hospital Frankfurt/Main
10/2012 – 09/2014	Master of Science “Technical Biology” at Technical University Darmstadt
10/2009 – 09/2012	Bachelor of Science “Biology” at Technical University Darmstadt
07/2009	*Abitur* at Claus-von-Stauffenberg-Schule in Rodgau